

Do subchondral bone chemical changes predict ankle osteoarthritis?

Thesis submitted for the degree of MD(Res)

Oliver Chan

Department of Medical Physics

University College London

Declaration

I, Oliver Chan confirm that the work presented in this thesis is my own. Where information has been derived from other sources, I confirm that this has been indicated in the thesis.

Acknowledgements

I would like to thank my supervisors Professor Allen Goodship and Mr Andy Goldberg for helping me conceptualise and complete the thesis. Without either of them, I would not have access to the patient samples or the control specimens vital for this project. I am also grateful to them for the useful feedback in the preparation of this thesis.

I am also thankful to Dr Helen Birch for helping me with the collagen biochemistry.

Lastly, I would like to thank Dr John Churchwell, who provided encouragement in all aspects of the study and was inspirational in terms of his knowledge about Raman spectroscopy. Without his technical nous in this area, the thesis would not have been completed and I am extremely grateful for his support.

Abstract

Introduction: Subchondral bone changes have been identified in hip and knee osteoarthritis (OA) and may serve as predictors of disease onset. Ankle OA in contrast is less common and strongly associated with trauma. The aims of the study were to determine whether subchondral bone changes are also associated with ankle OA.

Methods: Subchondral bone specimens were obtained from the distal tibiae of patients undergoing definitive surgery for ankle osteoarthritis. Samples were collected from patients with symmetrically and asymmetrically loaded (varus hindfoot deformity) wear patterns. Comparison was made with matched non-OA controls. Specimens were analysed using Raman spectroscopy and Sodium dodecyl sulphate polyacrylamide gel electrophoresis. Chemical markers of subchondral bone (phosphate: amide I, carbonate: amide I, phosphate:carbonate ratios, phosphate and amide I deconvolutional peak analysis) were calculated from the Raman spectra and principal component analysis was employed to detect inherent differences between the two groups. Sample mineral content and α -1 to α -2 type I collagen ratios were deduced from biochemical analysis.

Results: Significant differences within osteoarthritic subchondral bone were observed in the biochemical markers as deduced from Raman spectroscopy (phosphate:amide I, carbonate:amide I, Amide I (1690:1660) ratios ($p < 0.05$)). Biochemical Analysis revealed that osteoarthritic specimens were hypomineralised and had significantly greater α -1 to α -2 type I collagen ratios. Such changes were also noted to be present in subchondral bone collected from the relatively spared lateral joint surface from patients with a varus wear pattern.

Discussion: The results imply that subchondral bone is biochemically altered in patients with ankle osteoarthritis. This raises the possibility that certain patients may be biochemically predisposed to developing ankle osteoarthritis. Although trauma is strongly linked to the development of ankle osteoarthritis, it may be that trauma and/or subsequent joint instability may be an initiator for the disease process in subjects who are “biochemically predisposed”.

Impact Statement

Osteoarthritis of the ankle is a debilitating disease which causes pain, dysfunction and immobility in patients. An estimated 1% of the world's population is said to be affected by the condition. The pathoetiology however remains poorly understood.

The results from this thesis have identified subchondral bone changes within the distal tibial of patients with ankle osteoarthritis. This raises the possibility that a population with altered bone chemistry may be predisposed to developing ankle osteoarthritis, given the relative paucity of the condition compared to hip or knee osteoarthritis.

Spectral signatures from subchondral bone associated with ankle osteoarthritis have been identified using Raman spectroscopy in this study. With the further development of non-invasive modalities to acquire Raman spectra such as spatially offset Raman spectroscopy (SORS), it may be possible to identify healthy subjects prior to their development of clinical ankle osteoarthritis. This would then facilitate research into preventative interventions/patient factors which may potentially alter the natural history of the condition.

Abbreviations

RANKL	Receptor activator of nuclear factor kappa-B ligand
RANK	Receptor activator of nuclear factor
OPG	Osteoprotegerin
pH	Potential of Hydrogen
BMU	Basic multi-cellular unit
GPa	Gigapascals
OA	Osteoarthritis
ECM	Extracellular matrix
TNF-α	TNF-alpha
TRAP	Tartrate-resistant acid phosphatase
CTX-1	Carboxy-terminal crosslinked telopeptide
MRI	Magnetic Resonance Imaging
CT	Computed Tomography
DEXA	Dual-energy X-ray Absorptiometry
PCA	Principal Component Analysis
PC	Principal Component
CCD	Charge-coupled Device
SORS	Spatially Offset Raman Spectroscopy
SD	Standard Deviation
IQR	Inter-Quartile Range
DDRS	Drop-deposition Raman Spectroscopy
TAR	Total Ankle Replacement (Arthroplasty)
SDS-PAGE	Sodium dodecyl sulphate Polyacrylamide Gel Electrophoresis
SDS	Sodium dodecyl sulphate
Rf	Relative migration distance
EDTA	Ethylenediamine tetra-acetic acid

CONTENTS

Declaration	2
Acknowledgements	3
Abstract	4
Impact Statement	5
Abbreviations	6
<u>CHAPTER 1 – INTRODUCTION</u>	12
1.1 Bone	12
1.1.1 Bone composition, matrix and cells	12
1.1.2 Structure of bone	19
1.1.3 Mechanical Properties of Bone	22
1.2 Osteoarthritis	23
1.2.1 Macroscopic classification of OA	26
1.2.2 Pathogenesis of OA	27
1.2.2.1 Risk factors for OA	27
1.2.2.2 Pathobiology of OA	29
1.2.3 Role of Subchondral bone in OA	31
1.3 The ankle joint	35
1.3.1 Anatomy/Biomechanics of the ankle joint	35
1.3.2 Ankle osteoarthritis	38
1.4 Bone-imaging modalities	42
1.4.1 Plain radiography	42

1.4.2 Computed Tomography	42
1.4.3 Magnetic Resonance Imaging	43
1.4.4 Dual-energy X-ray absorptiometry	43
1.5 Raman Spectroscopy	44
1.5.1 Raman spectroscopy Background and theory	44
1.5.2 Raman spectroscopy instrumentation	46
1.5.3 Raman spectroscopy advantages and disadvantages	48
1.5.4 Kerr-Gate	49
1.5.5 Spatially Offset Raman Spectroscopy	50
1.5.6 Pre-processing	50
1.5.7 Interpretation of Raman spectra acquired from bone	51
1.5.8 Multivariate Analysis	54
1.5.9 Raman and studies of bone	55
<u>CHAPTER 2 – AIMS AND OBJECTIVES</u>	57
2.1 Aims	57
2.2 Hypotheses	57
2.3 Objectives	58
<u>CHAPTER 3 – VALIDATION OF METHODS</u>	59
3.1 Introduction	59
3.2 Methods	60
3.2.1 Calibration, reproducibility and repeatability	60

3.2.2 Natural variation by location of the tibial plafond	62
3.2.3 The effect of laser exposure time	64
3.3 Results	64
3.3.1 Calibration, reproducibility and repeatability	64
3.3.2 Natural variation by location of the tibial plafond	66
3.3.3 The effect of laser exposure time	67
3.4 Discussion	68
3.5 Power calculation	69
<u>CHAPTER 4 – ANALYSIS USING RAMAN SPECTROSCOPY</u>	70
4.1 Introduction	70
4.2 Methods	72
4.2.1 Ethical Approval	72
4.2.2 Specimen collection and preparation	73
4.2.3 Raman spectra acquisition	76
4.2.4 Raman spectra analysis	77
4.3 Results	81
4.3.1 Patient and donor demographic data	81
4.3.2 Results by sex	84
4.3.3 Osteoarthritis with a varus wear pattern	86
4.3.3.1 OA vs controls univariate analysis	86
4.3.3.2 OA vs controls multivariate analysis	88
4.3.3.3 Medial vs Lateral subchondral bone	89

4.3.4 Osteoarthritis with a balanced wear pattern	91
4.3.4.1 OA vs controls univariate analysis	91
4.3.4.2 OA vs controls multivariate analysis	93
4.3.4.3 Medial vs Lateral subchondral bone	94
4.4 Discussion	96
4.4.1 Male vs female patients and controls	96
4.4.2 Varus OA vs controls	96
4.4.2.1 Medial vs lateral subchondral bone	101
4.4.3 Balanced OA vs controls	102
4.4.3.1 Medial vs lateral subchondral bone	103
4.4.4 Summary of Raman results/Conclusion	103
<u>CHAPTER 5 – BIOCHEMICAL ANALYSIS OF SAMPLES</u>	105
5.1 Introduction	105
5.2 Methods	106
5.2.1 Mineral content	106
5.2.2 SDS-PAGE	107
5.3 Results	109
5.3.1 Specimen levels of mineralisation	109
5.3.1.1 Varus OA vs Matched controls	110
5.3.1.2 Balanced OA vs Matched controls	112
5.3.2 SDS-PAGE results	114
5.4 Discussion	118

5.4.1 Levels of mineralisation	118
5.4.2 SDS-PAGE Results	120
5.4.3 Summary of Biochemistry Results	122
<u>CHAPTER 6 – DISCUSSION & CONCLUSIONS</u>	123
6.1 Study Discussion	123
6.2 Conclusions	126
6.3 Future Work	127
REFERENCES	129

CHAPTER 1 – INTRODUCTION

1.1 Bone

1.1.1 Bone Composition

Bone is a complex, highly organized and specialized connective tissue. It is composed of specialized bone cells (osteoblasts, osteoclasts and osteocytes) and an extracellular matrix which has both organic and inorganic components.

Bone matrix

Examination of bone reveals that the matrix makes up roughly 90% of the volume of the tissue. Bone matrix is a composite material with both organic (largely type I collagen and other proteins) and inorganic components (predominantly calcium hydroxyapatite $(Ca_{10}(PO_4)_6(OH)_2)$). The removal of either component results in bone with altered mechanical properties. Demineralised bone behaves like a ligament or tendon and is flexible and resistant to fracture, while bone with the organic matrix removed is brittle and liable to fracture easily (Buckwalter 1995). The organic component therefore provides bone with the ability to resist tensile forces while the inorganic component allows bone to resist compressive forces (Viguet-Carrin 2006).

Organic Bone matrix

Organic bone matrix, accounts for roughly 20% of the wet weight of bone and is composed of mainly Type I collagen. This protein constitutes for roughly 90% of the organic matrix and is composed of three alpha polypeptide chains arranged in an alpha helical configuration (Two α -1 chains and 1 α -2 chain). A repetitive glycine-X-Y triplet (Where X is usually a proline and Y usually a

hydroxyproline) allows for such a configuration. The glycine is an absolute requirement as it is the smallest amino acid and can therefore occupy the limited space in the centre of the triple helix (Viguet-Carrin 2006).

Type I Collagen found in bone is synthesised by osteoblasts. Within the endoplasmic reticulum, the alpha chains are hydroxylated at the lysine and proline residues prior to helical formation and are then exported from these cells as procollagen. Procollagen undergoes further extracellular processing resulting in the cleavage of propeptides. The resulting fibrils are stabilised through the formation of intermolecular and intramolecular cross-links (Figure 1). This process is modulated by the enzymes Lysine hydroxylase and Lysyl oxidase (LOX) (Saito 2010). The importance of crosslink formation to the mechanical function of collagen is illustrated by Lathyrism. This is a clinical disorder associated with severe abnormalities of bone, joints and skin secondary to increased fragility of collagen fibrils. An animal induced lathyrism model has shown that affected individuals have a significantly decreased maximal force to failure and energy to failure of the lumbar vertebrae compared to unaffected controls. (Paschalis 2011).

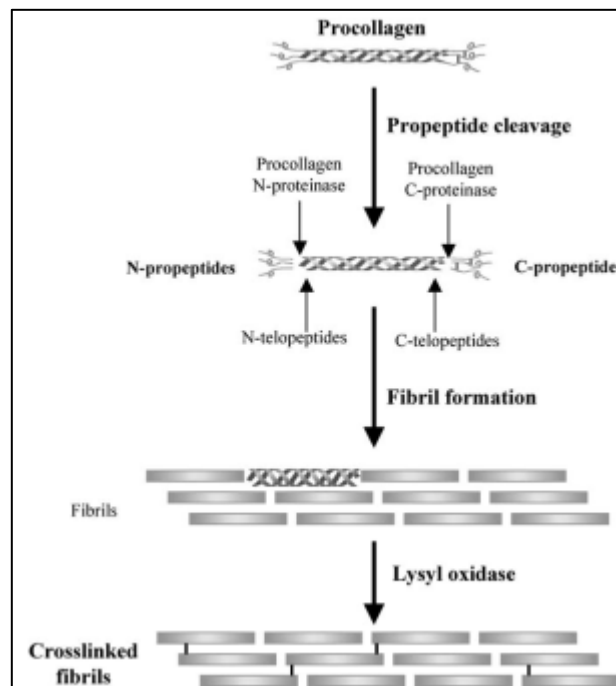


Figure 1. The synthesis and macroscopic structure of collagen fibrils. Adapted from Viguet-Carrin et al., 2006.

Small quantities of other collagen subtypes, namely types V and XII also exist in the organic bone matrix. Other constituents include non-collagenous matrix proteins such as fibronectin, osteocalcin, osteonectin, osteopontin and bone sialoproteins. These matrix proteins are primarily involved in bone cell regulation and metabolism (Ramachandran 2017). Growth factors such as bone morphogenetic proteins and insulin-like growth factors have also been identified within the matrix.

A large body of evidence indicates that type I collagen molecules are important in influencing the mechanical properties of bone. Several studies have demonstrated that collagen matrix contributes to bone toughness (Boskey 1999, Wang 2001, Zioupos 1999). Furthermore, the importance of Type I collagen to the mechanical properties of bone are highlighted in clinical disorders associated with bone collagen abnormalities. A mixture of normal and abnormal type I collagen is produced for example in patients with osteogenesis imperfecta. Mutations occur in the *COL1A1* and *COL1A2* genes which code for type I Collagen, the most common of which is a point mutation in the glycine residue. As a result, excessive brittleness of bone is observed.

Inorganic matrix

Within bone, collagen fibrils are stiffened by the integration of mineral. This is composed mainly of calcium phosphate crystals analogous to calcium hydroxyapatite ($\text{Ca}_{10}(\text{PO}_4)_6(\text{OH})_2$). Collagen molecules are precisely aligned within fibrils in a quarter-staggered end-overlap fashion (Figure 1). It is within these pores that the formation of calcium phosphate crystals occurs due to phase transformation of soluble calcium and phosphate. The inorganic matrix of bone serves to provide it with compressive strength and also acts as a reservoir for calcium and phosphate (Ramachandran 2017).

The inorganic matrix has the ability to influence mechanical properties within bone. The ratio of mineral to organic matrix increases

with age and this in turn is associated with a decrease in static toughness and impact strength of cortical bone in humans (Currey 1996). Calcium phosphate crystal chemical composition is also known to undergo changes with age particularly their carbonate and acid phosphate groups (Buckwalter 1995). Furthermore, in animal models the crystal size, calcium phosphate molar ratio and carbonate ion content of cortical bone have all been shown to increase with advancing age (Legros 1987).

Bone cells

The cells within bone carry out a diverse range of metabolic and homeostatic functions. They arise from two cell lines: a haematopoietic and a mesenchymal stem cell line.

Osteoblasts

Osteoblasts comprise roughly 4-6% of all bone cells and are largely known for their bone forming function. They arise from undifferentiated mesenchymal stem cells. Osteoblasts line the surfaces of bone and have great synthetic capacity. The expression of specific genes such as the synthesis of bone morphogenetic proteins and members of the wingless (Wnt) pathway are required to commit the stem cells down the osteoprogenitor lineage (Florencio-Silva 2015). The most apparent function of osteoblasts is to produce organic matrix of bone. This occurs in two-steps; the secretion of collagen type I and other non-collagen proteins (such as osteonectin, osteopontin and proteoglycans) and the subsequent mineralisation of bone matrix. Mature osteoblasts have three fates; 1. They may become inactive bone-lining cells or 2. They surround themselves with matrix and become osteocytes or 3. They disappear from the site of bone formation by apoptosis.

Osteocytes

Osteoblasts which have been surrounded by matrix and entrapped by calcified bone matrix are then known as osteocytes. They are by far the most abundant type of cell seen with bone (accounting for up to 90% of all bone cells). They possess long cytoplasmic processes which allow interaction with other bone cells. These are connected to the cytoplasmic processes of osteoblasts and bone lining cells on the bone surface, allowing the transport of small signalling molecules such as prostaglandins and nitric oxide (Civitelli 2002).

It has been postulated that via this vast network of intercellular connections, osteocytes have the capacity to detect mechanical loads and pressures and therefore act as mechanosensors (Rochefort 2010). Osteocytes are therefore important in the remodelling process of bone when subjected to mechanical stimuli. Bone is able to add bone matrix to improve resistance to increased loads while a decrease in this stimulus leads to resorption of bone. The mechanisms on how osteocytes are able to convert mechanical stimuli to biochemical signals are not well understood. A proposed idea on this function is that microdamage/microcrack formation secondary to loading is detected by osteocytes through either a change in pressure or via apoptosis through direct damage to osteocytes (Sims 2008). Indeed, mechanical loading in an ex-vivo human model is associated with increased osteocyte apoptosis and increased bone remodelling (Mann 2006). It is not known how osteocytes directly mediate or initiate bone remodelling, but they are known to produce chemical mediators such as nitric oxide and prostaglandins. The production of nitric oxide within bone is associated with the promotion of bone formation and the inhibition of bone resorption (Bakker 2001) and may also play a role in preventing osteocyte glucocorticoid-induced apoptosis (Bakker 2009).

Bone-lining cells

Osteoblasts act again as pre-cursors to this type of cell. They line the bony surface and also possess long cytoplasmic extensions that allow interaction with other bone cells such as osteocytes. Their function is not completely understood but they are thought to act as regulatory cells to osteoclasts. It has been shown that bone-lining cells prevent the direct interaction between osteoclasts and bone matrix when bone resorption is not desired (Andersen 2009). They are also thought to participate in osteoclast differentiation, producing Receptor activator of nuclear factor kappa-B ligand (RANKL) and osteoprotegerin (Moseley 2000).

Osteoclasts

Osteoclasts are multi-nucleated cells that arise from mononuclear cells from the haematopoietic bone cell lineage and are found in the bone marrow and circulating blood. Osteoclast genesis is regulated by the RANKL/RANK/OPG system (Florencio-Silva 2015). RANKL is produced by osteoblasts and osteocytes amongst other cell types. When bound to its receptor RANK in osteoclast precursors, osteoclast genesis is stimulated resulting in the fusion of osteoclast precursors to form multi-nucleated osteoclasts. Osteoprotegerin (OPG) on the other hand is an inhibitor of osteoclast formation, binding to RANK, thereby preventing the RANKL/RANK interaction on osteoclast precursor cells.

The main role of the osteoclast is to resorb bone. They achieve this by employing proton pumps to lower the pH within their resorption lacunae to enable dissolution of hydroxyapatite crystals (Crockett 2011). Remaining organic matrix is degraded via secreted proteases and also directly by osteoclast phagocytosis.

There is evidence that osteoclasts are not just bone-resorbing cells. They may regulate haematopoietic stem cells as well as

producing chemical mediators known as clastokines which regulate osteoblasts during bone remodelling (Charles 2014).

Bone Remodelling

Bone is a dynamic tissue that is constantly formed and resorbed in response to changes in mechanical loading, altered serum calcium levels and in response to a wide range of paracrine and endocrine factors. This is a highly complex process achieved by the combined efforts of osteoclasts, osteoblasts, osteocytes and bone-lining cells. Collectively they are often referred to as a basic multicellular unit or BMU (Florencio-Silva 2015, Sims 2008).

The bone remodelling cycle begins with an initiation phase which involves osteoclast formation and bone resorption mediated by osteoclasts. Following a transition or reversal phase, bone formation occurs via osteoblasts. The cycle is then completed by osteocytes and bone-lining cells (Sims 2008).

Mechanical loading has a profound effect on bone remodelling (Robling 2006). Wolff's law which was developed by the German anatomist Julius Wolff in the 19th century was based on such observations and states that bone in a healthy person or animal will adapt to the loads under which it is placed. Lack of loading causes increased bone turnover with bone resorption outweighing bone formation. This is evidenced by the loss of bone mass in astronauts, which occurs as a result of spending time in weightless environments. Conversely with regular loading, bone will remodel itself to become stronger in order to resist loading. A good example of this is shown by Robling et al., whereby a rat ulna was axially loaded for 3 minutes/day, 3 days/week for a total of 16 weeks. This resulted in new bone formation, an increase in strength by 64% and an increase in the energy required to fracture the bone (Figure 2).

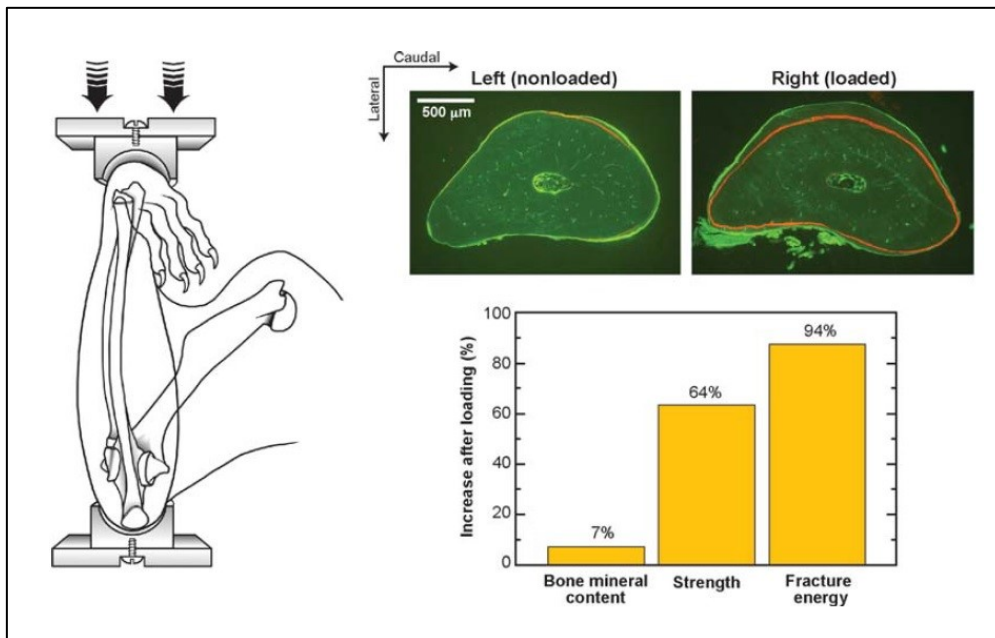


Figure 2. Mammalian Bone remodelling in response to repetitive loading. Adapted from Robling et al., 2006. Repeated axial loading of the rat ulna leads to an increase in bone formation and altered mechanical properties. The red outline of bone represents pre-loading.

1.1.2 Structure of Bone

Woven and Lamellar Bone

Above the level of the collagen fibril and its associated mineral phase, mammalian bone exists in two distinct forms:-woven and lamellar bone. Woven bone is found in the embryonic skeleton and within callous formation during fracture healing while mature lamellar bone forms the structural component of cortical and cancellous bone. These two types of bone differ in their formation, organization and mechanical properties. Woven bone is rapidly deposited at rates of up to 4 μm a day and has a high turnover. Several differences exist between the two types of bone. Woven bone contains 4 times as many osteocytes per unit volume and such cells vary in size and distribution. The collagen fibrils in woven bone appear to be aligned randomly and are not of uniform thickness-0.1–3 μm (Currey 2002). Mineralisation of woven bone appears to follow an irregular pattern i.e. mineral deposits vary in size and relationship to the collagen fibrils

(Buckwalter 1995). In contrast, collagen within lamellar bone vary less in size and are highly organised into parallel sheets with uniform distribution of mineral within them. The osteocytes within lamellar bone are also more of a uniform size and are orientated with other cells and collagen fibrils (Weiner 1998). As a result of these differences, woven bone is more flexible and weaker than lamellar bone (Webster 2001). The difference in orientation of collagen fibrils also accounts for woven bone displaying isotropic properties i.e. the material properties of woven bone are not affected by the direction of load whereas lamellar bone displays anisotropic properties i.e. its material properties are dependent on the direction of load.

Cortical and cancellous bone

Macroscopically, bone can be divided into cortical bone which has a higher density and cancellous bone which is more porous. Cortical bone comprises roughly 80% of the adult skeleton and is found predominantly in the diaphyseal region enveloping bone marrow and cancellous bone plates. Cortical bone is organized into units termed osteons or Haversian systems (Figure 3).

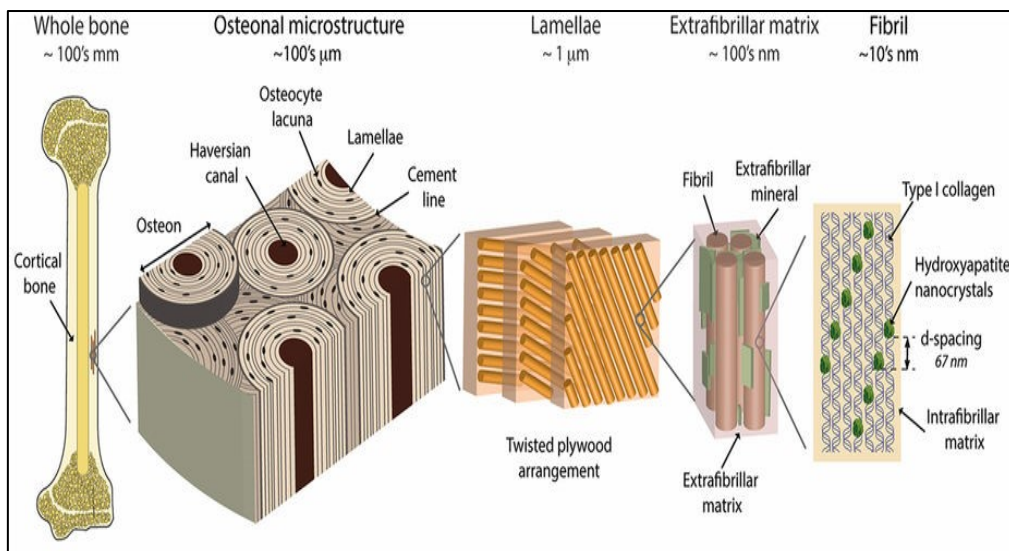


Figure 3. Cortical bone Micro-structure. Adapted from Zimmerman et al., 2016. The structure of cortical bone is shown at different microscopic levels.

In the centre of each Osteon, a Haversian canal exists which is lined by loose connective tissue and contains a blood vessel. Each canal is surrounded by lamellae of collagen fibres. Osteons are connected to each other and the bone marrow cavity by a structure known as Volkmann's canal.

Cancellous bone is found mainly in the metaphyses and epiphyses of long bones. Cancellous bone consists of a series of interconnecting rods and plates (~200µm thick) known as trabeculae. As cancellous bone predominates within the marrow cavity, cancellous bone by itself does not act as an efficient weight-bearing structure. It is however highly connected via trabeculae and is able to funnel the stresses imposed on it to stronger cortical bone (Burr 2003). The architecture of cancellous bone can be characterised by the thickness and number of trabeculae. The same volume of bone can present with different mechanical properties based on differences in this architecture. For example, cancellous bone segments with the same bone mass but with differences in the number inter-connecting trabeculae and architecture are able to support different loads (Figure 4).

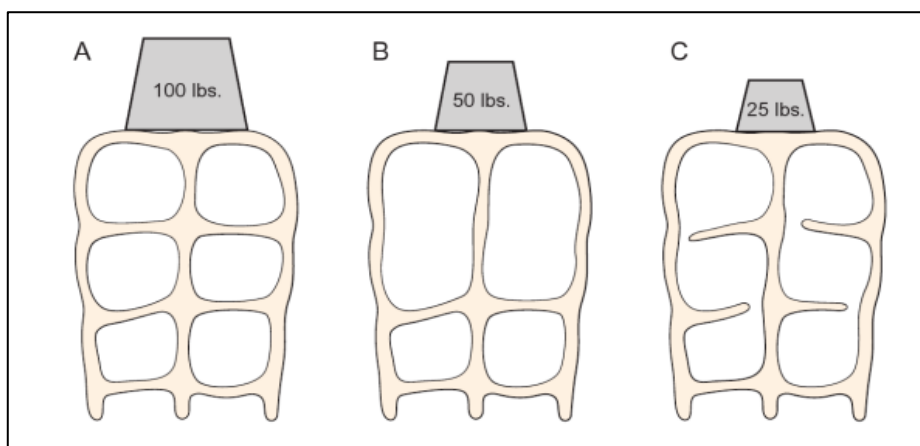


Figure 4. Illustration of how cancellous bone with the same mass but different architecture is able to support different loads. Adapted from Burr, 2013. A shows cancellous bone with a high number of interconnecting trabeculae, B shows the same bone with a reduced number of trabeculae and C shows cancellous bone with incomplete trabeculae.

1.1.3 Mechanical Properties of Bone

The mechanical properties of bone are determined by the relative amounts of its 3 major constituents; (organic matrix, mineral and water), the quality of these components and also how the resulting bone is arranged in space. A stress-strain curve (Figure 5) can be used to summarise such properties and allows bone to be compared with other materials. Stress is defined as the force per unit area applied while strain is defined as the change in length with respect to the original length of the material. The modulus of elasticity or Young's modulus refers to how stiff a material is i.e. the ability of a material to resist deformation against a load. The greater the modulus of elasticity or the steeper the stress-strain curve (within the linear elastic portion), the stiffer the material.

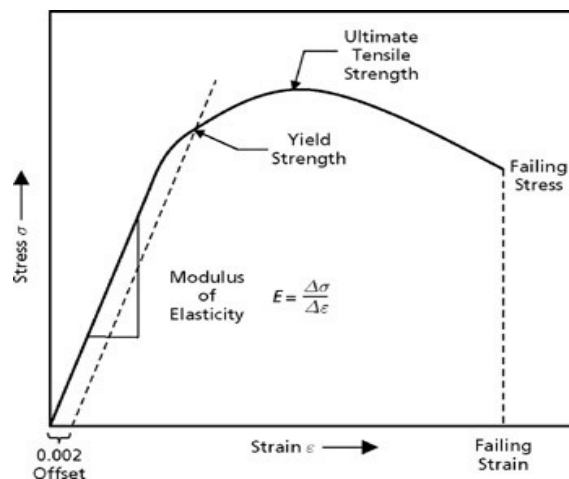


Figure 5. A stress-strain curve with important values shown. Adapted from <http://www.globalspec.com/reference/37452/203279/appendix-c-mechanical-and-environmental-properties>. Last accessed on 5th March 2018.

Cortical bone typically has a Young's modulus in the order of 12-24 GPa compared to cancellous bone which has a Young's modulus of 0.005-1.5 (Ramachandran 2017).

The yield strength refers to how much energy a material can absorb before undergoing irreversible change, while the ultimate tensile strength is the point at which a material fails and is a measure of its toughness.

The mineral phase of bone provides the material with stiffness (Viguet-Carrin 2006). Increasing the mineral component of bone leads to a significant rise in the Young's modulus. An increase from 200 mg calcium/g dry bone to 260 mg/g produces an increase in Young's modulus from about 5 GPa to 25 GPa (Currey 2003).

The organic phase of bone however contributes differently to the material properties of bone. This is shown by in vitro studies showing that ionizing radiation which damages bone collagen results in decreased bone toughness without modification of the Young's modulus (Currey 1997, 2003). The organic phase also contributes to the anisotropic properties of bone i.e. bone responds differently to forces depending on the direction of load. For example, the femur is capable of resisting significant axial load with no significant damage. In contrast, the same load applied transversally to the femur may result in fracture. This anisotropic behaviour is due to the orientation of collagen fibres. Martin et al (1998) reported that longitudinal fibres are found in regions supporting tensile loads, and transverse fibres correspond to regions under compressive loading.

The organic phase also allows bone to display visco-elastic properties i.e. it exhibits time-dependant properties. Bone therefore undergoes creep (time dependant deformation under a constant load), stress relaxation (a time-dependent decrease in load to maintain a constant strain) and hysteresis, which refers to a differing stress-strain curve during loading and unloading of bone.

1.2 Osteoarthritis

Osteoarthritis is a common disorder of synovial joints. It is associated with articular cartilage damage, new bone formation at joint margins (osteophyte formation), subchondral bone changes and variable degrees of synovitis (Abramson 2009, Egloff 2012). The physical impairment caused by a single osteoarthritic lower limb joint is thought to be comparable to that of a major life-altering disorder

such as end-stage kidney disease or heart failure (Saltzman 2006). At present there is no intervention that has been proven to prevent the development and progression of osteoarthritis. This condition is one of the most common causes of disability in the world. Epidemiological studies estimate that up to 15% of the world's population are currently affected (Egloff 2012). In the UK alone, 8.75 Million people have sought treatment for the condition (ARUK 2013). Osteoarthritis is associated with mobility impairment greater than due to any other medical condition in people over the age of 65 years (Guccione 1994) and often leads to social, psychological and economical burdens in patients with substantial financial consequences (Gupta 2005). In France for example, the health costs resulting from OA has almost doubled within a 10 year period (1993-2003) (Solignac 2004). The incidence of osteoarthritis is expected to increase due to a global increasing life expectancy as well as the increasing prevalence of obesity (Arias 2004).

Articular cartilage structure and function

Hyaline cartilage coats the articular surfaces within synovial joints and functions to reduce friction and distribute the weight-bearing forces within a joint. As such, it has a protective function to the underlying bone. It is a highly specialised type of connective tissue, comprising of chondrocytes within an extracellular matrix (ECM). Constituents of ECM include water (roughly 75%), Collagen (predominantly type II), proteoglycans and glycosaminoglycans (which are responsible for the water content) and a wide range of other glycoproteins and metalloproteinases.

The chondrocyte is the only cell type residing within the adult cartilage matrix. It survives under relatively hypoxic conditions and has low metabolic activity. This cell is ultimately responsible for remodelling and maintaining the structural and functional integrity of the cartilage matrix, however it possesses little regenerative capacity

(Goldring 2007). Chondrocytes have receptors for responding to mechanical stimulation and are able to react to direct biomechanical stimuli by upregulating synthetic activity or by increasing the production of inflammatory cytokines (Goldring 2007, Millward-Sadler and Salter, 2004).

Histologically, articular cartilage can be divided up into different layers (Figure 6). The superficial zone is the thinnest layer. It separates the cartilage from the synovial fluid and acts as a barrier to the passage of large molecules from the synovial fluid. The collagen fibres lie parallel to the articular surface and so-doing allow the articular surface to resist shear forces. In the middle zone, the fibres lie obliquely and act as a transition between the superficial and deep zones. The deep or radial zone forms the largest part of articular cartilage and has collagen fibres arrange perpendicular to the articular surface. This arrangement allows the cartilage to distribute load and resist compression (Ramachandran 2017). The tidemark lies beneath this and separates calcified and un-calcified cartilage.

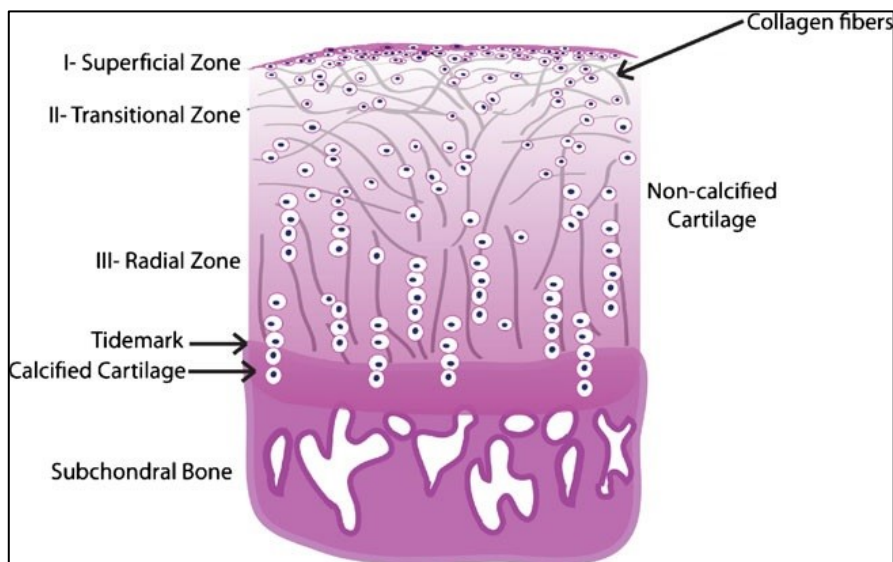


Figure 6. An illustration of the different articular cartilage zones. Adapted from Gadjanski et al., 2011.

Although osteoarthritis is characterised by articular cartilage loss and joint space narrowing, it is now widely accepted that it is a

disease of the whole joint. This includes subchondral bone changes as well as synovial inflammation. At present there is no recognised treatment to reverse osteoarthritic change i.e. articular cartilage damage. Treatment currently consists of symptomatic treatment for mild to moderate cases and surgical intervention for patients who have failed conservative measures, normally in the form of joint replacement surgery or joint fusion. There is also no current method that we can employ to detect sub-clinical patients that are going to go on and develop symptomatic osteoarthritic change. This would represent an important diagnostic achievement as this would allow the study of potential interventions on the development of osteoarthritis.

1.2.1 Macroscopic classification of OA

The Outerbridge classification system was first used to describe changes associated with chondromalacia patellae (Outerbridge 1961). However, it is also commonly used to describe macroscopic osteoarthritic change within the knee and the principles of the grading system can be applied to most joint surfaces coated by articular cartilage in the body:

Grade :	I	Softening and swelling of articular cartilage
	II	Fragmentation and fissuring of articular cartilage affecting an area of less than 0.5 inches
	III	Fragmentation and fissuring of articular cartilage affecting an area greater than 0.5 inches
	IV	Cartilage erosion to bone

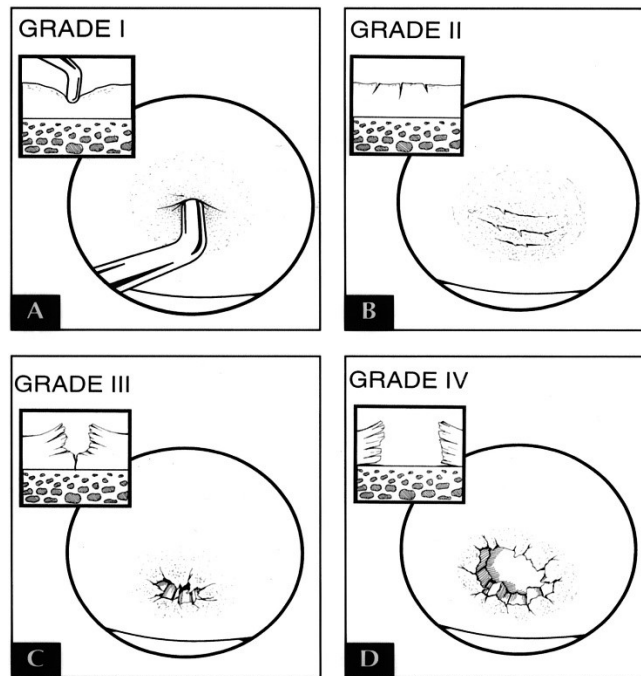


Figure 7. Illustration of the Outerbridge Classification for chondromalacia patellae. Adapted from Parker, RD. 2005.

1.2.2 Pathogenesis of Osteoarthritis

The pathogenesis of OA is complex and incompletely understood (Guilak 2011, Egloff 2012). It may be primary in origin where it occurs without an obvious identifiable cause or secondary to a traumatic event or separate disease process affecting the joint. Risk factors for OA can act as initiators that promote abnormal biochemical processes involving the joint synovium, bone or cartilage, which over a period of time can result in the development of osteoarthritis.

1.2.2.1 Risk factors for Osteoarthritis

Genetic Predisposition

A genetic contribution has been suggested in several epidemiological studies, twin studies and analysis of patterns of familial clustering (Loughlin 2002, Abramson 2009). Such studies have indicated that concordance for OA between monozygotic twins is

significantly higher than for dizygotic twins (Zhai 2007). Candidate gene studies have also revealed polymorphisms or mutations in genes encoding extracellular matrix and signalling molecules that may determine susceptibility to osteoarthritis (Loughlin 2005, Valdes 2007).

The precise genetic contribution to the pathogenesis of osteoarthritis has, however been difficult to determine given the extensive clinical heterogeneity of the condition (Abramson 2009).

Age

Age is significantly correlated with the development of osteoarthritis (Martin 2002). Chondrocytes, the native cells within articular cartilage become more predisposed to apoptosis with age (Todd 2004, Robertson 2006) and may also become less functional. A decrease in the synthetic activity of chondrocytes and a decreased responsiveness to growth factors has been associated with advancing age (Martin 2002).

Furthermore, an increase in joint mechanical stress may arise due to muscle weakness, altered gait, increase in body-weight and changes to proprioception with age (Abramson 2009).

Obesity

The joints of the body are subjected to millions of cycles of loading and under normal physiological conditions, there is no resulting adverse effect on the articular cartilage and surrounding tissues. In fact, biomechanical loading is required to facilitate one of the functions of synovial fluid i.e. to provide nutrition to the articular cartilage. Normal joint motion is also linked to the induction of a potent anti-inflammatory cytokine (Interleukin-10) (Helmark 2010). However, abnormal loading to joints is linked to the development of osteoarthritis.

Obesity is strongly associated with an increased risk of osteoarthritis (Oliviera 2010). This is believed to be due to an increase

in the mechanical forces around weight-bearing joints (Leach 1973). There is evidence that abnormal loading may alter the structure, metabolism and mechanical properties of articular cartilage. Increased chondrocyte apoptosis, damage to the ECM and tissue disruption have been observed in excessive loading (Guilak 2011). Furthermore, mechanical stress has been shown to directly influence the inflammatory cascade of chondrocytes to induce or inhibit the production of pro or anti-inflammatory cytokines (Lee 2003).

Adipocytes have also been implicated in the development and progression of osteoarthritis by regulating chondrocyte metabolism. Adipocyte derived factors such as C-reactive protein and Interleukin-6 appear to be catabolic stimulators for chondrocytes. Furthermore, leptin (an adipose-derived hormone) has been found to be present within the synovial fluid of osteoarthritic human knees with levels correlated with body-mass index and the grade of cartilage destruction (Dumond 2003).

1.2.2.2 Pathobiology of osteoarthritis

The chondrocyte and OA

The adult chondrocyte is believed to play a critical role in the pathogenesis of OA in responding to adverse environmental stimuli by promoting matrix degradation and downregulating processes essential for cartilage repair. In early osteoarthritis, there is evidence of increased chondrocyte synthetic activity (Goldring 2007).

Chondrocytes express several chemokines, as well as chemokine receptors that could participate in the induction of cartilage catabolism (Borzi 2004).

It is also believed that chondrocytes act as mechano-sensors, altering their metabolism in response to changes in their micro environment (Abramson 2007). In response to changes in mechanical stress, increases in levels of pro-inflammatory cytokines and matrix-

degrading enzymes has been noted as well as changes to gene expression (Fermor 2001).

Articular cartilage damage

Osteoarthritis is characterised by the loss of articular cartilage matrix, of which the degradation by proteolytic enzymes such as matrix metalloproteinases, plays a significant role (Tetlow 2001). The expression of matrix metalloproteinase 13 (MMP-13) has been shown to be greatly increased in osteoarthritis (Tetlow 2001). Furthermore, it is believed that mechanical stress can induce metalloproteinase production via transcription factors (Kawaguchi 2008).

Role of inflammation in OA

OA is not considered a classical inflammatory arthropathy, due to the absence of neutrophils in the synovial fluid and the lack of systemic manifestations of inflammation. Localised joint inflammation involving infiltration of B cells and T-lymphocytes however, is a well-recognised feature of many cases of early and late osteoarthritis (Benito 2005). This may be idiopathic in OA or be triggered by trauma, infection, overuse or crystal deposition (Egloff 2012). Synovial inflammation is a factor that likely contributes to dysregulation of chondrocyte function, favouring an imbalance between the catabolic and anabolic activities of the chondrocyte in remodelling the cartilage ECM (Loeser, 2006). Synovitis within the joint can lead to the production and release of pro-inflammatory cytokines such as TNF-alpha and interleukin-1. This can lead to the induction of metalloproteinases with subsequent cartilage degradation. Interestingly, movement of knee joints is known to stimulate the formation of interleukin-10, an anti-inflammatory cytokine (Helmark 2010). This suggests an interruption in inflammatory resolution as well as inflammatory induction in the pathogenesis of osteoarthritis.

Evidence from the literature also suggests overlap between abnormal mechanical loading and inflammation in the pathogenesis of osteoarthritis. Abnormal loading leads to proteoglycan depletion, collagen destruction and cartilage degradation (Oliviero 2010). In response, pro-inflammatory products are released that are postulated to lead to synovitis and joint damage secondary to inflammation.

1.2.3 Role of Subchondral bone

Subchondral bone Structure and Normal Function

Subchondral sclerosis and loss of articular cartilage are widely regarded as the hallmark of osteoarthritis. The evidence that subchondral bone plays a crucial role in the initiation and progression of osteoarthritis is growing (Li 2013, Castenada 2012, Henrotin 2012). There is however no universally agreed definition of subchondral bone. The most often used definition refers to bone lying immediately deep to the calcified zone of articular cartilage (Madry 2010, Li 2013). With this definition in mind, subchondral bone consists of the subchondral bone plate and the subarticular spongiosa (Figure 8). The “cement line” therefore, demarcates the border between articular cartilage and subchondral bone. The thickness of subchondral bone varies between different joints and also within different parts of the same joint. This appears to correlate to contact stresses with thicker subchondral bone observed in the center of the tibial plateau compared to the periphery (Madry 2010).

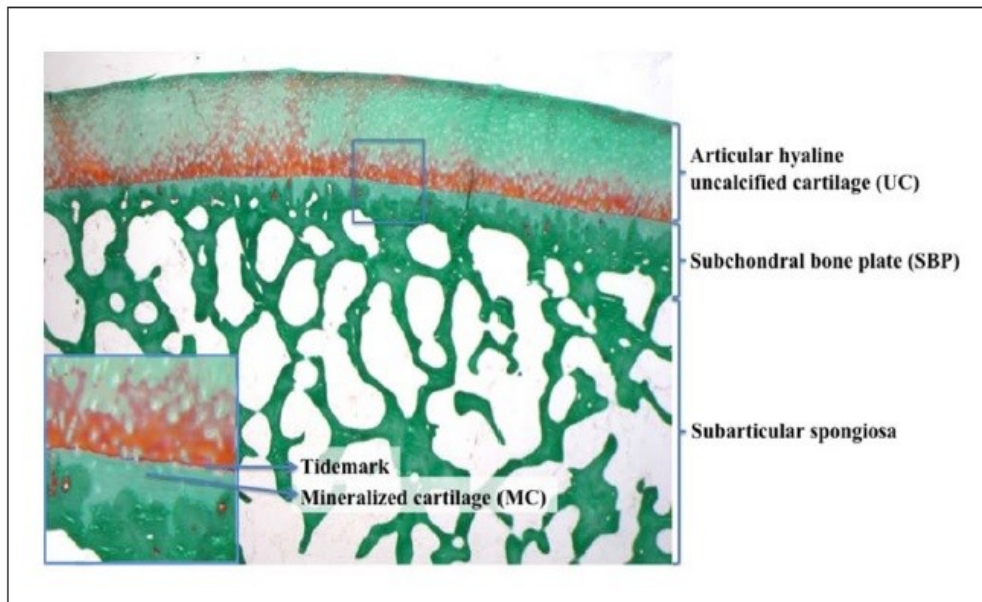


Figure 8. Subchondral bone schematic showing the different layers. Adapted from Buettner et al., 2013

Subchondral bone is recognised as a key factor in normal joint protection. It has been shown to exert shock-absorbing qualities and can attenuate 30% of the joint load (Imhoff 2000). Subchondral bone is also thought to play a vital role in nutrient supply and removal of metabolic waste products from articular cartilage.

The subchondral bone plate is highly porous and contains a number of channels that provide a direct link between the articular cartilage and the subchondral bone. It is traversed by a number of arteries, veins and nerves (Li 2013). The subchondral bone and articular cartilage are therefore regarded as a single functional unit by several authors (Castenada 2012, Imhoff 2000).

The role of subchondral bone in OA pathogenesis

Imaging techniques have revealed many structural changes in the subchondral bone of osteoarthritic joints. These include thickening of the calcified cartilage, tidemark duplication, subchondral sclerosis, subchondral cyst formation, bone marrow oedema like lesions and microdamage. It is widely accepted that subchondral bone changes are intimately linked in the osteoarthritic process but whether changes

in the subchondral bone initiate the development of OA or whether they are a consequence of OA remains highly debated. Animal models suggest that osteoarthritic change can be initiated by interruption in the subchondral bone. Malinin and Ouellette (2000) compared the effect of implanting osteochondral autografts into well vascularised cancellous bone wells with one separated from the underlying cancellous bone with a layer of methylmethacrylate. In this model with no contact between the cancellous bone and the osteochondral autograft, they were able to induce osteoarthritic change after 3 years. Muraoka et al., observed the subchondral bone in two different strains of guinea pig, one of which was prone to development of osteoarthritis. In the subchondral bone of the tibial plateau they observed bone formation in the subchondral region prior to the onset of cartilage degeneration. More recently alterations of Subchondral Bone Progenitor Cells in human knee and Hip OA have been found to lead to a bone sclerosis phenotype (Bianco 2018) suggesting that subchondral bone changes can initiate the disease process.

The potential role of subchondral bone in the initiation and progression of osteoarthritis was first proposed by Radin and Rose (Radin 1986). They proposed that alterations in the stiffness of subchondral bone may decrease its viscoelastic properties and produce a loss of its shock-absorbing ability. This in turn is postulated to cause extra mechanical load and damage to the overlying cartilage (Radin 1986). These findings were demonstrated in aged cynomolgus monkeys where cartilage damage in the medial compartment of the knee was related to sclerosis of the tibial plateau (Carlson 1996).

Increased subchondral bone turnover has been described in osteoarthritis by several studies using a variety of techniques (Kadri 2008, Dieppe 1993, Bettica 2002). These include biomarkers such as alkaline phosphatase and osteocalcin (markers of bone formation), TRAP, CTX-1 (markers of bone resorption), bone isotopic scintigraphy and imaging techniques such as magnetic resonance imaging (MRI) used to assess the bone microarchitecture. As a consequence of

increased turnover, greater levels of collagen synthesis, increased immature crosslinks between collagen fibres and collagen degradation has been observed (Bailey 2002). Interestingly, the subchondral bone in osteoarthritis is found to be hypomineralised (Grypnas 1991, Cucchiarini 2016). This is believed to be a result of an overproduction of the homotrimeric form (3 α -1 chains) of collagen as opposed to the normal (2 α -1 and 1 α -2 chains) form of collagen produced by osteoblasts with an altered phenotype (Mansell 1998, Bailey 2002, Couchourel 2009). A possible explanation is that increased levels of the homotrimeric form of type I collagen are not as readily mineralised as the classic form of collagen (Cucchiarini 2016). Furthermore, subchondral bone with this abnormal form of collagen type I is noted to have a reduced Young's modulus which may contribute to further cartilage degeneration (Li 2013).

The relevance of increased subchondral bone turnover and osteoarthritis appears to be related to the possible effect on the overlying articular cartilage. There appears to be close biological communication between the osteoblasts and osteoclasts in subchondral bone and the chondrocytes present in overlying articular cartilage (Castenada 2012, Lejueunesse 2003). Furthermore, it has been shown that subchondral bone cells can influence cartilage metabolism (Westacott 1997). It has been postulated that various cytokines, growth factors and prostaglandins produced by cells within the subchondral bone such as osteoblasts move through the subchondral bone-cartilage interface and promote cartilage breakdown (Castenada 2012).

Micro-damage of the subchondral bone can arise from overloading (Vener 1992). Micro-damage of the subchondral bone has been implicated in the initiation and progression of osteoarthritis (Li 2013, Burr 2003, Madry 2010). Microcracks, which arise as a result from damage may act as a focus for bone remodelling and may provide a further conduit between the joint space and the articular cartilage and subchondral bone. This process results in the influx of synovial fluid and the formation of pseudocysts. The relevance of

subchondral bone cysts on the osteoarthritic process is not entirely understood but their presence is shown to be associated with high bone turnover. The location of pseudocyst formation also appears to correspond to areas of high cartilage loss (Li 2013, Tamasas 2010). Activated osteoblasts, new bone formation and osteoclastic bone resorption have been detected around subchondral bone cysts (Sakobar 2000, Li 2013). The increased bone turnover may lead to the thickening of subchondral plates and calcified cartilage which eventually leads to thinning of articular cartilage (Kawcak 2001).

1.3 The Ankle joint

1.3.1 Anatomy and biomechanics of the Ankle Joint

The ankle joint complex is comprised of the lower leg and the foot. It forms a kinetic linkage allowing the lower limb to interact with the ground, a vital requirement for gait. The foot and ankle are made up of twenty-six bones and form a total of thirty-three joints (Brockett 2016). Motion at the foot is complex, with dorsiflexion and plantar flexion primarily occurring at the tibio-talar joint and inversion and eversion at the sub-talar joint.

The ankle or tibio-talar joint forms the junction between the distal tibia and fibula of the lower leg and the talus (Figure 9). Stability to the joint arises from joint congruence and stabilising ligaments, namely the medial deltoid ligaments, the lateral ligament complex and the syndesmotic complex. The joint is essentially a uniplanar hinge joint with movement occurring about a transverse axis joining the tips of the medial and lateral malleoli. The axis is oblique by roughly 10 degrees. As a result, during dorsiflexion of the ankle, the forefoot moves laterally and medially with plantarflexion (Ramachandran 2017).

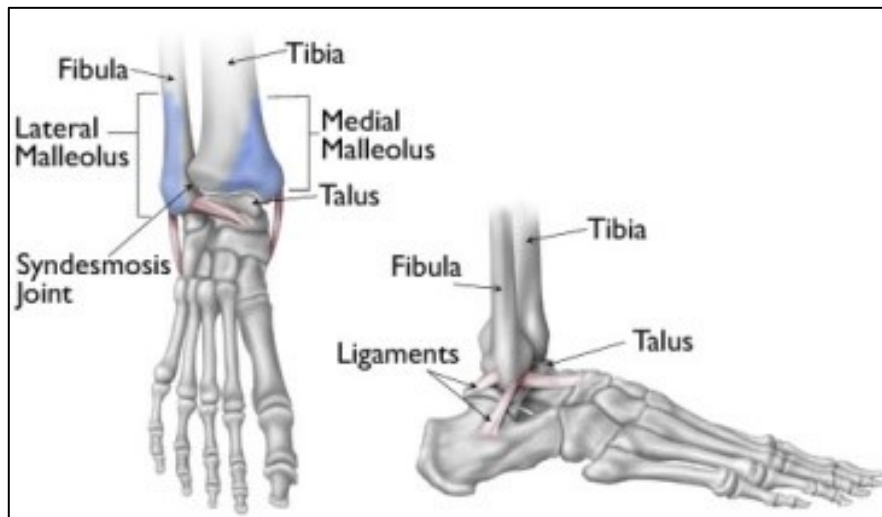


Figure 9. Illustrations of the ankle joint and supporting ligaments
 Adapted from <https://orthoinfo.aaos.org/en/diseases--conditions/ankle-fractures-broken-ankle/> Last accessed online: 3rd March 2017.

The ankle joint experiences higher forces than other major joints in the body. During stance phase, the ankle joint experiences stress in the magnitude of 5-7 times bodyweight compared to the knee which experience forces in the magnitude of 3-4 times (Michaels 2008). The articular surface area of the ankle joint is equivalent to the hip and knee joints. However, under load the area of articular surface contact is much smaller. With 500N of load, the hip joint has a contact area of 1100mm² compared to 350mm² at the ankle (Daniels 2008). During the normal gait cycle, the pressure distribution and contact area of the ankle joint change. The contact area on the talus is largest with the ankle joint in neutral or dorsiflexion which accounts for 50% of the stance phase (Deland 2000). This contact area decreases in the order of 13-18% with the ankle in plantar-flexion (Calhoun 1994). This normal change in pressure distribution is hypothesised to have a beneficial impact on cartilage nutrition and lubrication (Huch 1997).

Variation by location in the thickness of the articular cartilage has been noted in the non-pathological ankle joint. The articular cartilage has been found to be thickest at the mid and posterior talar dome as well as the tibial plafond and lowest in the anterior portion of the talus. (Buettner 2013). Interestingly, the thickness of the articular

cartilage appears to be inversely correlated to stiffness. This has been verified by cartilage indentation stiffness measurement (Buettner 2013).

Several differences exist in the cartilage of the ankle joint compared to other major joints in the body such as the knee and hip joints. Shepherd and Seedhom (1999) studied the articular cartilage in the joints of the lower limb. They found the cartilage in the ankle joint to be the thinnest and also the most uniform (ankle cartilage with thickness ranging from 1mm to 1.7mm in specimens examined) compared to the knee with thickness ranging from 1mm to 6mms. They also found that thin articular cartilage had a high compressive modulus and proposed that the thickness of articular cartilage was related to the congruence of a joint. A model has been proposed by Wynarsky and Greenwald (1983) as to how the ankle is able to cope with such high loads. They were able to demonstrate a change in congruence of the ankle joint with load and that as pressure was increased, the load-bearing area increased significantly. This increased congruence allows the resulting applied forces to be distributed over a larger area. There is also evidence to suggest that the articular cartilage found in the ankle is more resilient compared to the hip with age. Kempson et al., 1991 studied the effects of ageing on the normal mechanical properties of normal intact cartilage in the hip and ankle joints. He observed that the tensile strength of cartilage from the femoral head decreased significantly with age while the tensile strength from the talus decreased significantly less.

The thickness of subchondral bone within the ankle joint also appears to vary by location. In a cadaveric study, Buettner et al., 2013 found that the subchondral bone plate was thickest anteromedially in the talus and lowest in the posterolateral portion of this bone. With regards to the tibial plafond, the subchondral bone plate thickness was observed to be homogenous but with augmentation in the posteromedial portion of the tibia.

1.3.2 Ankle osteoarthritis

Osteoarthritis of the ankle is a debilitating disease which causes pain, dysfunction and immobility in patients. An estimated 1% of the world's population is said to be affected by ankle OA (Barg 2013) and at least 29,000 symptomatic cases are referred to foot and ankle surgeons in the UK alone (Goldberg 2012).

Compared to hip or knee osteoarthritis, primary ankle OA is relatively less common and the joint appears far less susceptible to degenerative processes such as osteoarthritis (Barg 2013, Brockett 2016). This may be due to the differences in joint stability or to the cartilage in the respective joints as outlined in section 1.3.1. There are many epidemiological and clinical studies which have helped to identify previous trauma as the most common aetiological factor for ankle OA. Saltzman et al., 2005 conducted analysed a consecutive series of 639 patients with end-stage ankle OA presenting to a tertiary referral centre, 445 (70%) were post-traumatic, 76 (12%) were rheumatoid disease and 46 (7%) were idiopathic (primary osteoarthritis). This trend was echoed by Valderrabano et al., 2009 who evaluated the cause of OA in a cohort of 390 patients with ankle OA. 78% of these patients presented with post-traumatic OA. Of these patients, ankle fracture was the most common previous trauma, affecting 156 patients of their cohort, whilst proven ligamentous injury affected 60 patients. Primary Ankle OA accounted for only 7.7% of the aetiology for their cohort. Previous trauma appears to be the biggest single risk factor in the development of ankle osteoarthritis. Ankle osteoarthritis may present with normal alignment or may be associated with a varus or valgus deformity in the coronal plane. A varus deformity appears to be the most common, accounting for 55% of all patients in a cohort study including patients with primary OA, post-traumatic and secondary ankle OA. (Valderrabano 2009). This predominance of varus ankle OA may be explained biomechanically. A kinematic study looking at ankles with lateral ligament injury found that such ankles abnormally pronate and rotate externally at the time

of heel strike and abnormally supinate and rotate internally during the acceleration phase (Hashimoto 1997). It is postulated that these changes in ankle mechanics, due to lateral ligament injury and ankle instability as well as peroneal muscle dysfunction may lead to repetitive cartilage damage of the medial ankle and may support the development of varus ankle OA (Valderrabano 2009).

Ankle OA with valgus malalignment is less common than varus ankle OA or ankle OA with a balanced or symmetrical alignment (Valderrabano 2009). The aetiology of ankle OA with valgus malalignment has been linked to distal tibial malunions, shortening fibula malunions, medial ankle ligament instability, hindfoot coalitions, posterior tibial tendon insufficiency and posttraumatic valgus sequelae of the hindfoot (Barg 2013). Ankle OA can be classified according to radiological severity. A system was first proposed by Takakura et al., in 1995 based on weight-bearing radiographs (Table 1)

Stage	Radiographic Osteoarthritis Signs
1	No joint-space narrowing, but early sclerosis and osteophyte formation
2	Narrowing of the joint space medially
3	Obliteration of the joint space with subchondral bone contact medially
4	Obliteration of the whole joint space with complete bone contact

Table 1. Radiographical classification of ankle osteoarthritis. Adapted from Takakura Y, et al., 1995.

Giannini et al., 2007 also suggested a radiological classification of ankle osteoarthritis (Table 2). It is similar to that proposed by Takakura et al., and is based on radiographic evaluation of degenerative changes of the tibiotalar joint (e.g., presence of osteophytes or narrowing of joint space). However, it does not assume that wear in the ankle joint occurs medially in the first instance.

Stage	Radiographic Osteoarthritis Signs
0	Normal joint or subchondral sclerosis
1	Presence of osteophytes without joint-space narrowing
2	Joint-space narrowing with or without osteophytes
3	Subtotal or total disappearance or deformation of joint space

Table 2. Ankle osteoarthritis classification system (as suggested by Giannini and colleagues). Adapted from Giannini S et al., 1997.

Post-traumatic Ankle OA

Traumatic injuries include ligamentous injuries around the ankle and fractures of the tibial plafond, the medial and lateral malleoli and talus as well as isolated osteochondral fractures of the talar dome. Post-traumatic OA is thought to develop in the ankle due to two main mechanisms. This may arise from irreversible cartilage damage at the time of injury or chronic cartilage overloading due to ligamentous instability; eventually predisposing to the onset of osteoarthritis.

Ankle fractures and ankle sprains are often associated with osteochondral lesions. Stufkens et al., 2010 performed a long-term prospective cohort study on patients who had sustained an ankle fracture. All patients underwent ankle arthroscopy and cartilage damage seen during this assessment after the injury was found to be a risk factor for the development of osteoarthritis. The idea that irreversible cartilage damage is sustained at the time of injury was further supported by a cadaveric study conducted by Tochigi et al., 2011. They harvested normal human ankle joints post amputation and subjected them to impaction forces to generate fractures of the tibial plafond and using live-dead assays were able to ascertain acute chondrocyte death which was progressive with time.

Chronic overloading of cartilage following trauma may arise due to joint incongruity and/or ankle instability. In a cadaveric study with a constrained ankle, Ramsey and Hamilton (1976) demonstrated that a 1-mm lateral talar shift of the ankle mortise reduced the ankle contact

area by 42%. Similarly, the anatomical reduction of a posterior malleolar fracture of the distal tibia appears to be important for the maintenance of the ankle joint contact area. It has been shown that the ankle joint contact area decreases in an inverse relationship to the size of the posterior malleolar fragment. A fragment spanning half the articular surface appears to decrease the ankle joint contact area by as much as 35% (Macko 1991).

Mckinley et al., 2008 have shown that incongruity in the distal tibia leads to a substantial rise in contact stresses in a cadaveric model. Furthermore, if an element of instability is added to the group with joint incongruity, contact stresses are increased further when compared to joint incongruity alone. A further cadaveric study aimed to recreate ankle joint instability by transection of the anterior talo-fibular ligament also revealed increases in joint contact stresses (Tochigi 2008).

Certainly not all ankle trauma leads to the onset of ankle osteoarthritis and the prevalence is estimated to be 14% from one study (Lindsjo 1985). The latency following a traumatic injury to the ankle and the onset of symptomatic ankle osteoarthritis appears to be highly variable. Of the limited studies available assessing this aspect, risk factors for the earlier development of ankle OA appear to be type of fracture/fracture reduction, complications arising during injury healing, age at the time of injury, body/mass index and varus malalignment of the hindfoot (Horisberger 2009, Lubbeke 2012).

Although trauma is strongly associated with the development of ankle OA, it's specific role in the pathoaetiology of osteoarthritis is not clear. The nature of trauma can vary widely within the ankle joint, from simple ankle sprains to complex fracture-dislocations. The reasons why some people who experience trauma to an ankle go on to develop osteoarthritis whilst others do not are unknown. The studies that reported the incidence of ankle OA due to trauma also do not report whether such patients have other pathologies which could also lead to the development of OA such as inflammatory or metabolic conditions.

1.4 Bone-imaging modalities

1.4.1 Plain radiography

Plain radiography relies on the production of x-rays which are a form of high-energy radiation within the electromagnetic spectrum. They are generated by a process known as thermionic emission whereby a fine filament is heated resulting in the generation of free negatively charged electrons. They are attracted towards the positive anode and on collision produce x-rays.

As x-rays pass through matter they can either be transmitted, absorbed or scattered depending on the composition of the matter. Tissue with a high atomic number e.g. calcium, absorbs a high proportion of x-rays thereby producing a radiopaque appearance compared to tissue with low absorption of x-ray such as air which produces a radiolucent appearance. X-rays are subsequently captured by a detector (either photographic film or a digital detector) and then a 2D representation of the matter is produced.

Radiographs are good for assessing bone due to its high calcium content and are cheap and easy to obtain. The limitation however is that plain radiography produces a 2D representation of a 3-dimensional structure (Ramachandran 2017).

1.4.2 Computed Tomography

The limitations of plain radiography led to the development of computed Tomography (CT). CT employs a rotating x-ray source around the subject combined with multiple detectors which record the attenuated x-rays that have passed through the patient. By combining these images with digital processing, cross-sectional images can be produced. As with plain radiography employing x-rays, tissues that attenuate x-rays to a higher degree such as bone appear more radiopaque. CT is able to clearly differentiate bone, soft tissue, fat and air (Ramachandran 2017).

As well as the ability to produce cross-sectional and 3D imaging, CT can also be used to guide interventional procedures. Disadvantages of CT however include that the patient is usually subjected to a significant ionizing radiation dose (Davies 2011) as well as having a limited value in evaluating soft tissues compared to MRI.

1.4.3 Magnetic Resonance Imaging

MRI is based on using superconducting magnets and radiofrequency (RF) coils to manipulate hydrogen protons, creating a detailed, high-contrast image (Hartley 2012). A patient is placed in an MRI scanner and energy is applied in the form of radiofrequency pulses. This energy is designed to match the resonant frequency of hydrogen atoms as these are by far the most abundant nuclei in the body. Once the energy has been absorbed by the hydrogen atoms, the energy is re-emitted as a magnetic resonance signal which induces a small voltage in a receiver next to the patient. Hydrogen atoms return to a relaxed state via two different mechanisms, known as T1 and T2. T1 and T2 values vary for different tissues and it is this difference which is used for forming an image from the MRI scanner (Ramachandran 2017).

MRI can be used to generate high quality, high resolution images and is therefore good at evaluating soft tissues such as chondral surfaces as well as bone (Hartley 2012). Additionally, MRI does not involve exposure of ionising radiation and is therefore safe. It is however time consuming and contra-indicated in certain patients e.g. patients with pacemakers.

1.4.4 Dual X-ray Absorptiometry (DEXA)

Dual-energy X-ray absorptiometry or DEXA scanning is used to assess bone mineral density. X-rays of two different wavelengths are used which are absorbed in differing amounts by bone. This allows

the bone mineral density to be calculated. DEXA scanning is the current gold standard for diagnosing osteoporosis and allows for the indirect assessment of fracture risk. It can also be used to evaluate the effect of preventative interventions. However, DEXA scanning is unable to distinguish between cortical and cancellous bone and as DEXA-measured bone mineral density is thought to account for 60-70% of the variation in bone strength (Ammann 2003), some important factors are therefore not captured regarding mechanical properties of bone from DEXA.

1.5 Raman Spectroscopy

1.5.1 Raman Spectroscopy Background and theory

Raman spectroscopy is a spectroscopic technique used to observe vibrational, rotational and other low-frequency modes in a system (Gardiner 1989). It is widely used to identify substances from characteristic spectral patterns (so-called fingerprinting) and can be used to determine the amount of a substance in a sample. It is named after the Indian scientist, Sir Chandrasekhara Venkata Raman who first observed the Raman effect in the 1920s. He was later awarded the Nobel Prize for Physics in 1930. He discovered that, when light traversed a transparent material, some of the scattered light changed in wavelength. This observation is now referred to as Raman scattering.

When light interacts with matter, the photons which make up light may either pass through the matter or be absorbed and/or scattered. In the scattering process, the incident photon typically excites a molecule into a higher “virtual” vibrational energy level. Subsequently, the molecule decays back to a lower level therefore emitting a scattered photon. The vast majority of scattered photons have the same energy (and wavelength) as the incident photons and are said to be elastically scattered. This is referred to as Rayleigh

scatter. A small fraction of light however (roughly 1 in 10^7 photons) is scattered at different frequencies to the incident photons (inelastic scatter). This is referred to Raman scattering and the change in frequency is dependent on the specific molecule, its chemical and physical environment.

There are two common types of Raman scattering. When the incident light is shifted to a lower frequency or lower energy, the scattered light is referred to as Stokes scattering. When the incident light is shifted to a higher frequency, the scattered light is referred to as Anti-Stokes scattering (Figure 10).

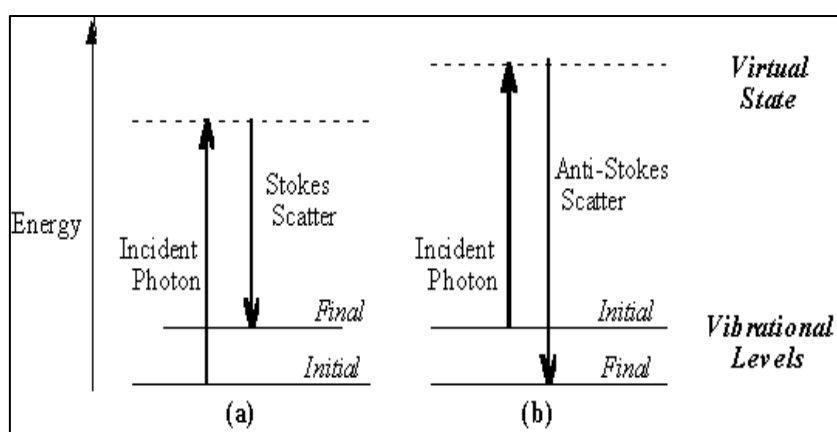


Figure 10. Illustration depicting Raman scatter. Adapted from http://www.kosi.com/na_en/products/raman-spectroscopy/raman-technical-resources/raman-tutorial.php. Last accessed March 17th, 2018.

The difference between the incident radiation frequency and the Raman scattered radiation is known as the Raman shift. The Raman spectrum is a plot of the intensity of Raman scatter as a function of its frequency difference from the incident radiation. The Raman shift is independent of the frequency of the incident radiation. The energy of the scattered photons is recorded on the x-axis with the unit inverse centimetres (cm^{-1}) and this is plotted against the Raman signal intensity on the y-axis. An example Raman spectrum is shown in Figure 11.

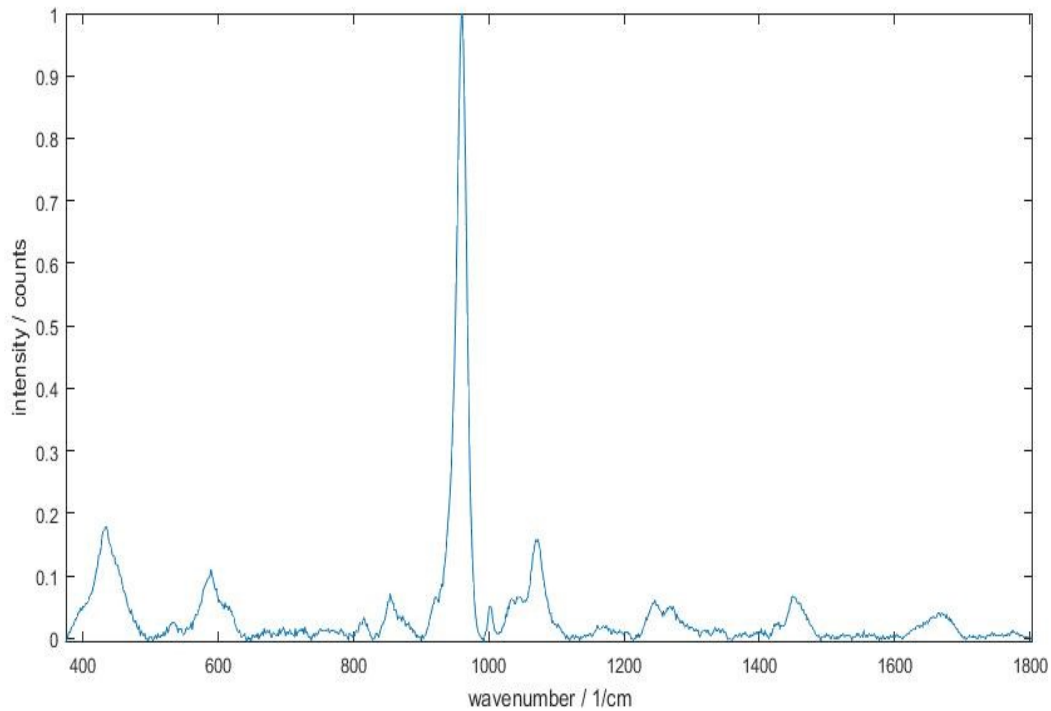


Figure 11. An example Raman spectrum which was acquired from bone (Baseline corrected and normalised to the 960 cm^{-1} peak. The shift in wavenumber is plotted on the x-axis with the intensity on the y-axis

Each spectrum has several bands. Each band corresponds to light which has been shifted by a certain frequency. For example, the Amide I band at 1650 cm^{-1} corresponds to incident photons which were inelastically scattered from the Amide I in the sample and in this process, the photons lost energy and shifted to a lower frequency corresponding to a wavenumber shift of 1650 cm^{-1} .

1.5.2 Raman spectroscopy instrumentation

Commercially available Raman spectrometers are composed of five main components:

1. An excitation source, usually a laser. Lasers are ideal excitation sources for Raman spectroscopy. Laser beams are highly monochromatic with extraneous lines much weaker. The extraneous lines may be further eliminated by using notch

filters. Most laser beams also have small diameters which can be focused on small samples. Theoretically samples as small as $2\mu\text{m}$ can be studied (Ferraro 2003).

2. A sample illumination system. As the Raman scattered light is relatively weak, the excitation source needs to be focused properly onto the sample and the scattered light collected efficiently.
3. A wavelength selector. As the intensity of Rayleigh scatter is far greater than that of Raman scatter, a filter is required to separate the elastically scattered light, to cut-off spectral range of $\pm 80\text{-}120\text{ cm}^{-1}$ from the laser line. This method is efficient in stray light elimination.
4. Diffraction grating. The different components of the inelastically scattered light are separated before reaching the detector.
5. A detector. This normally incorporates a charge-coupled device (CCD). A CCD is a silicon-based semi-conductor arranged as an array of photosensitive elements. Electrical charge is produced when stimulated, read by electrodes and recorded by a computer.
6. A computer to read and interpret the signals from the CCD.

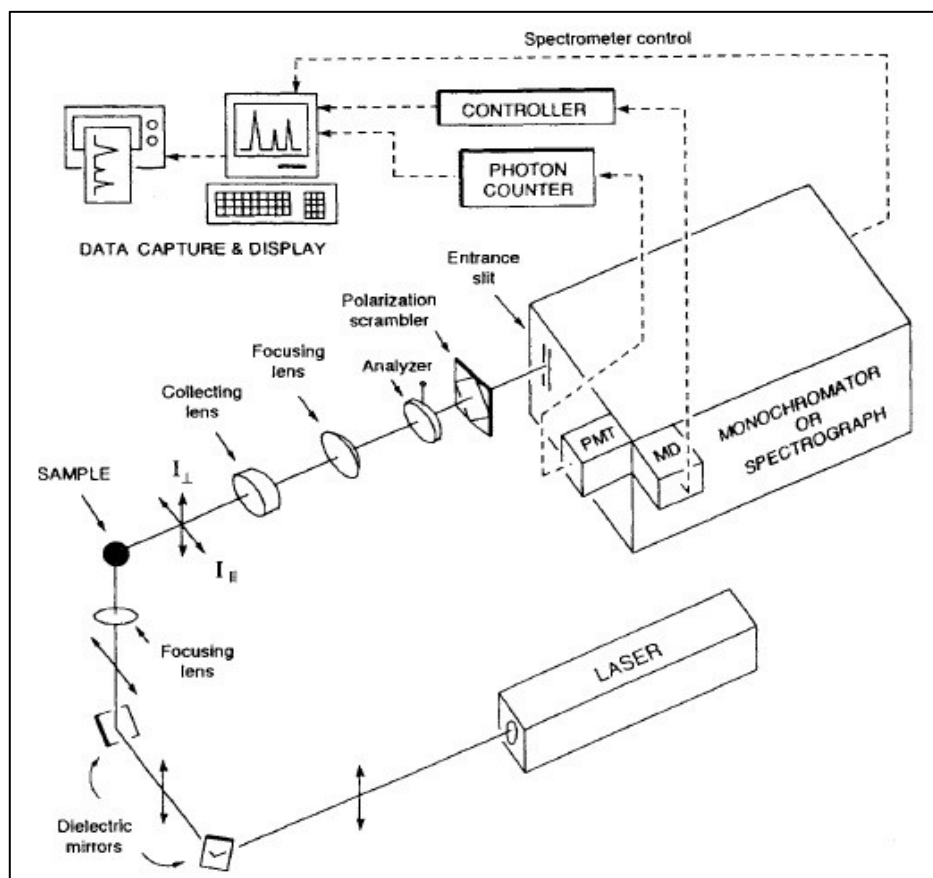


Figure 12. An illustration depicting the major components in a Raman spectrometer. Adapted from Ferraro JR. ed., (2003) *Instrumentation and Experimental Techniques in: Introductory Raman spectroscopy, 2nd ed.*

1.5.3 Advantages and disadvantages of Raman spectroscopy

Raman spectroscopy has several advantages as a chemical analysis modality:

- Unlike most other techniques, sample preparation prior to acquisition of Raman spectroscopy is relatively minimal.

- Furthermore, this process is non-destructive of the sample at moderate laser powers/limited acquisition times.

- Water is a weak Raman scatterer and is therefore ideal for studying biological tissues.

-As the intensity of the Raman band in a spectrum is proportional to the number of molecules giving rise to the band, the Raman bands can be used for quantitative analysis.

-Raman spectroscopy does not utilise ionizing radiation. There is therefore no risk from ionizing radiation to subjects during in-vivo studies.

Disadvantages of Raman spectroscopy include:

-The laser used to elicit a Raman shift can cause heating and thermal degradation to the sample. This is potentially an issue for small samples and for specimens which require a relatively long acquisition time (>30 minutes).

-Raman spectroscopy is not suitable for analysing pure metals.

-Conventional Raman spectroscopy may have limited use investigating samples exhibiting strong fluorescence in the spectral region of interest for the available laser illumination wavelengths.

1.5.4 Kerr-Gate

This technology employs pulsed lasers to overcome fluorescence (a disadvantage to conventional Raman spectroscopy). This method exploits the fact that when a pulse of light passes through an appropriate medium, it can cause changes in the dielectric properties of the medium. This effect can rotate the plane of polarization of the incident light is rotated by 90 degrees.

The Kerr-Gate setup includes using a pulsed laser split into two parts so that the scattered light from one part of the pulse excites the sample at the same time as the Kerr medium is stimulated by the other part of the pulse. Scattered radiation from the sample passes through a polarizer into a Kerr medium and then through a second

polarizer onto the detector. During the closed state of the Kerr gate, no light can pass from the sample to the detector as the polarizers are 90 degrees to each other. However, if a sample is excited by one part of the pulse and the second part passes through the Kerr medium, it will rotate the plane of polarization of the scattered light by 90 degrees so that radiation can pass through the analyser and be detected. This is the open gate.

Since Raman scattering is normally faster than fluorescence emission, it is possible to setup a Kerr gate system so that it collects only the first few picoseconds of emission following the laser pulse. This can therefore be used to effectively eliminate the effect of background fluorescence.

1.5.5 Spatially Offset Raman spectroscopy (SORS)

Spatially Offset Raman spectroscopy is a variant of Raman spectroscopy that allows chemical analysis of objects beneath a surface. The technique is based on the collection of Raman scattered light from surface regions that are laterally offset away from the excitation laser spot on the sample. The Raman spectra obtained from the sample in this way exhibit a change in relative spectral intensities of the surface and subsurface layers (Matousek 2005). A SORS measurement will make at least two Raman measurements; one at the source and one at an offset position of typically a few millimetres away. The two spectra can be subtracted using a scaled subtraction to produce two spectra representing the subsurface and surface spectra.

Matousek et al., 2006 performed the first transcutaneous Raman spectroscopy of human bone in vivo using SORS at a depth of up to 4mm from the skin. The development of this technique has potentially wide ranging in-vivo applications.

1.5.6 Pre-processing

Following Raman spectral acquisition from a specimen, pre-processing can be employed to improve the spectral signal for further analysis. This can be done in a number of ways. Smoothing can be employed to remove noise from spectra that have a low signal-noise ratio. However, excess smoothing will also remove useful information.

Normalisation allows different spectra to be combined or compared by ensuring that the intensity range of spectra are on similar scales. The scales can be made similar by normalising all the spectra in a dataset to a particular band's intensity. Alternatively, the spectra can be normalised to the mean spectral intensity.

Fluorescence which is sometimes several orders of magnitude greater than the Raman scatter can interfere with the Raman spectra and cause a phenomenon known as baseline drift making the analysis of Raman spectra difficult. Baseline correction aims to reduce the effect of this and can be done both instrumentally and mathematically.

1.5.7 Interpretation of Raman spectra acquired from bone

The use of Raman spectroscopy to study bone quality is a relatively new but rapidly expanding field. Most of the bands of a bone Raman spectrum can be assigned to phosphate, carbonate or matrix collagen (Figure 13).

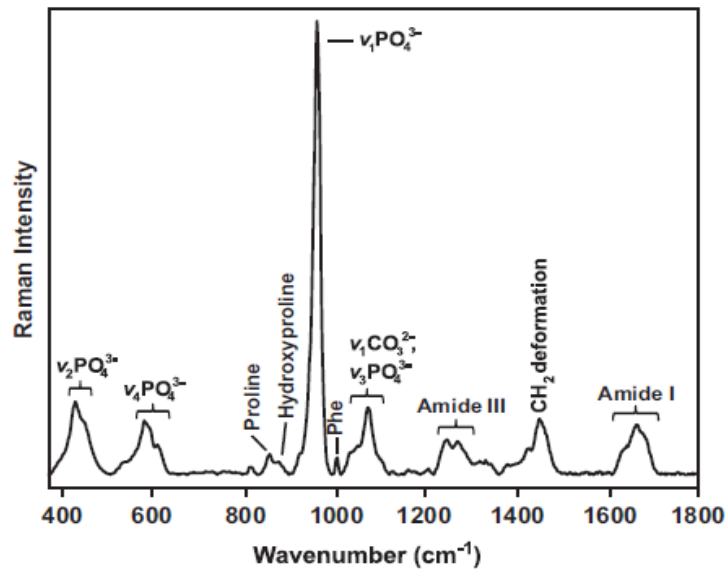


Figure 13. An illustration showing the Raman spectra acquired from the mouse tibia. Adapted from Mandair et al., 2015.

Most bone spectra are reported through a wavenumber interval from about 400cm⁻¹ to about 1750cm⁻¹. The most widely used mineral band is a phosphate band at 955-962cm⁻¹, whilst the most widely reported collagen band is the amide I band.

The interpretation of absolute peak intensities arguably has limited value as the efficiency of Raman scatter, grain size and surface roughness of the specimen can all affect the peak values (Morris 2011). For this reason, many studies have reported the relative peak intensities. For example, the phosphate to amide I ratio corresponds to the mineral to matrix ratio and indicates the amount of mineralisation. The carbonate to phosphate ratio can provide insight into the chemical composition of bone as it varies with bony architecture and crystallinity (Legros 1987, Yerramshetty 2006), while the carbonate to amide I ratio can provide an indication about bone remodelling (McReadie 2006). Such Raman compositional measures are correlated with mechanical properties of bone with the phosphate:amide I and carbonate:amide I ratios thought to be the strongest predictors of this (Akkus 2004).

Further information can be gained from the various spectral peaks as they are in fact the combination of several related peaks. For example, the dimensions of the main phosphate peak at ~959cm⁻¹ are

actually a combination of several peaks. Its main constituents are believed to be a combination of a peak at 955cm^{-1} (representative of a transient bone mineral (P–O) phase, usually seen in immature bone), and a peak at $959\text{--}962\text{cm}^{-1}$ (mature bone mineral) (Morris 2011). Likewise, the amide I band is the summation of a combination of several components, with the two most important at 1660cm^{-1} (relates to the alpha-helix of collagen I) and 1690cm^{-1} (relates to beta-sheet/secondary structure of collagen I) (Morris 2011). Sub-analysis of these components can yield further information regarding the structure and properties of bone. The identification of the separate components of a Raman spectral peak is known as deconvolution and involves a process of curve fitting. Figure 14 provides an example of the sub-peak components of the phosphate and amide I peaks:

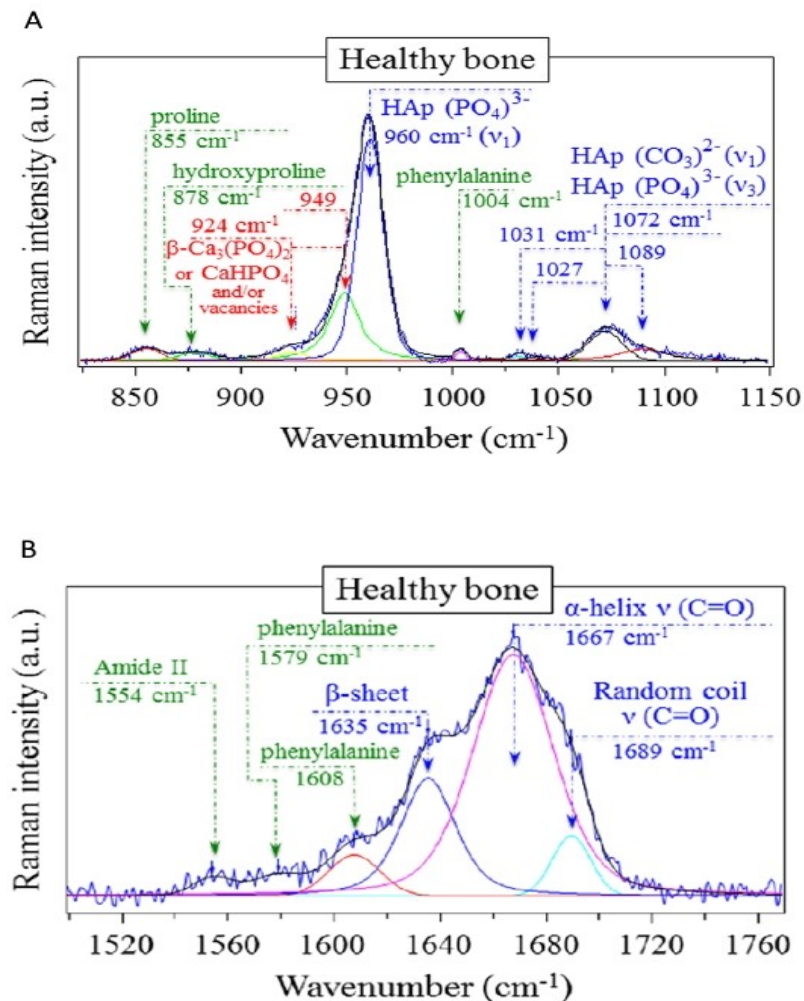


Figure 14. Deconvoluted Raman spectra in the phosphate (A) and amide I (B) regions showing the various different components. Adapted from Pezzotti et al., 2017.

Similar to the acquired base Raman spectra, the relative peak intensities of the deconvoluted spectra can be calculated to provide more information regarding the properties of the bone. An increase in the ratio of the two most important bands in the amide I peak at 1660cm^{-1} and 1690cm^{-1} has been used to infer the presence of pathological cross-links within the collagen I structure. (Carden 2003, Morris 2015). Likewise, analysis of the deconvoluted spectra in the main phosphate peak at 960cm^{-1} allows comparison of immature phosphate (957cm^{-1}) relative to mature phosphate ($959\text{-}962\text{cm}^{-1}$) (Pezzotti 2017).

1.5.8 Multivariate analysis

Principal component analysis (PCA) can be used to analyse and inspect the multi-dimensional nature of Raman spectra. PCA is a non-parametric statistical technique that linearly transforms a large set of variables into a representative smaller set of uncorrelated variables or so-called principal components. It was first conceived by Pearson in 1901. The aim of PCA is to reduce the dimensionality of the original data set. The rationale being that a smaller set of uncorrelated variables is much easier to understand and use in further analysis.

Principal components are linear combinations of the original variables constructed such that the first principal component explains the greatest variance within the data, the second principal component explains the maximal variance in the data not accounted for by the first principal component and so on and so forth. The number of principal components extracted is equal to the number of observed variables being analysed, however in most analyses the first few components account for meaningful amounts of variance, so only these first few components are retained, interpreted, and used in subsequent analyses.

The principal components can be used as axes on scores plots where Raman spectra can be represented by individual points or scores (Figure 15).

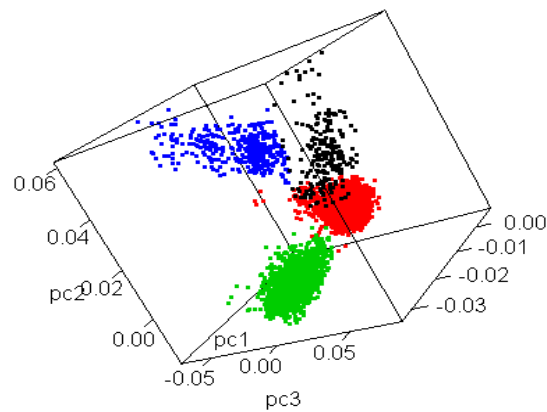


Figure 15. An example of a 3D PCA scores plot with different spectra represented by the four different colours. Figure adapted from: <https://www.r-bloggers.com/a-new-dimension-to-principal-components-analysis/> accessed: 3rd March 2018.

Representing the data in this way allows variation in the individual spectra to be identified. The closer the scores are, the more similar the spectra are. Conversely the further away the scores are, the more different the spectra are and it is therefore inferred that they differ biochemically. In addition, the principal component loadings can be plotted as functions of the original variables thereby identifying the biggest contributors to any inherent difference within the data.

1.5.9 Raman spectroscopy and studies of bone

Raman spectroscopy has been used to study metabolic bone conditions such as osteoporosis. A comparison of specimens from low trauma fracture victims against controls matched for bone and volume fraction showed that fracture specimens had a higher carbonate to phosphate, phosphate to amide I and carbonate to amide I ratios (McCredie 2006). An explanation from the authors given was that osteoporotic bone underwent greater remodelling and was therefore of reduced mineralisation as a result.

The study of ageing bone has also revealed changes to bone chemistry. In a cadaveric study, the spectra obtained from the humerus bone from donors with differing ages highlighted differences

in the Amide I and Amide III peak intensities relative to the CH₂ wag spectrum (Ager 2003) (Figure 16).

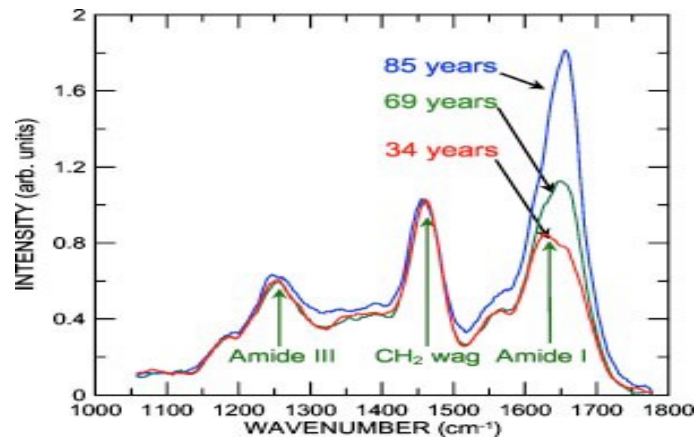


Figure 16. UV Raman spectra acquired from human humerus bone from donors of differing ages. Adapted from Ager et al., 2003.

The amide I and amide III bands are believed to be good indicators of protein conformation because of the role of amide in cross-linking and bonding. These results are therefore suggestive of age related changes in the organic component of the bone matrix.

As stated earlier, bone is a dynamic tissue and one that adapts constantly to the mechanical loads that it is placed under as suggested by Wolff's law. Buckley et al., 2012 have provided evidence of this and used Raman spectroscopy to "map" the chemical composition of the entire length of cadaveric human tibiae in fine spatial resolution. Their results showed that the average mineral to collagen ratio for mid-shaft cortical tibial bone was ~20% higher than cortical bone seen towards either end of the tibia. The authors theorised that this difference was a functional adaptation; that a decrease in the mineral to collagen ratio could be expected to lead to a significant decrease in the Young's modulus (Buckley 2012) of cortical bone closer to the joints. This bone would provide a better load transfer function compared to bone at the midshaft thereby providing protection to the nearby cartilage.

CHAPTER 2 – AIMS AND OBJECTIVES

2.1 Aims of the Study

The aims of this study are to investigate the chemical composition of subchondral bone in osteoarthritic ankle joints and to compare this to non-osteoarthritic controls using Raman spectroscopy and biochemical analysis. After acquiring Raman spectra from subchondral bone, univariate and multivariate techniques will be used to analyse the data.

Biochemical testing will be used to further investigate the biochemical composition and secondary structure of subchondral bone and to validate results obtained from Raman spectroscopy.

2.2 Hypotheses

The following hypotheses will be tested:

1) Raman spectra acquired from osteoarthritic specimens differ significantly to spectra acquired from non-osteoarthritic controls and that the following peak ratios are altered:

-The phosphate:amide I ratio in osteoarthritic ankle samples is decreased compared to non-osteoarthritic controls.

-The carbonate: phosphate and carbonate: amide I ratios in osteoarthritic ankle samples are increased compared to non-osteoarthritic controls.

2) Osteoarthritic subchondral bone specimens are hypomineralised compared to controls.

3) Osteoarthritic subchondral bone specimens have a greater alpha-1 to alpha-2 type I collagen ratio compared to controls.

4) Biochemical differences within subchondral bone vary according to the macroscopic severity of osteoarthritis.

2.3 Objectives

1) Obtain ethical approval to acquire human specimens.

2) To acquire Raman spectra from subchondral bone specimens from the tibial plafond of osteoarthritic patients and non-osteoarthritic cadveric controls and to subsequently process the data with univariate and multi-variate analysis.

3) To determine levels of mineralisation of subchondral bone in osteoarthritic specimens and compare them to controls using biochemical analysis.

4) To determine the alpha-1 to alpha-2 ratio of type I collagen within subchondral bone of osteoarthritic specimens and controls.

5) To compare subchondral bone from different locations of the ankle joint i.e. medial vs lateral and to relate this to the observed osteoarthritis wear pattern i.e. varus vs balanced osteoarthritis.

6) To run a pilot study to develop protocols and power the study.

7) To develop models/theories as to the role of subchondral biochemistry and/or trauma have on the development of ankle OA.

CHAPTER 3 – VALIDATION OF METHODS

3.1 Introduction

Several pilot experiments were undertaken to inform the final methodology and to ensure that results obtained from Raman spectroscopy were reproducible and repeatable. This was important as only a handful of studies employing Raman spectroscopy have assessed subchondral bone from human osteoarthritic specimens.

The thickness of the subchondral bone plate is known to vary according to different joints and also according to location across a particular joint (Buettner 2013). This variation is believed to be related to differing contact stresses across the joint (Madry 2010).

Subchondral bone is believed to be a key factor in normal joint protection with its shock-absorbing qualities. It is thought that it can attenuate 30% of the joint load (Imhoff 2000). It would therefore be important to establish whether the subchondral bone chemistry varies according to ankle joint location prior to establishing experimental procedure.

The use of a laser to acquire Raman spectroscopy is associated with a local heating effect on the sample. Even low powered lasers can raise the temperature of the specimen and can affect the Raman measurement (Kouteva-Arguirova 2003). The heating effect is dependent on the sample properties i.e. thermal conductivity, laser power, laser wavelength and the length of time that the sample is exposed to the laser (Pope 2011). Taking this into account, it would therefore be important to evaluate the duration of time that subchondral bone specimens could be used to gather Raman spectroscopy prior to significant alteration in the measurement.

3.2 Methods

3.2.1 Calibration, reproducibility and repeatability

The Raman spectrometer was calibrated prior to use using silicon. This produces an intense sharp peak with a Raman shift of 520 cm^{-1} . The spectrometer was calibrated until this change in wavelength was obtained.

Reproducibility of the Raman spectrometer was investigated. A freshly frozen cadaveric donor distal tibia was thawed and allowed to acclimatise to room temperature for 6 hours. A cylindrical core bone was removed from the articular surface using an 8-gauge Jamshidi needle. The resultant core was roughly 3.2 mm in diameter and 10mm in length. As bone is abundant in lipids which can cause Raman peaks which can interfere with peaks of interest to the study such as the amide I peak, the core was defatted using 5ml of pure acetone at 37°C for 90 minutes. Following this, the core was rinsed thoroughly with de-ionised water and subjected to 2 further 90-minute cycles of delipidation with acetone. The specimen was placed horizontally onto the inVia Renishaw spectrometer sample stage and a random location within the subchondral bone was chosen. The co-ordinates of the microscope objective with respect to the sample were noted (X, Y and Z co-ordinates) and a Raman spectrum was acquired in this location using a laser with a power of 300mW, 830nm wavelength and a 5 times objective lens. The spectra were acquired over a period of 60 seconds (60 accumulations with a 1 second acquisition time). The position of the sample was then changed but subsequently reverted to the initial co-ordinates and 9 further Raman spectra acquired for comparison (under the same spectrometer settings as the initial scan). The 10 spectra were pre-processed and analysed using MATLAB (2016b). The raw data was baseline corrected for background fluorescence using an in-house implementation of the improved polynomial background correction method of Zhao et al., 2007. The raw spectral data was normalised to the phosphate peak at 960 cm^{-1} .

The spectral band ratios (phosphate: carbonate and phosphate: amide I) were calculated using MATLAB (2016b). This was based on dividing the height of the respective peaks as shown in figure 17.

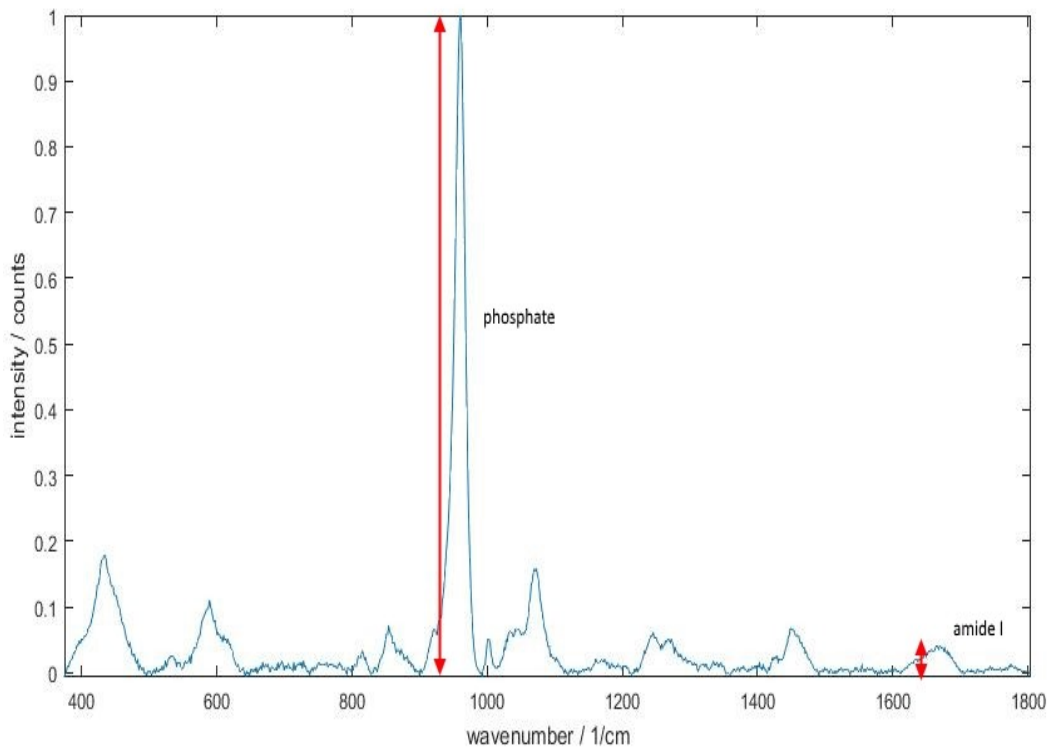


Figure 17. An illustration of how the phosphate:amide I ratio was calculated using MATLAB. The height of the phosphate peak is divided by the height of the amide I peak.

The variation in spectral band ratios would serve as a marker of reproducibility.

Repeatability was also tested. The same defatted cylindrical core of bone was used for this pilot experiment and was placed horizontally onto the spectrometer sample stage. A different location within the subchondral bone was chosen and 10 spectra were acquired from this location. The same spectrometer settings were used to acquire the spectra (5x objective, laser power 300mW, 1 second acquisition, 60 accumulations). The raw data was subjected to the same processing as in the previous pilot experiment using MATLAB (2016b). The spectral band ratios (phosphate: carbonate

and phosphate: amide I) were again calculated and the variability would serve as a marker of repeatability.

3.2.2. Natural variation of spectra by location of the tibial plafond

A freshly frozen cadaveric donor distal tibia was thawed and allowed to acclimatise to room temperature for 6 hours. The tibial plafond was examined by an orthopaedic surgeon and was noted to show no macroscopic evidence of ankle osteoarthritis (no articular cartilage loss, no fissuring or softening of articular cartilage noted). Ten cylindrical cores were obtained from different locations of the tibial plafond joint surface specimen (Figure 18) using an 8 gauge Jamshidi needle. The resultant cores were roughly 3.2mm in diameter and 10mm in length. The cores were defatted using 5ml of pure acetone at 37°C for 90 minutes. Following this, the core was rinsed thoroughly with de-ionised water and subjected to 2 further 90 minute cycles of delipidation with acetone. The cores were scanned using an InVia Raman spectrometer at room temperature with a 300mW laser light source, 830nm wavelength with cosmic ray removal.



Figure 18. A photograph showing the distal tibial joint surface from a cadaveric specimen and the location of cylindrical cores for analysis.

The cores were placed horizontally on the sample stage with the articular cartilage at one end (Figure 19).

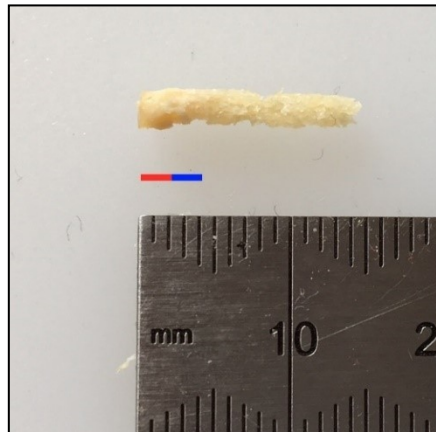


Figure 19. A bony core placed horizontally as shown on the spectrometer sample stage. The red line indicates the thickness of the articular cartilage and the blue line represents the area of subchondral bone scanned.

A 5x Leica microscope objective was used to focus the laser onto the sample. The laser was focused over the cartilaginous end of the core and at the midpoint of the core on the Y axis. To ensure that tibial plafond subchondral bone was analysed, the cartilage was identified and confirmed from the spectral signature. Using real-time cyclical spectral acquisition, the site of spectral acquisition on the cylindrical core was moved at 50 μ m increments away from the cartilage until the Raman spectra returned signature consistent with bone. Once subchondral bone was identified, spectra were acquired within the subchondral bone using 1 second acquisitions for 60 accumulations using circularly polarised light and cosmic ray removal. The laser was then focused a further 300 μ m away from the cartilage edge of each core and further spectra acquired. This process was repeated until spectra had been acquired from subchondral bone across a depth of 0.9mm thickness i.e. three spectra from each core. Once acquired, the raw spectral data was subjected to normalisation, baseline correction and analysis using multivariate analysis (principal component analysis).

3.2.3 The effect of laser exposure time on Raman measurement

The tibial plafond from a cadaveric donor was left to thaw and equilibrate at room temperature for 6 hours. A core of bone was then harvested using an 8 gauge Jamshidi needle. The resultant core was roughly 3.2mm in diameter and 10mm in length. Following defatting as described in the previous pilot experiments, the core was then placed horizontally on the sample stage within the Raman spectrometer. Spectra were acquired from the subchondral bone using a 5x working objective to focus the laser and circularly polarised light. 60 Spectra were acquired at this location with 60 accumulations and 1 second acquisition times per spectra. The sample was therefore exposed to the laser from within the spectrometer for roughly 60 minutes. The raw spectral data was subjected to baseline correction and normalised to the phosphate peak at 960 cm^{-1} . The spectra were analysed using MATLAB (2016b) and were subjected to principal component analysis. This would allow for a subtle change in the spectral signature to be detected.

3.3 Results

3.3.1 Calibration, reproducibility and repeatability

The spectra obtained investigating reproducibility are shown in figure 20. The ten different spectra are represented by a different colour and are superimposed on one another.

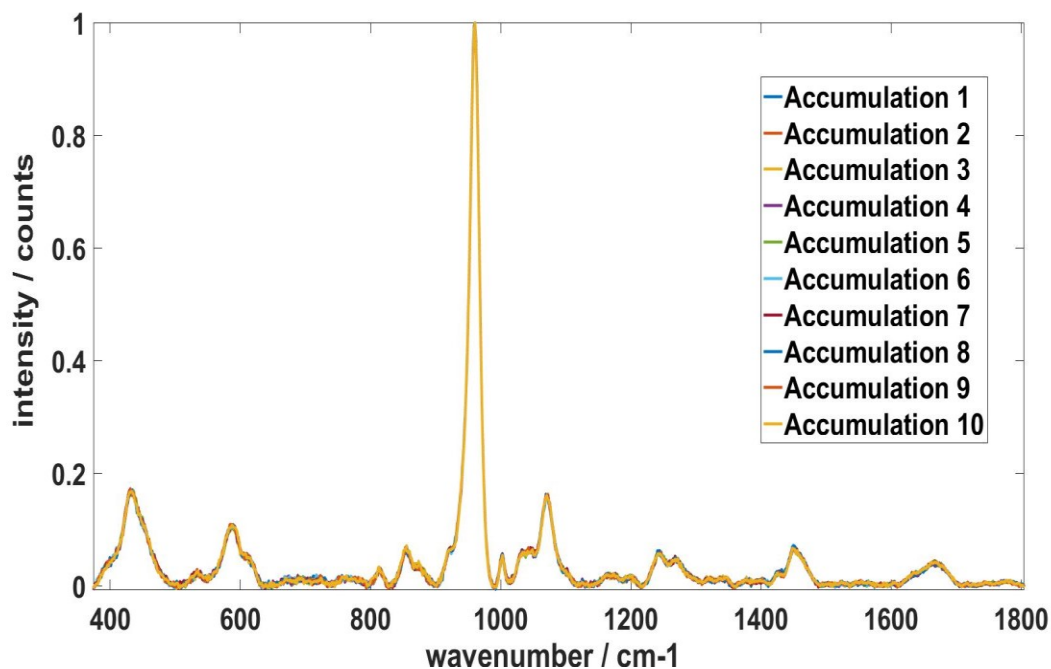


Figure 20. Raman spectra acquired whilst investigating reproducibility. The separate spectra are represented by different colours and are superimposed on one another. Wavenumber (cm^{-1}) is shown on the x axis and peak intensity is shown on the y axis.

Using the relative height of the peaks, peak ratios were calculated and are shown in Table 3.

Ratio	Mean	SD	IQR
Phosphate:amide I	25.13	0.57	0.94
Phosphate:carbonate	6.37	0.08	0.08

Table 3. Mean, standard deviation (SD) and inter-quartile range (IQR) of biochemical ratios as calculated from the ten spectra investigating reproducibility.

The results show no significant variation between the ten spectra and little variation with the phosphate:amide I and phosphate:carbonate ratios.

The ten spectra obtained investigating repeatability are shown in figure 21. Once again, the different spectra are represented by different colours and are superimposed on one another.

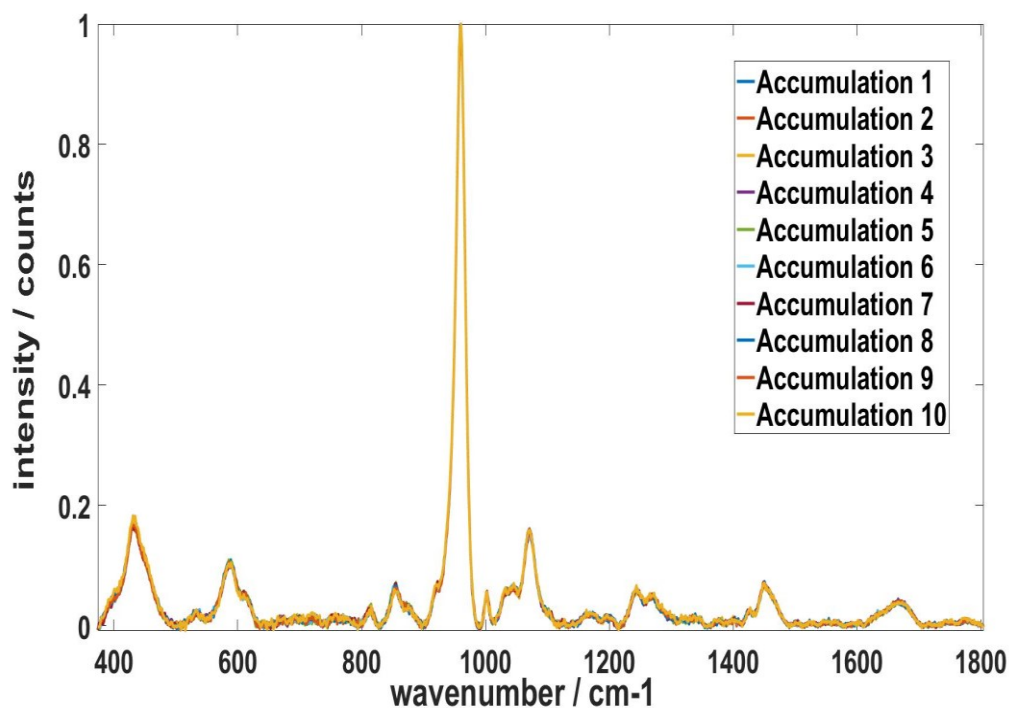


Figure 21. Raman spectra acquired from investigating repeatability. The separate spectra are represented by different colours and are superimposed on one another. Wavenumber (cm-1) is shown on the x axis and peak intensity is shown on the y axis.

Using the relative height of the peaks, peak ratios were again calculated and are shown in Table 4.

Ratio	Mean	SD	IQR
Phosphate:amide I	24.55	0.58	0.77
Phosphate:carbonate	6.33	0.06	0.11

Table 4. Mean, standard deviation (SD) and inter-quartile range (IQR) of biochemical ratios as calculated from the ten spectra investigating repeatability.

Once again both the spectra and peak ratios show no significant variation.

3.3.2 Natural variation of spectra by location of the tibial plafond

Three spectra were acquired from each core location. The spectra were subjected to principal component analysis and the results are shown in a scores plot (Figure 22).

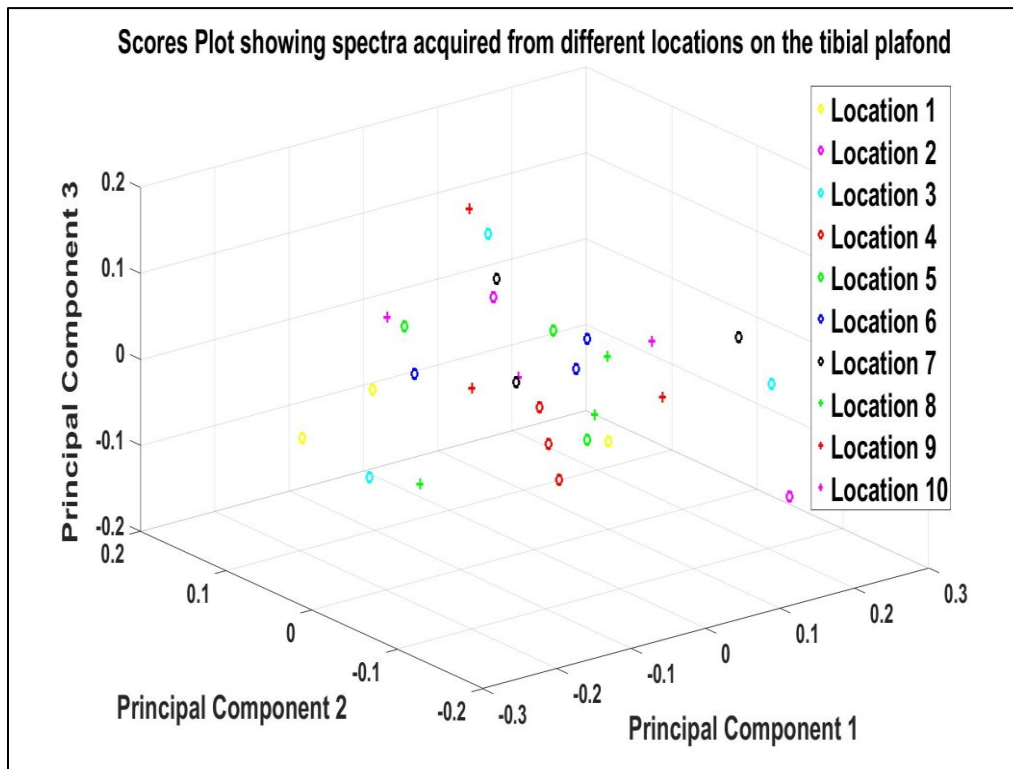


Figure 22. Scores plot showing spectra acquired from different subchondral bone locations. Scores are plotted against the first 3 principal components. Spectra acquired from different locations are represented by different symbols/colours.

The scatter plot shows that there is random distribution of principal component score values as a function of core anatomical location with no clear clustering.

3.3.3 The effect of laser exposure time on Raman measurement

The scores plots vs number of spectral acquisitions were examined, and the second principal component showed the greatest change. PC2 is therefore plotted against spectral number in figure 23.

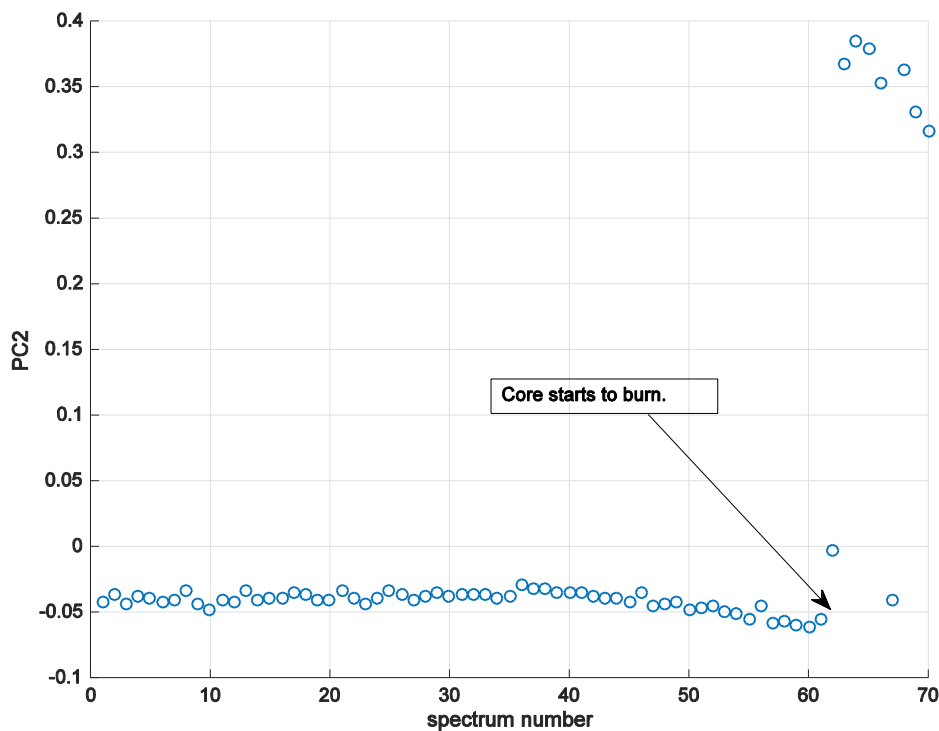


Figure 23. Spectral number against the second principal component. Each spectrum was acquired for 60 seconds. The spectral number is shown on the x axis with the principal component 2 scores shown on the y axis

The graph above represents the data with the spectral number on the x axis against the second principal component on the y-axis. Each spectrum represents 60 seconds of laser exposure. The first to 35th spectra remain stable. Following this, there is a subtle change to the 61st spectra. Beyond this point, a sudden and large change is noted in the second principle component indicating irreversible thermal damage from the laser source.

3.4 Discussion

The pilot studies show that results acquired from the Raman spectrometer are reproducible and repeatable.

With regards to whether spectra appear to vary according to subchondral bone location, our results show that within the joint of our pilot specimen, the Raman spectra and therefore the subchondral

bone biochemistry does not appear to change according to location on the joint. This observation is in keeping with the results observed by Kearns et al., 2014 i.e. biochemical changes in knee OA subchondral bone was observed not only within the affected compartment but also in the macroscopically normal part of the joint.

Harvesting subchondral bone from the exact same position relative to the joint position consistently on patient specimens and control specimens is technically challenging. Although steps should be taken to ensure consistency in terms of sample acquisition location, the observations suggest that subchondral bone sampling by location is not a significant factor to affect the overall results.

The time of laser exposure during Raman acquisition has been shown to affect the measurements with frank sample degradation observed around the 60-minute mark and subtle change noted at 35 minutes. To minimise this variable on Raman acquisition, samples should be scanned in the Raman spectrometer for less than 35 minutes using a 300mW power laser with a 830nm wavelength.

3.5 Power Calculation

An F-test was used to calculate the required sample size for the study. Based on a desired effect size of 0.8 and using standard deviations of phosphate: amide I and phosphate: carbonate ratios collected from a recent knee study on subchondral knee bone chemistry (Kearns et al., 2014), a sample size of eight patients was determined for each cohort of ankle osteoarthritis patients. Therefore, samples from a total of at least 16 patients would be required.

CHAPTER 4-ANALYSIS OF SAMPLES USING RAMAN SPECTROSCOPY

4.1 Introduction

The investigation of osteoarthritis using Raman spectroscopy is a relatively new development and therefore there are only a few published papers currently focusing on this application. Esmond-White et al., 2009 were one of the earliest groups to investigate osteoarthritis using Raman spectroscopy. Using a technique known as drop-deposition Raman spectroscopy (DDRS), they were able to assess the synovial fluid in patients undergoing elective knee surgery (knee arthroplasty and arthroscopy). This included patients with osteoarthritis and with only minimal OA changes. Their results revealed a statistically significant increase in the Amide I band in the synovial fluid from arthritic knees and that this correlated with increasing OA severity i.e. higher Kellgren-Lawrence grades. An increase in the Amide I intensity indicates more disorder in protein secondary structure (Pelton 2000). They surmise that the change in chemical environment of synovial fluid from osteoarthritic knees may either be due to a lower pH therefore partially denaturing synovial proteins or that there are increased levels of degraded type II collagen fragments in the diseased synovial fluid.

The remaining previous studies that used Raman spectroscopy to investigate osteoarthritis all focused on chemical changes (compositional/structural) to subchondral bone (Buchwald 2012, Kearns 2014, Kim 2015). These studies have focused on either the hip or the knee joint. Buchwald et al., 2012 compared femoral head subchondral bone from osteoarthritic hips undergoing total joint arthroplasty to subchondral bone specimens from non-osteoarthritic controls (patients under-going surgery for fractured neck of femur without signs of pre-existing metabolic disease or osteoarthritis). Their results revealed some significant differences in the chemical composition in subchondral bone of osteoarthritic patients. This

included a statistically significant decrease in hydroxyapatite to collagen ratio. This ratio is a marker of bone mineralisation and the authors suggested that demineralization of subchondral bone was a result of greater remodelling of OA bone tissue. They also measured the carbonate apatite to hydroxyapatite ratio and this was found to be significantly higher in the OA specimens. This indicated an increased carbonate ion substitution into hydroxyapatite and the authors inferred that this occurs as a response to a decline in mineralization. The carbonate ions may be replacing the lost phosphate ions within apatite crystals in an attempt to limit loss of mineral within the bone (Buchwald 2012). This also further highlights altered chemistry within subchondral bone of osteoarthritic joints. Interestingly these chemical alterations were found in both the most and least weight-bearing surfaces of the femoral head but were absent in the cancellous bone underlying the subchondral bone.

Differences in subchondral bone chemical composition have also been noted in osteoarthritic knees. Kim et al., 2015 investigated the chemical composition of subchondral bone from the medial femoral condyle using a cadaveric model. They found significant differences in the subchondral bone of specimens with macroscopically advanced osteoarthritis. This included statistically significantly decreased maximum intensity in the phosphate, amide I and carbonate Raman peaks. However, the value in interpreting the peak intensities is debatable as the efficiency of Raman scatter, grain size and surface roughness of the specimen can all affect the peak values (Morris 2011).

Changes have also been found in the other major bone of the knee joint. Kearns et al., 2014 investigated the bone chemistry of the tibial plateau from patients undergoing total knee replacement for end-stage osteoarthritis. This was compared to non-osteoarthritic cadaveric specimens and also from patients undergoing above knee or through knee amputations with normal knee joints. As well as studying such changes using Raman spectroscopy, subchondral bone specimens were also subjected to biochemical analysis. Statistically

significant differences in the phosphate:amide I and bioapatite: collagen ratios were detected in the OA samples using Raman. Interestingly, such changes were also present in areas of the tibial plateau which macroscopically did not show OA changes i.e. the changes were observed in the subchondral bone of the lateral tibial plateau which was macroscopically unaffected by the osteoarthritic process. This observation raises an interesting question, that is whether certain individuals are predisposed to the development of osteoarthritis given their subchondral bone composition or indeed whether the biochemical changes observed within subchondral bone from osteoarthritic patients are secondary to the development of the condition. The non-osteoarthritic patient controls that were used however were not age matched to the patient osteoarthritic specimens. The mean age of patients with non-OA controls was 30 compared to a mean of 68 for the patient osteoarthritic specimens. As it is known that spectra acquired from bone of patients varies with age (Ager 2003), this may have contributed to the differences in subchondral bone chemistry they observed.

The use of Raman spectroscopy has not been used to study ankle osteoarthritis before and whether subchondral bone biochemical differences exist as seen in osteoarthritic hip and knee patients is unknown. Furthermore, deconvolution of specific Raman peaks as a technique has not been used in the study of osteoarthritic subchondral bone before. Inherent differences within the ankle joint and differing aetiologies of ankle osteoarthritis compared to osteoarthritis of the hip and knee raise questions as to whether similar biochemical differences will be found.

4.2 Methods

4.2.1 Ethical Approval

Ethical approval was sought and granted from the Research and Ethics Committee (REC) for the collection of bone specimens

from patients undergoing ankle fusion or ankle arthroplasty at the Royal National Orthopaedic Hospital (RNOH), Stanmore. Approval included the transfer, storage and analysis of specimens at the Institute of Orthopaedics and Musculoskeletal Science (IOMS). Ethical approval was also granted for the collection, transfer and storage of cadaveric tibiae from The Vesalius Clinical Training Centre at the University of Bristol (08/H0724/34), from people who had previously consented to donate their bodies for medical research.

4.2.2 Specimen collection and preparation

Bony specimens were collected from the tibial plafond of eligible patients undergoing ankle fusion or ankle arthroplasty for clinically and radiologically diagnosed ankle osteoarthritis at the RNOH, Stanmore. This included patients with symmetrically loaded and varus patterns of osteoarthritis. All patients gave informed written consent to allow retention and analysis of their specimens for the study.

Patients with a predominantly valgus pattern of wear were excluded from the study due to the low relative incidence of this pattern of ankle wear. Other exclusion criteria were as follows:

- Diagnosis of inflammatory arthropathy such as rheumatoid arthritis.
- Diagnosis of metabolic bone disease such as osteoporosis.
- Drug treatments affecting the metabolism of bone such as bisphosphonates.
- patients with a recent (< 2 months) history of smoking.

Patient demographic data was captured (age, sex and side of operation). Pre-operative investigations including x-rays and weight-bearing CT scans were reviewed. The wear pattern of osteoarthritis was noted (varus or symmetrically loaded) and the macroscopic severity of the disease was graded according to the Outerbridge

classification system. The aetiology of the osteoarthritis was recorded if known i.e. traumatic vs primary.

For patients undergoing open ankle fusion, an 8-gauge Jamshidi needle was used to collect bony cores from the tibial plafond intra-operatively. Following exposure of the ankle joint by the surgical team and prior to bony preparation of joint surfaces for fusion, the tibial plafond joint surface was inspected macroscopically, and the medial and lateral aspects of the joint were scored according to the Outerbridge classification. Two cores of subchondral bone were taken from each patient, one medial and one lateral of the midline in the coronal plane and as close to the midline in the sagittal plane as possible. Collected cores were ~3.2mm in diameter and measured at least 5mm in length. After collection, samples were transferred to the Institute of Orthopaedic and Musculoskeletal Sciences (IOMS), University College London for defatting.

For patients undergoing total ankle replacement, the distal tibial resection was retained and transferred to the IOMS, University College London. Cores of bone were taken from the specimens using an 8-gauge Jamshidi needle. The joint surface was divided up into medial and lateral sides according to the midline of the joint surface in the coronal plane and inspected and scored macroscopically according to the Outerbridge classification. Two cores of bone were harvested from each side and as close to the midline in the sagittal plane as possible (Figure 24).

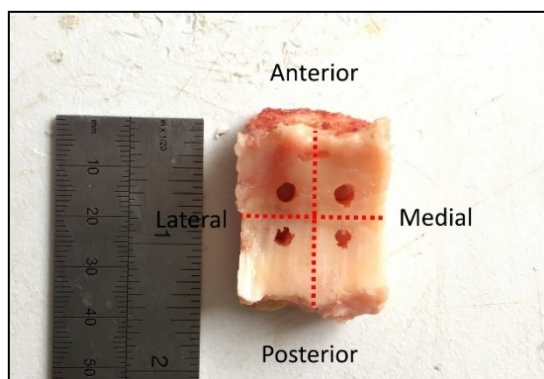


Figure 24. Photograph showing the distal tibial resection from total ankle replacement and showing the location of core sampling. A ruler measuring inches and millimetres gives an indication of the size of the specimen.

Collected cores were ~3.2mm in diameter and measured at least 5 mm in length.

Twenty-four fresh frozen cadaveric ankles were obtained from the Vesalius Clinical Training Centre at the University of Bristol, UK for the purposes of non-osteoarthritic controls. Cadaveric donors were age (within 8 years), sex and laterality matched to participant specimens. Where possible, donor medical history was reviewed, and donors were selected on absence of inflammatory bone disease and absence of metabolic bone disease. The controls were examined macroscopically and confirmed not to have any macroscopic features of osteoarthritis according to the Outerbridge classification (intact articular cartilage without signs of fissuring, softening or fibrillation). Cadaveric samples were thawed and equilibrated to room temperature for 6 hours prior to bone sampling. Four cores were taken from each donor tibia, two medial and two lateral of the midline in the coronal plane and as close to the midline in the sagittal plane as possible (Figure 25).

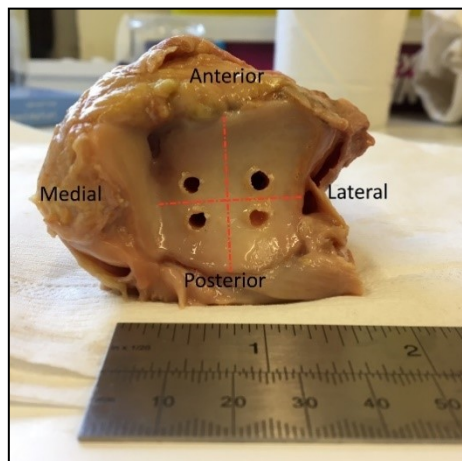


Figure 25. Photograph of a cadaveric control ankle specimen showing the location of core sampling. A ruler measuring inches and millimetres is shown giving an indication of the size of the specimen.

Collected cores were ~3.2mm in diameter and measured at least 5mm in length.

The removal of lipids was required because lipids have large Raman scattering cross-sections and have spectral peaks that overlie some of the spectral peaks from bone matrix. Cores were defatted with 5ml of pure acetone at 37°C using a water bath for 90 minutes, after which the cores were rinsed with de-ionised water. 2 further 90-minute cycles of delipidation with acetone were carried out-a total time of 270 minutes. Samples were then stored in a -80°C freezer (Sanyo Biomedical, Japan) prior to processing and analysis at IOMS, University College London.

4.2.3 Raman spectra acquisition

All cores were thawed and equilibrated to room temperature for 60 minutes prior to Raman spectral analysis. The Raman spectrometer was calibrated prior to use using crystalline silicon. This produces a strong sharp Raman phonon band at 520 cm^{-1} . The spectrometer's detector was iteratively calibrated until this band was found at the correct wavenumber position. The cores were placed horizontally on the spectrometer sample stage (Figure 19, page 61).

Spectra were acquired with a Renishaw inVia Raman spectrometer using a class 3B 300 mW laser, 830nm wavelength. A Leica microscope with a 5x working objective was used to focus the laser on the sample. Such a working objective was utilised to acquire Raman spectra from a relatively large surface area of bone to remove the potential effect of local variations in subchondral bone chemistry. The laser was focused over the cartilaginous end of the core and halfway along the core on the Y axis. To ensure that tibial plafond subchondral bone was analysed, the cartilage was identified using real-time cyclical spectral acquisition by moving along the cylindrical core at 50 μm increments from macroscopically visible cartilage until Raman spectra returned a signal with a strong phosphate peak, indicative of bone. The core was moved a further 50 μm from this point to ensure that Raman acquisition of calcified cartilage was not

captured. This served as the first starting point for spectral acquisition of subchondral bone for each cylindrical core. In osteoarthritic cores which did not contain any cartilage (due to the degenerative process of osteoarthritis), a starting point of 50 μm from the distal edge of the core was chosen as the first location of Raman spectral acquisition. Raman spectra were acquired at room temperature using 1 second acquisitions and 60 accumulations using circularly polarized light, cosmic ray removal with the region of interest centred at wavelength change 1150cm^{-1} . Following Raman spectral acquisition at this location, the sample was moved at further 50 μm increments from the cartilage and scanned under the same settings. A total of twenty Raman spectra were acquired this way from each core ensuring that spectra were captured from a variety of locations from a total thickness of 0.75mm of tibial plafond subchondral bone.

4.2.4 Raman spectra analysis

The data collected using the inVia Renishaw Raman spectrometer was pre-processed using MATLAB (version R2016b). The raw data was baseline corrected for background fluorescence using an in-house implementation of the improved polynomial background correction method of Zhao et al., 2007. The background corrected spectral data was subsequently normalised to the phosphate peak at 960 cm^{-1} .

The osteoarthritic specimens were grouped according to wear pattern (varus and balanced wear). The patient specimens within these two groups were matched with sex, laterality and age matched (to 8 years) cadaveric controls. Within the osteoarthritic groups, the biochemical markers were also compared according to location of the bone specimen i.e. medial vs lateral. Possible differences within the bone chemistry according to sex were also investigated within both control and osteoarthritic specimens.

Bivariate analysis was utilised for direct comparison of bands of interest. The phosphate: amide I, carbonate: amide I and carbonate:

phosphate ratios were calculated using MATLAB by dividing the heights of the relevant peaks. For example, to calculate the phosphate: amide I ratio, the height of the phosphate peak was divided by the height of the amide I peak (figure 26)

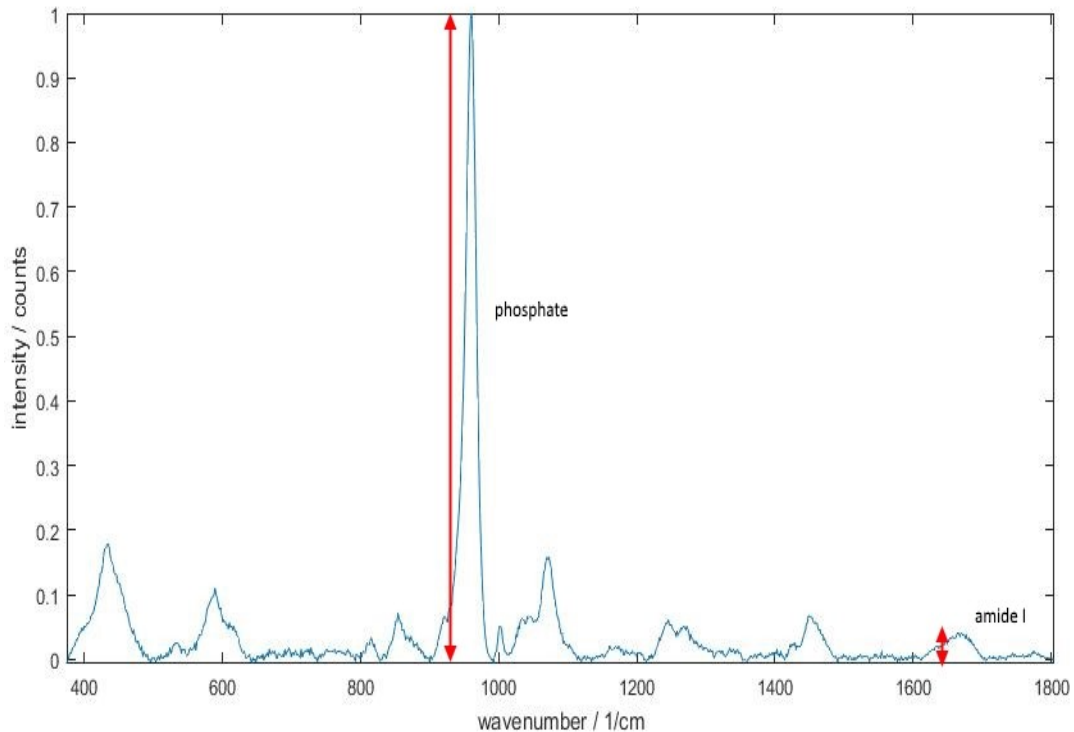


Figure 26. An illustration of how the phosphate:amide I ratio was calculated using MATLAB. The red arrows correspond to the heights of the respective peaks normalised to the phosphate peak. The height of the phosphate peak is divided by the height of the amide I peak.

The mean ratios from the twenty spectra from each bone specimen were calculated. Using SPSS, the Mann-Whitney U test was used to assess the presence any statistically significant difference in the phosphate: amide I, carbonate: amide I and carbonate: phosphate ratios between the separate groups with p values < 0.05 found to be significant.

Deconvolution of the phosphate and amide I peaks into their underlying constituent peaks was also undertaken for the osteoarthritic groups and their matched controls to provide further information regarding the secondary structure of subchondral bone. From the 20 spectra acquired from each specimen, the mean spectral signature was calculated using MATLAB. Deconvolution of these mean spectra was undertaken using Origin Pro (v9) by a process of multiple curve-fitting using to Gaussian-Lorentzian (Voigt) functions. For the amide I peak, the relative peak intensities of the peaks at 1690cm^{-1} and 1660cm^{-1} were calculated by dividing the height of the 1690cm^{-1} peak against that of 1660cm^{-1} (Figure 27) to gain information regarding the secondary structure of collagen, notably the presence of immature crosslinks.

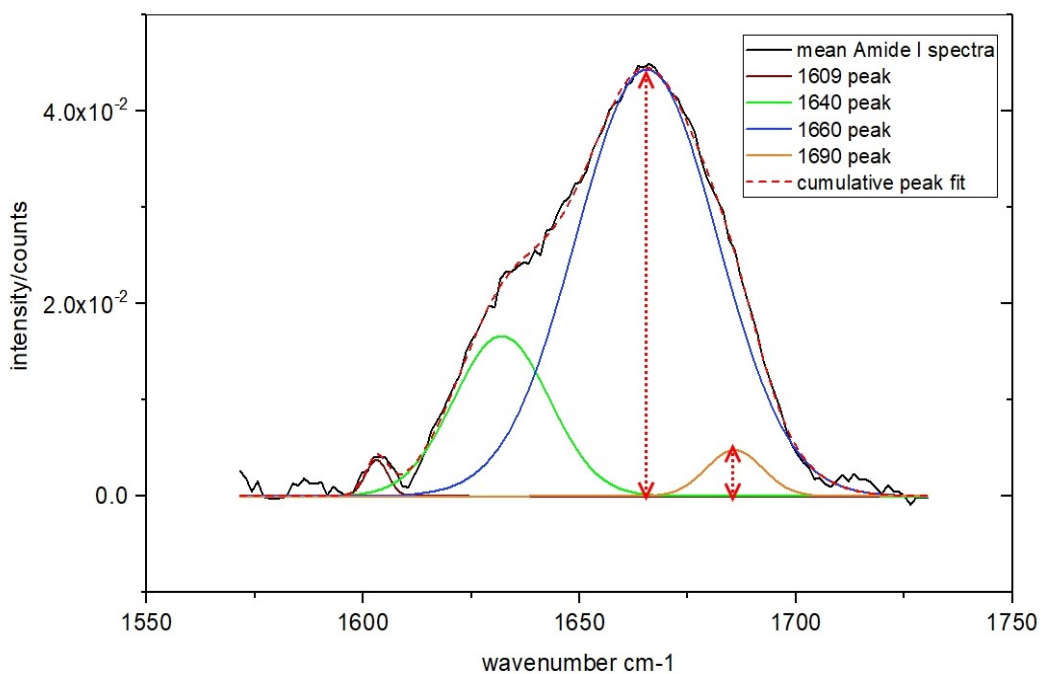


Figure 27. Deconvoluted Raman spectra of the Amide I region. The four different underlying peaks are shown contributing to the cumulative peak fit. The red arrows illustrate the height of the peaks at 1660 and 1690. The height of the 1660 peak is divided by the height of the peak at 1690.

For the phosphate peak, the relative peak intensities of the peaks at 955 and 959 were calculated by dividing the height of the 959cm^{-1} peak against that of 955cm^{-1} (Figure 28) to gain information

regarding the crystal structure of the mineral phase of subchondral bone.

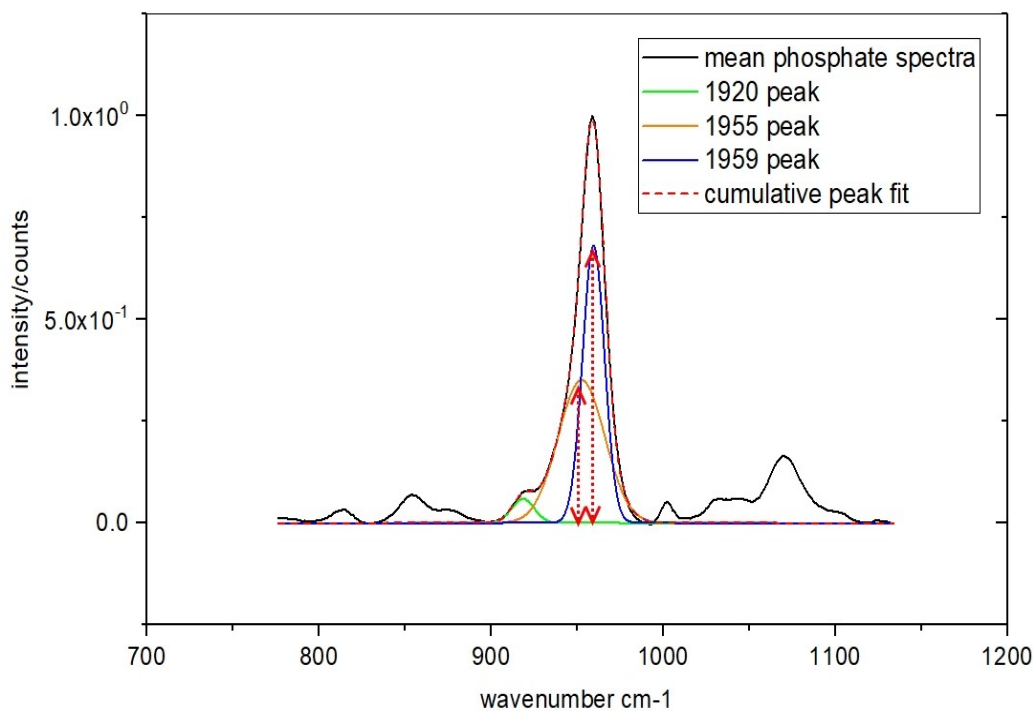


Figure 28. Deconvoluted Raman spectra of the phosphate region. The three different sub peaks are shown contributing to the cumulative peak fit. The red arrows illustrate the height of the peaks at 955 and 959. The height of the 959 peak is divided by the height of the peak at 955.

Statistical analysis was performed on the ratios calculated from deconvolution of the phosphate and amide I peaks by using the Mann-Whitney U test with significance found when $p < 0.05$. Osteoarthritic specimens (varus and balanced) were compared to matched controls.

Principal component analysis (PCA) was used to perform exploratory analysis of the data to identify the presence of any segregation of spectra between the different groups. 3-dimensional scatter plots of the resulting scores obtained from PCA allowed for differences to be identified objectively. The principal component loadings were also plotted for cohorts where a significant separation was found. This was performed to identify the specific Raman peaks contributing to any difference observed.

4.3 Results

4.3.1 Patient and donor demographic data

Following screening for exclusion criteria, 25 patients undergoing open ankle fusion or total ankle replacement between March 2016 and February 2017 for osteoarthritis were recruited to the study. All patients were operated on by the same consultant foot and ankle surgeon through an anterior approach to the ankle. One patient was later excluded from the study (participant 11) as a routine synovial biopsy result available 2 weeks after surgery was suggestive of an inflammatory arthropathy. Consent was given to collect, retain and analyse bone from the tibial plafond. There were 13 male and 11 female participants that remained in the study. The average age was 67.28 years and all but 3 participants had a clear history of trauma to the ankle. The participant details are summarised in table 5.

Participant number	Age	Sex	Side	Wear pattern	History of trauma?	Operation
1	69	Male	Right	Balanced	Y	Fusion
2	70	Male	Left	Varus	Y	TAR
3	69	Female	Right	Varus	Y	Fusion
4	65	Female	Left	Balanced	Y	TAR
5	68	Male	Left	Varus	Y	TAR
6	64	Male	Left	Varus	N	TAR
7	54	Female	Left	Varus	Y	TAR
8	76	Female	Left	Varus	Y	fusion
9	69	Female	Right	Balanced	N	fusion
10	62	Female	Left	Varus	Y	TAR
11	62	Female	Right	Balanced	N	TAR
12	69	Female	Left	Balanced	Y	TAR
13	71	Male	Right	Balanced	Y	TAR
14	67	Male	Right	Balanced	Y	TAR
15	70	Female	Left	Balanced	Y	TAR
16	67	Male	Right	Varus	Y	TAR
17	69	Female	Right	Varus	Y	TAR
18	59	Male	Right	Balanced	Y	TAR
19	83	Male	Left	Varus	Y	Fusion
20	76	Male	Right	Varus	Y	fusion
21	52	Male	Left	Balanced	Y	TAR
22	65	Male	Left	Varus	Y	TAR
23	69	Female	Left	Balanced	Y	TAR
24	55	Female	Left	Balanced	Y	TAR
25	80	Male	Left	Varus	Y	TAR

Table 5. Patient characteristics with the osteoarthritic wear pattern, radiological grading and operation undertaken.

The cadaveric tibiae transferred from the Versalius Centre Bristol were confirmed to be free of macroscopic signs of osteoarthritis. The specimen/donor characteristics are shown in table 6.

Specimen number	Age	Side	Sex
10-16	82	R	Male
10-16	82	L	Male
21-16	76	R	Male
21-16	76	L	Male
22-16	83	R	Female
22-16	83	L	Female
23-16	76	R	Male
23-16	76	L	Male
30-16	79	R	Male
30-16	79	L	Male
78-14	57	R	Male
78-14	57	L	Male
53-16	63	R	Male
53-16	63	L	Male
42-16	63	R	Female
42-16	63	L	Female
48-16	76	R	Female
48-16	76	L	Female
51-16	77	R	Female
51-16	77	L	Female
64-16	57	R	Male
64-16	57	L	Male
70-16	72	R	Female
70-16	72	L	Female

Table 6. Cadaveric donor specimen characteristics.

4.3.2 Results by sex

Subchondral bone specimens were collected from 13 male patients (Mean age 68.69 years), 11 female patients (mean age 65.75 years), 7 male cadaveric tibiae (Mean age 70 years) and 5 female cadaveric tibiae (Mean age 74.2 years). The mean phosphate: amide I, carbonate: amide I and carbonate: phosphate ratios as ascertained from processed Raman spectra are summarised in the table below.

Cohort	Phosphate:amide I ratio	Carbonate:amide I ratio	Carbonate:phosphate ratio
Male patients	20.698+/-1.416	3.519+/-0.218	0.170+/-0.003
Female patients	20.044+/-1.574	3.376+/-0.263	0.169+/-0.004
Male donors	22.800+/-1.165	3.804+/-0.169	0.167+/-0.004
Female donors	21.540+/-0.675	3.573+/-0.127	0.167+/-0.006

Table 7. Mean biochemical ratios with standard deviations shown to 3 decimal places, obtained from subchondral bone specimens from male and female patients as well as male and female cadaveric donors.

No statistically significant differences were identified within the biochemical ratios between the male and female patient specimens, male and female donor specimens.

When the individual spectra are subjected to principal component analysis, no significant separation is noted on the scores plot representing the first 3 principal components when male and female patients and male and female donors are compared. The scores plots are shown below in figures 29 and 30.

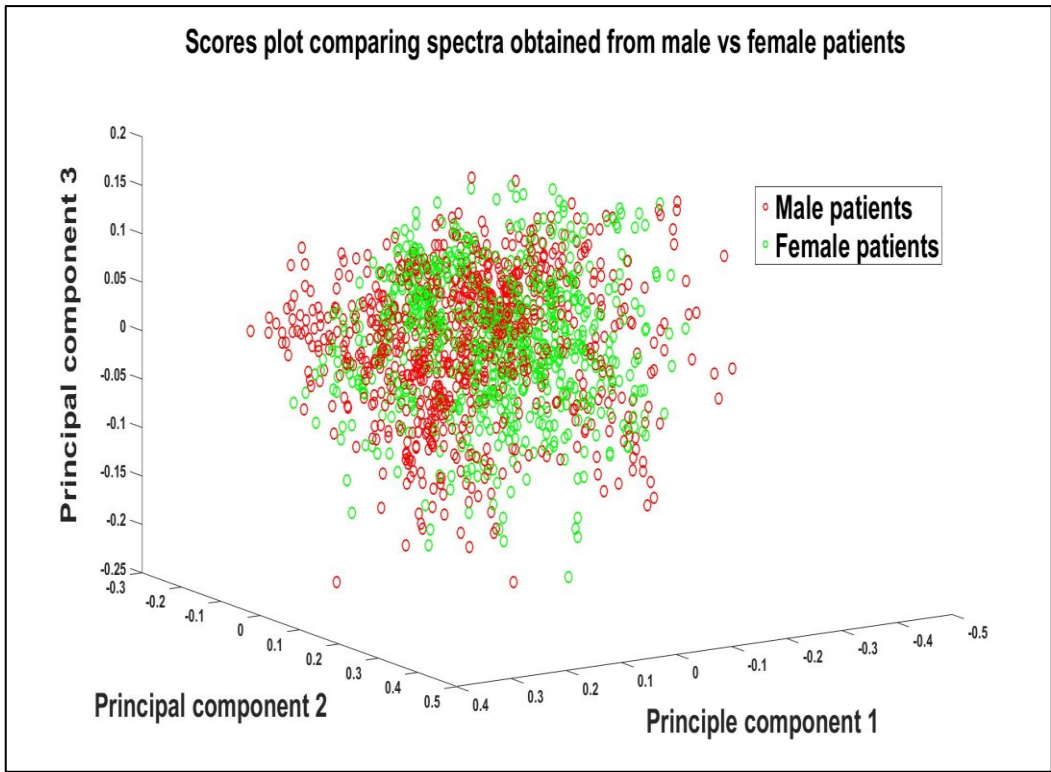


Figure 29. PCA scores plot comparing all spectra acquired from male and female patients. The first 3 PCAs are represented. Spectra obtained from male patients are shown in red and female patients in green.

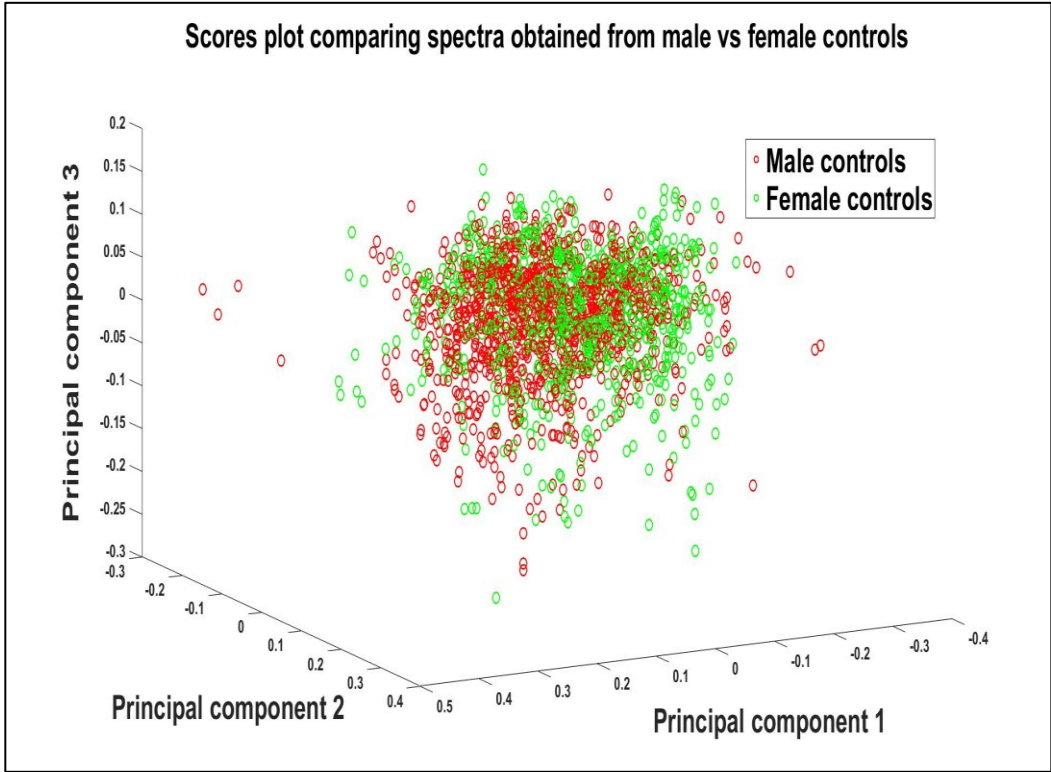


Figure 30. PCA scores plot comparing all spectra acquired from male and female patients. The first 3 PCAs are represented. Spectra obtained from male controls are shown in red and female controls in green.

4.3.3 Osteoarthritis with a varus wear pattern

4.3.3.1 OA vs matched controls univariate analysis

The following patients undergoing surgery for ankle osteoarthritis with a varus wear pattern were age (to within 8 years), sex and laterality matched with the following control specimens:

Patient number	Medial OA grade	Lateral OA grade	Operation	Matched control
2	4	2	TAR	21-16 L
3	3	2	Fusion	70-16 L
5	3	1	TAR	23-16 L
6	4	3	TAR	64-16 L
8	2	2	Fusion	51-16 L
10	3	2	TAR	42-16 L
16	4	3	TAR	53-16 R
17	3	2	TAR	48-16 R
19	4	3	Fusion	22-16 L
20	4	2	Fusion	30-16 R
22	4	2	TAR	78-14 L
25	4	2	TAR	10-16 L

Table 8. The patients recruited to the study with a varus pattern of OA and the age, laterality and sex matched non-OA controls used. Medial and Lateral OA gradings are based on the Outerbridge classification.

A suitable control could not be found for participant 7, the data collected from participant 7 was therefore excluded from the analysis comparing patients with a varus wear pattern of osteoarthritis with matched controls. The OA grade on the medial side was generally higher than that of the lateral side (median medial grade = 4, median

lateral grade = 2). The biochemical ratios between such patients and their controls are compared in table 9.

Cohort	Phosphate: amide I ratio	Carbonate: amide I ratio	Carbonate: phosphate ratio
Varus OA patients	20.907+/-1.366	3.523+/-0.213	0.169+/-0.005
Matched controls	22.191+/-0.975	3.694+/-0.154	0.167+/-0.005
P value	0.018	0.028	>0.05

Table 9. Mean biochemical ratios with standard deviations shown to 3 decimal places, obtained from subchondral bone specimens obtained from patients with a varus osteoarthritic wear pattern and compared against matched controls.

The mean phosphate: amide I and carbonate: amide I ratios were found to be significantly higher in the non-OA control group ($p=0.018$ and $p=0.028$ respectively). A difference was also noted in the carbonate: phosphate ratios but this was not found to be statistically significant.

Deconvolution of the amide I and phosphate peaks provided a good cumulative peak fit using 4 sub peaks in the amide I peak and 3 sub peaks in the phosphate peak. The ratios of the subpeaks 1690cm^{-1} to 1660cm^{-1} within the amide I peak and of subpeaks 1955cm^{-1} and 1959cm^{-1} are shown in table 10.

Cohort	Amide I (1690:1660) ratio	Phosphate (959:955) ratio
Varus OA patients	6.858+/-2.590	1.930+/-0.084
Matched controls	9.436+/-2.544	1.963+/-0.083
P Value	0.038	>0.05

Table 10. Mean ratios with standard deviations shown to 3 decimal places, acquired from deconvolution of amide I and phosphate peaks. Specimens obtained from patients with a varus osteoarthritic wear pattern and compared against matched controls.

The amide I 1690:1660 ratio was found to be significantly lower compared to matched controls on performing the Mann-Whitney U test ($p=0.038$). The phosphate 959:955 ratio was also found to be lower in the OA group, however this difference was not found to be statistically significant.

4.3.3.2 OA vs matched controls multivariate analysis

All separate Raman spectra acquired from osteoarthritic patients with a varus wear pattern were compared against spectra obtained from matched controls. A scores plot obtained from principal component analysis is shown in figure 31.

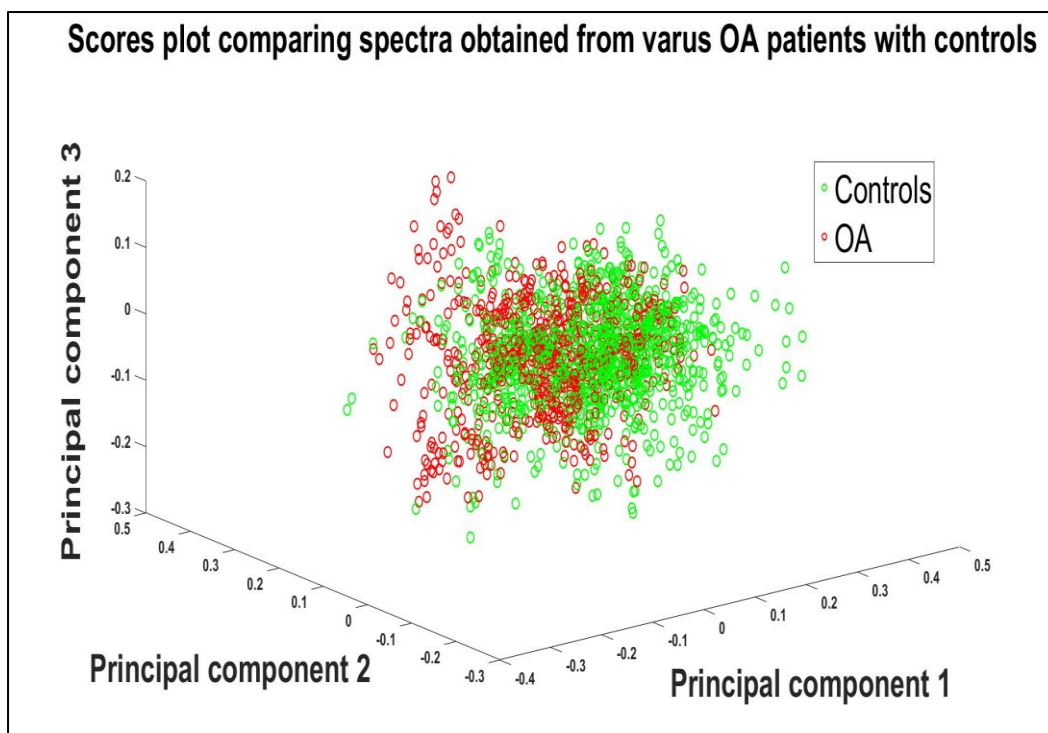


Figure 31. PCA scores plot comparing all spectra acquired from patients with a varus osteoarthritic wear pattern with age, sex and laterality matched non-OA controls. The first 3 PCAs are represented. Spectra from controls are represented in green and patients with varus OA in red.

Multivariate analysis with PCA did reveal some separation between the two groups as illustrated in the above figure between spectra acquired from varus osteoarthritic specimens and non-OA

matched cadaveric controls. The principal loadings for varus OA vs matched controls are shown in figure 32:

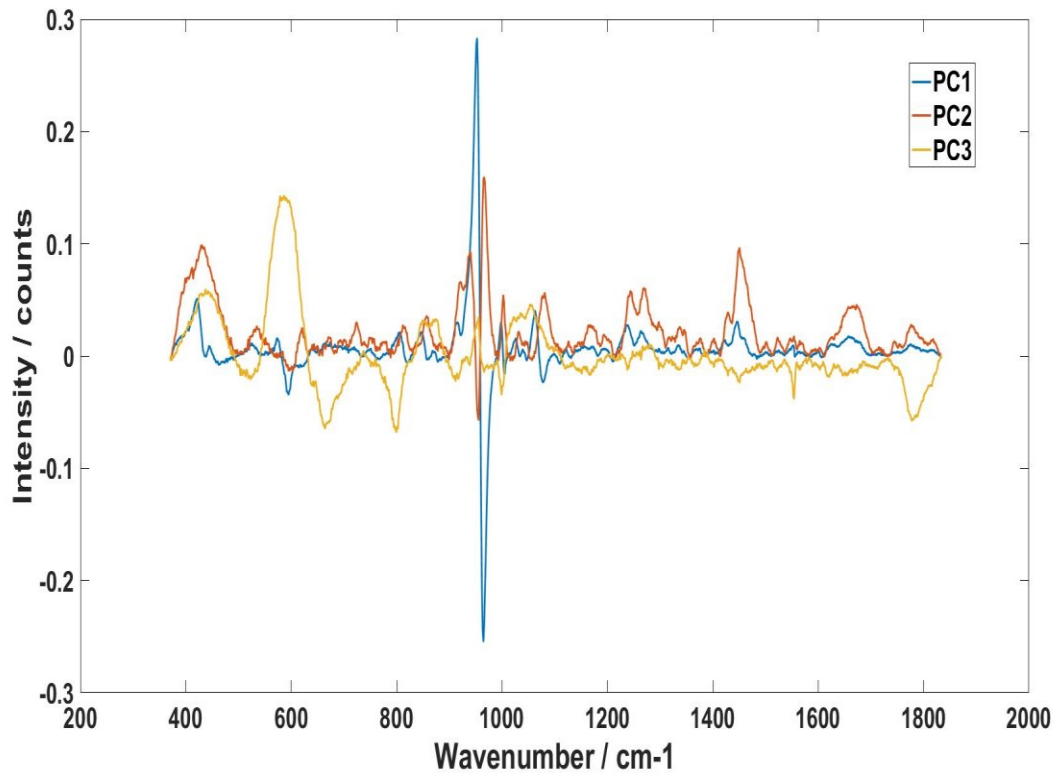


Figure 32. Graphical representation of PCA (1-3) loadings for varus OA vs non-OA controls with their respective wavenumbers and relative intensities shown.

The loadings suggest that the for the first three principal components, differences within the phosphate, amide I, amide III and phenylalanine peaks contribute to the separation observed within the scores plot.

4.3.3.3 Medial vs Lateral subchondral bone

The median Outerbridge grading for the medial joint surface was 4, compared to the median lateral joint surface grading of 2. The mean biochemical ratios as deduced from the spectra acquired from the medial vs the lateral side of the joint are shown in table 11.

Cohort	Phosphate: amide I ratio	Carbonate: amide I ratio	Carbonate: phosphate ratio
Varus OA medial cores	21.244+/-1.810	3.576+/-0.280	0.169+/-0.004
Varus OA lateral cores	20.612+/-1.345	3.478+/-0.197	0.169+/-0.005
P value	>0.05	>0.05	>0.05

Table 11. Mean biochemical ratios with standard deviations shown to 3 decimal places, obtained from subchondral bone specimens obtained from patients with a varus osteoarthritic wear pattern. Subchondral bone from the medial surface is compared to subchondral bone from the lateral surface.

The subchondral bone from the lateral side of the joint was found to have a lower mean phosphate: amide I and carbonate: amide I ratios, however this difference was not found to be significantly different. The PCA scores plot obtained from principal component analysis is shown in figure 33.

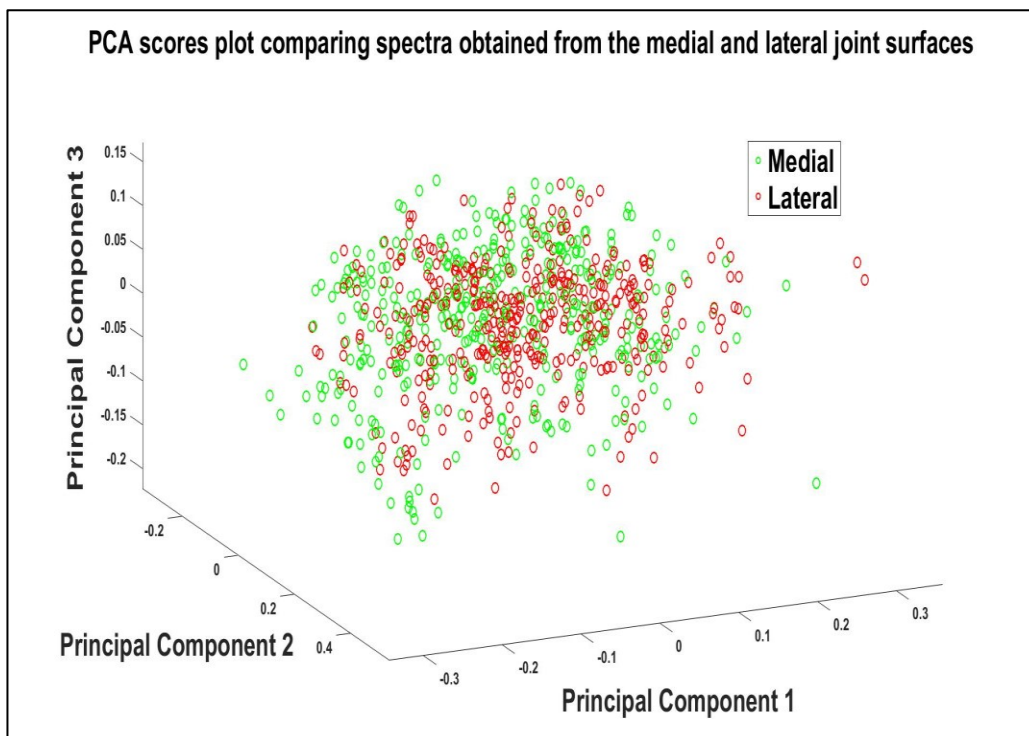


Figure 33. PCA scores plot comparing all spectra acquired from the medial and lateral subchondral bone from patients with a varus osteoarthritic wear pattern. The first 3 PCAs are represented. Spectra from medial bone are represented in green and lateral in red.

No separation was identified from multivariate analysis as illustrated in figure 33.

4.3.4 Osteoarthritis with a balanced wear pattern

4.3.4.1 OA vs matched controls univariate analysis

The following patients undergoing surgery for ankle osteoarthritis with a balanced wear pattern were age, sex and laterality matched with the following control specimens:

Patient number	Medial OA grading	Lateral OA grading	Operation	Matched control
1	2	2	Fusion	23-16 R
4	4	4	TAR	42-16 L
9	4	4	Fusion	70-16 R
12	4	3	TAR	48-16 L
13	4	3	TAR	21-16 R
14	3	4	TAR	53-16 R
15	4	3	TAR	22-16 L
18	3	4	TAR	64-16 R
21	4	4	TAR	78-14 L
23	3	4	TAR	51-16 L

Table 12. The patients recruited to the study with a balanced pattern of OA and the age, laterality and sex matched non-OA controls used. Medial and Lateral OA gradings are based on the Outerbridge classification

A suitable control could not be found for participant 24, the data collected from participant 24 was therefore excluded from the analysis comparing patients with a balanced wear pattern of osteoarthritis with age, sex and laterality matched controls. The medial and lateral OA

gradings were comparable with a median of 4 on both sides. The biochemical ratios between such patients and their controls are compared in table 13.

Cohort	Phosphate: amide I ratio	Carbonate: amide I ratio	Carbonate: phosphate ratio
Balanced OA patients	19.936+/-1.471	3.401+/-0.255	0.171+/-0.003
Matched controls	22.008+/-1.400	3.671+/-0.224	0.167+/-0.006
P value	0.01	0.034	>0.05

Table 13. Mean biochemical ratios with standard deviations shown to 3 decimal places, obtained from subchondral bone specimens obtained from patients with a balanced osteoarthritic wear pattern and compared against matched controls.

The phosphate: amide I and carbonate: amide I ratios were found to be significantly higher in the non-OA matched controls (p=0.01 and p=0.034 respectively). Although the carbonate: phosphate ratio was lower in the non-OA group, this difference was not found to be statistically significant.

Deconvolution of the amide I and phosphate peaks provided a good cumulative peak fit using 4 sub peaks in the amide I peak and 3 sub peaks in the phosphate peak. The ratios of the subpeaks 1690cm⁻¹ to 1660cm⁻¹ within the amide I peak and of subpeaks 955cm⁻¹ and 959cm⁻¹ are shown in the table 14.

Cohort	Amide I (1690:1660) ratio	Phosphate (959:955) ratio
Balanced OA patients	6.306+/-1.902	1.924+/-0.071
Matched controls	8.566+/-1.632	1.941+/-0.086
P value	0.019	>0.05

Table 14. Mean ratios with standard deviations shown to 3 decimal places, acquired from deconvolution of amide I and phosphate peaks. Specimens obtained from patients with a varus osteoarthritic wear pattern and compared against matched controls.

The amide I 1690:1660 ratio was found to be significantly lower compared to matched controls on performing the Mann-Whitney U test ($p=0.019$). The phosphate 959:955 ratio was also found to be lower in the OA group, however this difference was not found to be statistically significant.

4.3.4.2 OA vs matched controls multivariate analysis

All separate Raman spectra acquired from osteoarthritic patients with a balanced wear pattern were compared against spectra obtained from match controls. A scores plot obtained from principal component analysis is shown in figure 34.

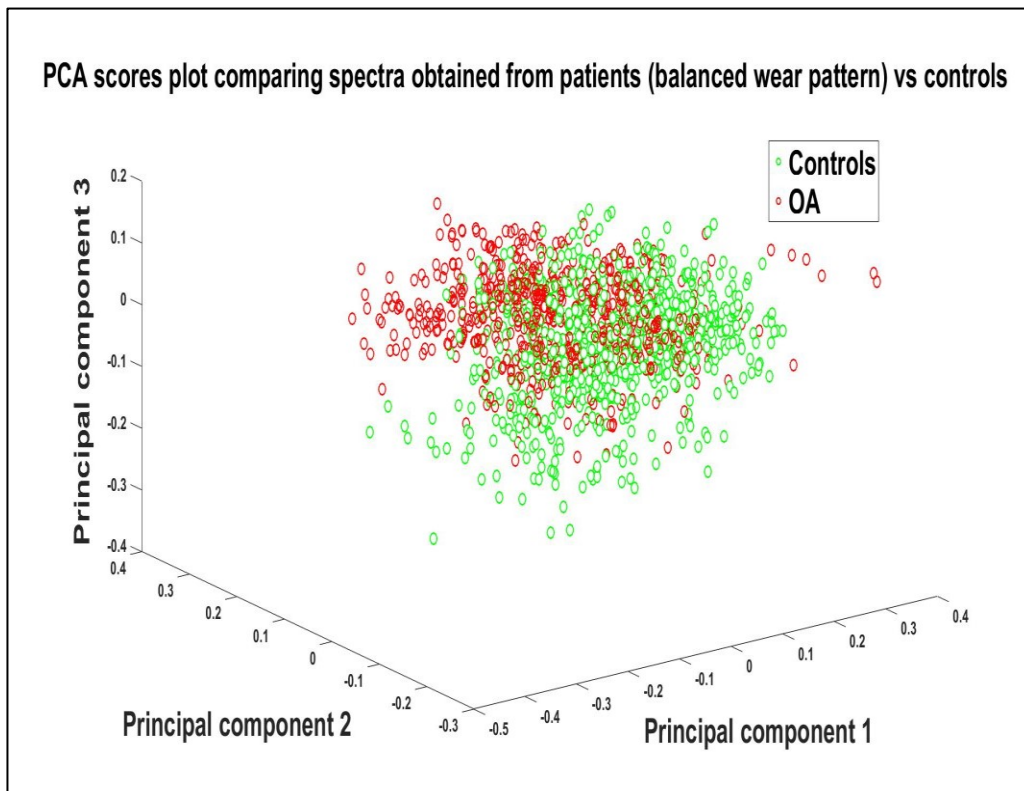


Figure 34. PCA scores plot comparing all spectra acquired from patients with a balanced osteoarthritic wear pattern with age, sex and laterality matched non-OA controls. The first 3 PCAs are represented. Spectra from controls are represented in green and patients with balanced OA in red.

Multivariate analysis with PCA did reveal some separation between the two groups as illustrated in the above figure between spectra acquired from patients with a balanced osteoarthritic wear pattern and non-OA matched cadaveric controls. The PCA loadings are shown in figure 35:

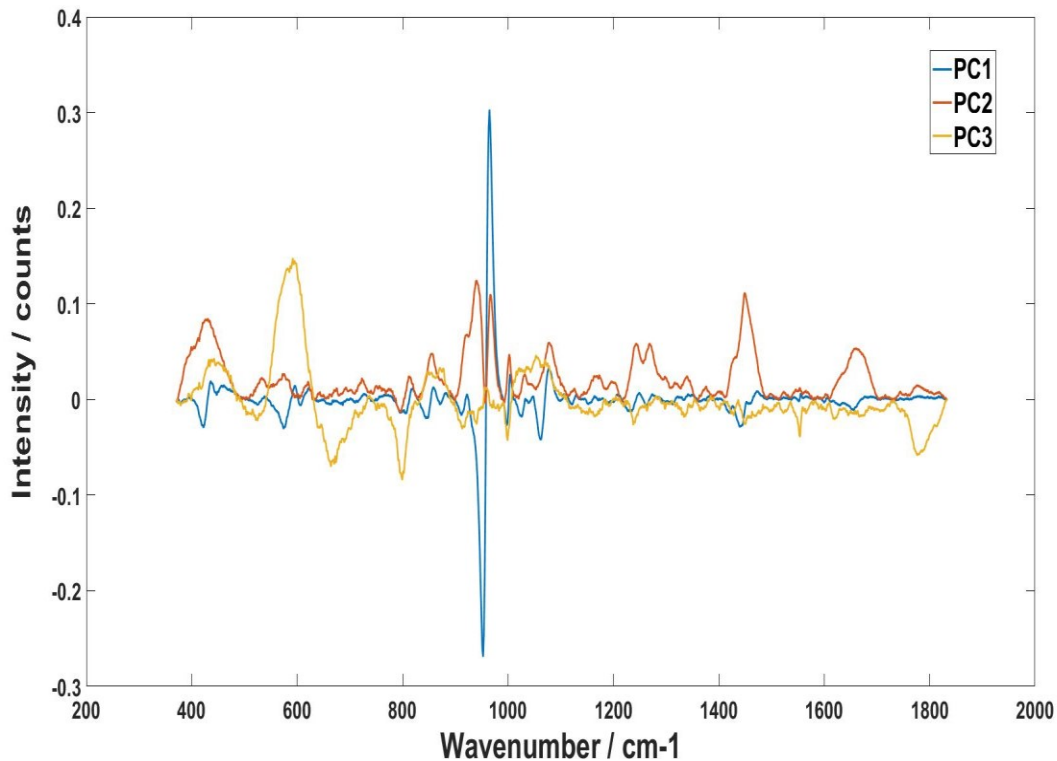


Figure 35. Graphical representation of PCA (1-3) loadings for balanced OA vs non-OA controls with their respective wavenumbers and relative intensities shown.

The loadings suggest that the for the first three principal components, differences within the phosphate, amide I, amide III and phenylalanine peaks contribute to the separation observed within the scores plot.

4.3.4.3 Medial vs Lateral subchondral bone

Subchondral bone from the medial and lateral sides was also compared. The median Outerbridge grading for the medial side and

lateral sides was 4. The mean biochemical ratios as deduced from the spectra are shown in table 15.

Cohort	Phosphate: amide I ratio	Carbonate: amide I ratio	Carbonate: phosphate ratio
Balanced OA Medial cores	19.806+/-1.928	3.369+/-0.297	0.171+/-0.005
Balanced OA lateral cores	19.674+/-1.728	3.355+/-0.311	0.171+/-0.003
P value	>0.05	>0.05	>0.05

Table 15. Mean biochemical ratios with standard deviations shown to 3 decimal places, obtained from subchondral bone specimens obtained from patients with a balanced osteoarthritic wear pattern. Subchondral bone from the medial surface is compared to subchondral bone from the lateral surface.

No statistically significant difference between subchondral bone obtained from the medial and lateral sides of the joint from patients with a balanced osteoarthritic wear pattern was identified in the biochemical ratios. The PCA scores plot obtained from principal component analysis is shown in figure 36.

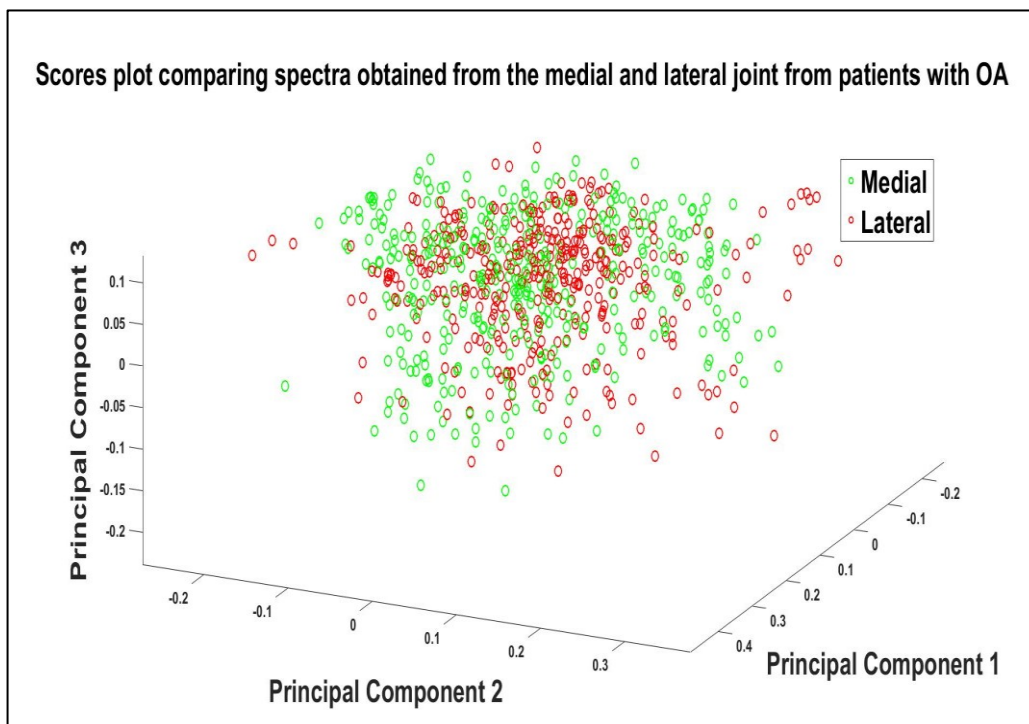


Figure 36. PCA scores plot comparing all spectra acquired from the medial and lateral subchondral bone from patients with a balanced osteoarthritic wear pattern. The first 3 PCAs are represented. Spectra from medial bone are represented in green and lateral in red.

No significant separation was identified from multivariate analysis as illustrated in figure 36.

4.4 Discussion

4.4.1 Male vs female patients and controls

No significant differences were observed in the biochemical ratios when male patients were compared to female patients and when specimens from male cadaveric controls were compared to those from female cadaveric controls. This is supported by no obvious separation when PCA was performed comparing these groups. Males are known to have greater bone mass density and bone mineral content (Nieves 2005) so one might expect to observe some differences in the phosphate: amide I ratio between the sexes. The study did not find this but is limited to the fact that the mean age of male patients was greater than their female counterparts (68.5 years vs 65.8 years). It is also known that the spectral changes are observed with increasing age. The amide I group appears particularly prone to this (Ager 2003). The cadaveric controls are also limited by numbers in this analysis as there were 7 male cadaveric controls and 5 female cadaveric controls.

4.4.2 Varus OA vs controls

The ratio parameters deduced from Raman spectroscopy revealed some interesting results. When osteoarthritic specimens from the varus and balanced osteoarthritis cohorts were compared to age, sex and laterality matched controls, statistically significant differences were observed in the phosphate: amide I ratios. The phosphate: amide I ratio is a compositional measure of the amount of mineralisation within the bone (Morris 2011). The lower phosphate: amide I ratio found within this cohort of osteoarthritic patients therefore suggests that osteoarthritic subchondral bone is hypomineralised

compared to non-osteoarthritic bone. This is consistent with the majority of literature and supports our hypothesis. Grynepas et al., 1991 assessed the mineralisation of osteoarthritic subchondral hip bone from patients undergoing total hip arthroplasty using density fractionation and chemical analysis. They found that both weight-bearing and non-weight-bearing surface subchondral bone became thickened but showed a lower degree of mineralization compared to non-OA controls. This finding is supported further by studies from Mansell et al., 1998 and more recently by Buchwald et al., 2012. Both these papers again assessed the subchondral bone from osteoarthritic hips and found OA subchondral bone to be less mineralised than controls. The hypomineralised subchondral bone observed in the osteoarthritic specimens is believed to be due to increased turnover and remodelling (Mansell 1998, Buchwald 2012), a known finding during the progression of osteoarthritis (Li 2013).

It is known that the chemical composition of long bones differs depending on location highlighting that complex adaptive changes are involved for various parts of the skeleton. It has also been suggested that a decrease in the mineral to collagen ratio could be expected to lead to a significant decrease in the Young's modulus of bone (Buckley 2012, 2014). For osteoarthritic subchondral bone, this would suggest a protective/adaptive function i.e. to aid in load transfer at the joint thereby an attempt to preserve the remaining overlying cartilage.

The results from Kearns et al., 2014, who looked at the subchondral bone from osteoarthritic knees using Raman spectroscopy contrasts with the literature as well as the results from this study with regards to osteoarthritic subchondral bone becoming hypomineralised. In their study, they observed an increase in the phosphate: amide I ratio within the subchondral bone of osteoarthritic tibias from patients undergoing total knee replacement. This difference could have arisen due to the age discrepancy of their controls. Half their controls were taken from young patients undergoing lower leg amputation and the difference in age was therefore significant. Bone mineralisation is known to increase with

age (Ager 2005) and the difference in phosphate: amide I found in their study could have been due to the significant difference in age. The other possibility for this differing trend could be due to location of osteoarthritis. Kearns et al., 2014 looked at the knee, whilst the studies suggesting hypomineralisation of osteoarthritic subchondral bone were all based on the hip joint.

The carbonate: phosphate ratios from osteoarthritic subchondral bone were found to be higher when compared to age, sex and laterally matched controls (Varus OA vs controls: 0.169 ± 0.005 vs 0.167 ± 0.005). Although the observed differences were not statistically significant, the increased ratios are consistent with increased carbonate: phosphate ratios observed within subchondral osteoarthritic hip bone when compared to non-OA hip specimens (Buchwald 2012). As discussed earlier in this section, it is believed that osteoarthritic subchondral bone becomes hypomineralised because of increased turnover and remodelling (Mansell 1998, Buchwald 2012). It is believed that carbonate ions replace the lost phosphate ions within apatite crystals in an attempt to limit mineral loss during this decline in mineralization (Buchwald 2012).

The carbonate: amide I ratios from osteoarthritic subchondral bone (both varus and balanced OA) were found to be significantly lower compared to non-osteoarthritic cadaveric controls. This was not supportive of the hypothesis and goes against the increased carbonate: amide I ratio observed in osteoarthritic knees (Kearns 2014). The carbonate: amide I is believed to be a marker of bone remodelling (McCredie 2006) and as bone remodelling is known to be increased in osteoarthritic bone (Mansell 1998, Buchwald 2012), one would expect the carbonate: amide I ratio to be higher in osteoarthritic bone. This unexpected result from this study could be explained by a greater increase in our Amide I peak intensities within our osteoarthritic subchondral bone relative to the carbonate peak on spectral analysis. This would imply that the amide I group (a marker of collagen secondary structure) could be altered to a greater extent in osteoarthritis of the ankle compared to the knee. Another possibility

for the unexpected difference in the carbonate: amide I ratios may be due to specimen age. Although the patient osteoarthritic specimens were age matched to within 8 years, the age of cadaveric donors was generally older (mean of 67.2 years in the osteoarthritic group vs 71.75 years in the cadaveric control group). In male cortical bone, skeletal mineralization and mineral carbonation is thought to increase with age (Mandair 2015) and the observed difference may be because of this difference in age between the osteoarthritic patients and control specimens.

Analysis of sub-peaks in the amide I region obtained through deconvolution of the Raman spectra revealed a statistically significant decrease in the ratio of the 1660:1690 peaks. The 1660 cm^{-1} peak is the strongest amide I component whereas the 1690 cm^{-1} peak is believed to correlate with immature cross-links within collagen and relates to a disordered secondary structure (Mandair 2015). A decrease in the 1660:1690 peak ratio therefore suggests a relative increase in the levels of immature cross-links within the collagen secondary structure. This finding taken in combination with a decreased phosphate: amide I ratio would suggest that OA is associated not only with hypomineralised subchondral bone but also with a disordered secondary matrix structure. Although hypomineralised bone is associated with a decreased Young's modulus and may therefore preserve the joint, its protective effect may be limited by a disordered matrix secondary structure which has been postulated to lead to increased stiffness and brittleness, limiting the intrinsic capacity of energy dissipation of the bone matrix (Pezzotti 2017).

Deconvolution of the phosphate region and analysis of the peaks did not reveal a statistically significant difference in the 959:955 peak ratios between varus OA and matched non-OA controls. The main peak at 959 cm^{-1} is associated with mature bone mineral whereas that of 955 is believed to represent immature mineral (Mandair 2015). Although the lower phosphate: amide I ratios observed in our OA samples indicate hypomineralisation, spectral deconvolution of the

phosphate peak suggests that the proportions of mature and immature mineral are not changing when compared to non-OA controls.

The differences identified through univariate analysis were also supported by those gained from multivariate analysis. Principal component analysis performed for all spectra acquired from varus OA patients and matched controls did reveal some separation in the first three principal components. The plotting of PC loadings also revealed contributions to the inherent differences in the spectra primarily attributable to the phosphate, amide I, amide III and phenylalanine regions. There was however also significant overlap between the two groups as shown on the scores plot (Figure 31). When compared to the analysis of subchondral bone taken from knee osteoarthritis by Kearns et al., 2014, a comparative scores plot of OA vs controls appears to separate with less overlap (Figure 37).

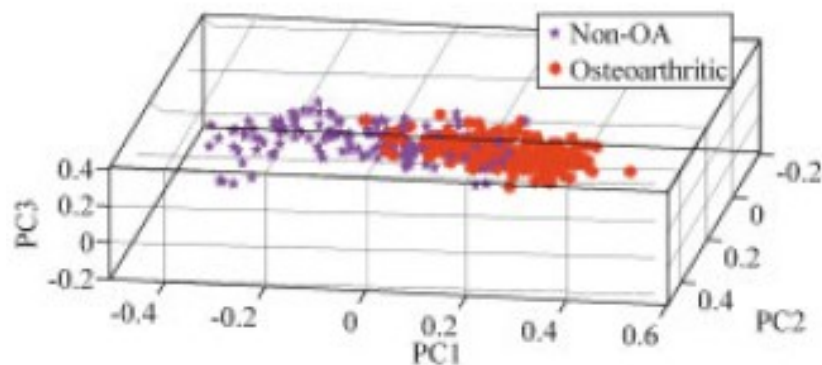


Figure 37. PCA scores plot for knee OA specimens vs non-OA controls. OA specimens are shown in red. Adapted from Kearns et al., 2014.

This observed difference may be due to the inherent difference in aetiology for osteoarthritis at the two different joints. Whereas knee OA is predominantly primary with a lower incidence of secondary OA due to trauma/inflammation, ankle osteoarthritis primarily has a strong association with trauma (Barg 2013, Valderabano 2009) with a much lower incidence of primary OA-believed to be under 10% (Valderabano 2009). If we accept the premise that individuals with certain subchondral bone chemistry are predisposed to developing

osteoarthritis, then this could account for the difference observed in the study on OA knees (Kearns 2014) and the results from this study. The relatively small overlap seen between OA and non-OA knees could be accounted for by a small number of patients who may have developed OA of the knee due to trauma/inflammation but were otherwise not predisposed to develop OA.

This could also hold true for the results observed in this study for ankle osteoarthritis. As primary ankle osteoarthritis is thought to be relatively uncommon compared to trauma related ankle osteoarthritis (Barg 2013, Brockett 2016, Valderrabano 2009), the overlap is therefore greater i.e. there are more patients with ankle osteoarthritis who have a similar subchondral bone chemistry to the non-OA controls however they may develop ankle OA due to preceding trauma.

4.4.2.1 Medial vs lateral subchondral bone in patients with varus OA

No significant differences were observed in the phosphate: amide I, carbonate: amide I or carbonate: phosphate ratios when subchondral bone taken from the medial tibial plafond was compared to bone taken from the lateral tibial plafond in patients with a varus pattern of wear. Such results support the hypothesis that there are no differences in biochemical composition between subchondral bone acquired from the medial and lateral joint areas of the joint regardless of differences to macroscopic articular cartilage wear.

Patients with a varus pattern of wear have an asymmetrically affected joint surface i.e. osteoarthritis predominantly affects the medial compartment of the ankle. Our results therefore indicate that subchondral bone changes associated with osteoarthritis are present even in areas of the joint with relatively well preserved macroscopic joint surfaces. These results are in keeping with the study of osteoarthritic knees in which subchondral bone from patients undergoing total knee replacement for osteoarthritis (with

predominantly varus or medial compartment osteoarthritis) was analysed using Raman spectroscopy (Kearns 2014). Subchondral bone from the greater affected medial side was compared to that of the relatively unaffected lateral side and no significant difference was found in various spectroscopic measures. These findings can be explained by the concept that subchondral bone changes precede macroscopic joint surface changes and that osteoarthritis is a “whole joint” disease.

4.4.3 Balanced OA vs controls

The results when comparing subchondral bone specimens obtained from balanced OA specimens to matched controls showed a statistically significant decrease in the phosphate: amide I ratio and an increased carbonate: amide I ratio. This mirrors the findings from the varus OA cohort and the reasons as to why these ratios are altered in the balanced OA cohort also mirrors the previously discussed possibilities i.e. osteoarthritic subchondral bone appears to be hypomineralised and that the raised carbonate: amide I ratio could indicate that the amide I region is altered to a greater extent in ankle osteoarthritis relative to the carbonate group.

Analysis of amide I and phosphate peaks revealed a statistically significant decrease in amide I 1960:1990 sub peak ratio and no statistical difference in the phosphate 959:957 band ratio. This again mirrors the results obtained from the varus OA cohort and suggests that OA subchondral bone has a disordered secondary matrix structure associated with more immature cross links but no increase in the amount of immature mineral.

The differences observed through univariate analysis are supported by the results of principal component analysis. A separation was observed between balanced OA specimens and matched controls albeit with some overlap. This once again mirrors the findings

from the varus OA cohort and when compared to samples taken from the knee do not as much of a separation on the scores plot.

4.4.3.1 medial vs lateral subchondral bone in patients with balanced OA

No significant differences were observed in the biochemical markers when subchondral bone from the medial tibial plafond was compared to that of the lateral tibial plafond. This was supported by no obvious separation on principal component analysis. When taken together with comparable results obtained from patients with varus OA, this is in keeping with the notion that osteoarthritis of the ankle is a whole joint disorder and supports the hypothesis that there are no differences in biochemical composition between subchondral bone acquired from the medial and lateral joint areas of the joint

4.4.4 Summary of Raman results/Conclusion

Raman spectra acquired from subchondral bone specimens from osteoarthritic ankle samples show changes when compared to non-OA controls. This is evident from both multivariate analysis as well as univariate analysis in the form of biochemical ratios. Notably osteoarthritic samples were found to have a decreased phosphate: amide I and decreased carbonate: amide I ratios. Spectral deconvolution of the amide I band was also suggestive of increased levels of immature cross-links as well as a disordered secondary structure within OA subchondral bone. These biochemical markers suggest changes to both the mineral and matrical elements of subchondral bone. Osteoarthritis of the ankle like osteoarthritis of the knee appears to be a whole joint disease with even the subchondral bone from the relatively unaffected lateral side in varus OA displaying no difference to the more severely affected medial side. The same changes were common to both osteoarthritic cohorts (varus and

balanced wear) suggesting that these two cohorts are the same disease entity differing perhaps only with respect to different injured ligamentous and soft tissue support structures resulting in the different wear patterns as implicated by Barg et al., 2013.

CHAPTER 5- BIOCHEMICAL ANALYSIS OF SAMPLES

5.1 Introduction

SDS-PAGE (sodium dodecyl sulphate-polyacrylamide gel electrophoresis) is a commonly used technique used to separate proteins based on their molecular weight in a polyacrylamide gel. In this technique, the normally amphoteric proteins are mixed with SDS (sodium dodecyl sulphate) to acquire a net negative charge and in the presence of an electric field, causing the proteins to move towards the positively charged anode. Proteins of different molecular weight separate in the gel as the relative migration distance (Rf) is inversely proportional to the log of its weight. SDS-PAGE can be used to estimate the molecular weights of proteins and to determine the relative quantities of major proteins within a sample.

The Biochemical analysis of subchondral bone samples was undertaken to detect sample levels of mineralisation as well as provide information regarding the type I collagen quaternary structure, notably the α -1 to α -2 chain ratios which would provide an indication of the quantity of α -1 homotrimers within the type I collagen. Furthermore, biochemical analysis would help to validate and support the results obtained from Raman spectroscopy.

Previous studies investigating the structure and composition of osteoarthritic subchondral bone have found several differences compared to non-osteoarthritic bone including hypomineralisation of bone (Grypnas 1991, Cucchiarini 2016) and increased levels of type I collagen containing α -1 homotrimers (Bailey 2002, Kearns 2014). Bone hypomineralisation is believed to be as a result of increased levels of the type I collagen homotrimer because of altered osteoblast phenotypes (Coucherel 2009) and therefore being less readily mineralised than the normal subtype (Cucchiarini 2016). Such studies however have assessed bone acquired from the hip and the knee and no such published work has investigated the levels of subchondral

bone mineralisation or attempted to quantify the α -1 to α -2 type I collagen ratios in the context of the ankle joint.

5.2 Methods

Following acquisition of Raman spectra from the osteoarthritic and non-osteoarthritic samples, the specimens underwent biochemical analysis. Osteoarthritic specimens from patients with varus and symmetrically loaded wear patterns were compared to age (within 8 years), sex and laterality matched controls. Samples were matched to the same controls as per analysis with Raman spectroscopy.

5.2.1 Mineral content

Following delipidation of subchondral bone (as described in chapter 4) and acquisition of Raman spectra, samples were freeze dried under vacuum for 24 hours at a pressure of 0.02mBar. The cores were then ground using a pestle and mortar (to increase then surface area for digestion by pepsin) and weighed using a digital balance (approximate weight of samples 20-30 mg). Following this the specimens were decalcified by being immersed in 5 ml of 10% ethylenediamine tetra-acetic acid (EDTA), pH 7.5 for 7 days at 20°C on a roller. Samples were then spun in a centrifuge at 3000 rpm for 5 minutes and the EDTA removed from the pellet. The bone pellet was rinsed with 5ml of deionised water to remove EDTA and re-centrifuged. Rinsing with fresh deionised water was repeated a further two times and the supernatant removed. The bone pellets were freeze-dried for a further 24 hours to remove the deionised water and a dry-weight of decalcified samples was obtained using a digital balance. The mineral weight per sample was calculated by subtracting the post-EDTA weight by the pre-EDTA weight and a percentage of mineral present in the samples was determined. Mineral content was expressed as a percentage of the dry weight of bone tissue.

The degree of mineralisation from samples with varus and balanced osteoarthritis wear patterns was compared to age (within 8 years), sex and laterality matched non-osteoarthritic controls. Statistical significance was assessed using the Mann Whitney U-test and $P < 0.05$ was taken to be statistically significant.

5.2.2 SDS-PAGE

In order to release the type I collagen chains within the samples, the demineralised dry specimens were digested using porcine pepsin. 5 mg of dry weight porcine pepsin were dissolved in 0.5M acetic acid to produce a pepsin solution with a concentration of 25 µg/ml (3200-4500 units/mg). 1ml of the final pepsin solution for every 5 milligrams of demineralised sample was added. Pepsin digestion was carried out for 48 hrs at 4°C with gentle agitation. Following this, the samples were centrifuged at 3,000 revolutions per minute for 30 minutes to isolate the collagen containing supernatant. The supernatant was subsequently removed and freeze-dried for 24 hours. The resulting protein samples were dissolved in 0.25mls of Sodium dodecyl sulphate–polyacrylamide gel electrophoresis (SDS-PAGE) sample buffer (composition: 125mM tris(hydroxymethyl)aminomethane, 2% Sodium dodecyl sulphate, 10% Glycerol, 0.01% bromophenol blue) for smaller samples or 0.5mls of SDS-PAGE sample buffer for larger samples.

SDS-PAGE electrophoresis was performed using a Mini-Protean II apparatus (Bio-Rad, UK). Two precast 7.5% polyacrylamide gels (Bio-Rad Mini-PROTEAN TGX Stain-Free Gels) were inserted into the apparatus. 10 microlitres of each sample was exclusively inserted into a single well using a micro pipette. Type I collagen standards prepared from rat and human skin as well as molecular weight markers (Kaleidoscope – Bio-Rad Precision Plus Protein Standards Catalog #161-0375) were inserted into wells alongside the samples. Current was applied to the gels (40mA or 20mA per gel)

until the dye front reached the end of the gel. After electrophoresis, the gels were stained with Coomassie blue (0.005%) to visualize protein for 24 hours at room temperature, and then destained with 10% acetic acid and 20% methanol solution for a further 24 hours at room temperature.

Following staining and destaining, a digital image of the gel was obtained (Figure 38). The migration distance of the protein bands (Rf) from the molecular weight standards were plotted against their $\log(\text{MW})$ (logarithm of their known molecular weights). A line of best fit was applied, and the resultant line equation was used to estimate the molecular weights of the $\alpha 1$ and 2 chains. ImageJ software was then used to quantify the relative intensities of the α -1 and 2 chain bands. Given the lower molecular weight of the α -2 chain, a correction factor of (α -1 molecular weight/ α -2 molecular weight) was applied when calculating the relative intensities.

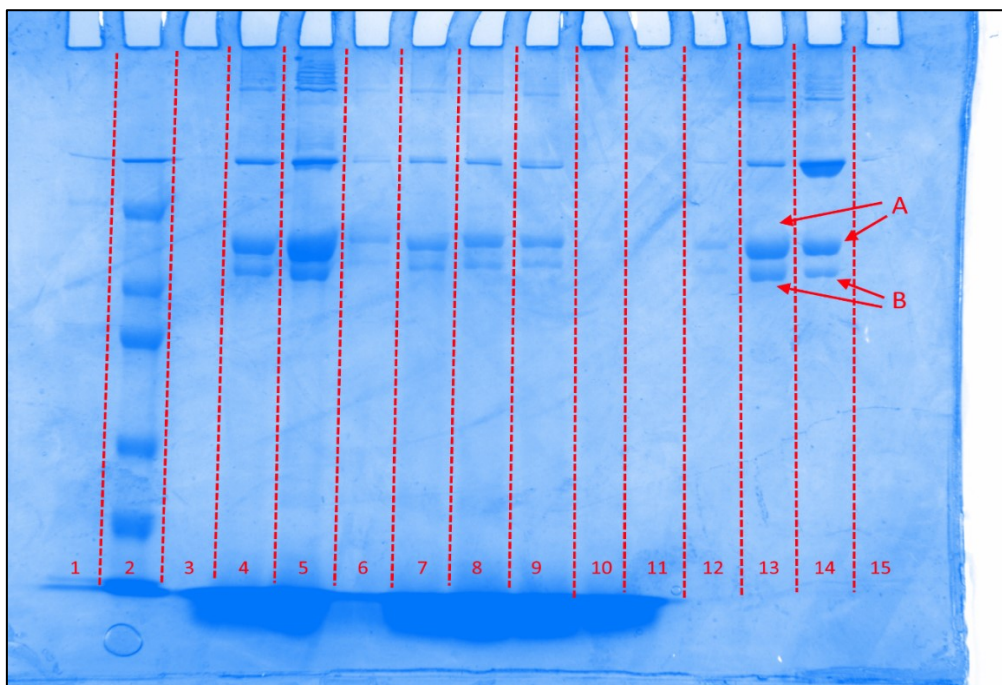


Figure 38. An image of a gel obtained following SDS-PAGE, staining with Coomassie Blue and subsequent destain. The separate lanes are annotated with the red dashed lines and example alpha-1 (A) alpha-2 (B) collagen bands are shown. Lane 2 in the example above shows the stained molecular weight marker whilst lanes 4 and 5 show the human and rat collagen standards. Lanes 10 and 11 are examples of when samples did not produce readable bands.

The α 1:2 chain ratios from samples with varus and balanced osteoarthritis wear patterns were compared to age (within 8 years), sex and laterality matched non-osteoarthritic controls. Statistical significance was assessed using the Mann Whitney U-test and $P < 0.05$ was taken to be statistically significant.

5.3 Results

The quantity of bone collected intra-operatively from patients undergoing open ankle fusion was insufficient to analyse biochemically and were therefore excluded from biochemical analysis. Patient specimens without a matched control also did not undergo biochemical analysis. This left 16 patient samples (8 with a varus wear pattern and 8 with a balanced wear pattern) and their matched controls for biochemical comparison. These are shown in tables 16 and 17.

5.3.1 Specimen levels of mineralisation

The samples weights before and after demineralisation by EDTA and the proportion of mineral within each sample is shown in Tables 16 and 17.

5.3.1.1 Varus OA vs Matched controls

Sample	pre-EDTA weight (g)	post-EDTA weight (g)	mineral weight (g)	Percentage mineral of sample total
OA specimens				
2M	0.0499	0.0118	0.0381	76.36
2L	0.0368	0.0094	0.0274	74.43
5M	0.0347	0.0088	0.0259	74.63
5L	0.0357	0.0095	0.0262	73.39
6M	0.0468	0.015	0.0318	67.95
6L	0.0508	0.0151	0.0357	70.28
10M	0.0406	0.0106	0.0300	73.89
10L	0.0236	0.0061	0.0175	74.19
16M	0.0375	0.0099	0.0276	73.60
16L	0.0352	0.0101	0.0251	71.31
17M	0.0124	0.0039	0.0085	68.55
17L	0.0182	0.0063	0.0119	65.46
22M	0.0328	0.0076	0.0252	76.83
22L	0.0504	0.0119	0.0385	76.40
25M	0.0596	0.0148	0.0448	75.16
25L	0.0297	0.0072	0.0225	75.73
Mean				73.01
Non-OA controls				
21-16 L medial	0.0532	0.0144	0.0388	72.95
21-16L Lateral	0.0521	0.0136	0.0385	73.90
23-16 L medial	0.0201	0.0050	0.0151	75.10

23-16 L lateral	0.0376	0.0094	0.0282	75.02
64-16 L medial	0.0366	0.0081	0.0285	77.89
64-16 L lateral	0.0342	0.0078	0.0264	77.17
42-16 L medial	0.0536	0.0139	0.0397	74.07
42-16 L lateral	0.0601	0.0147	0.0454	75.54
53-16 R medial	0.0652	0.0182	0.0470	72.09
53-16 R lateral	0.0510	0.0138	0.0372	72.94
48-16 R medial	0.0215	0.0061	0.0154	71.56
48-16 R lateral	0.0077	0.0021	0.0056	72.83
78-14 L medial	0.0636	0.0145	0.0491	77.19
78-14 L lateral	0.0710	0.0173	0.0537	75.63
10-16 L medial	0.0302	0.0073	0.0229	75.83
10-16L lateral	0.0201	0.0052	0.0149	74.13
Mean				74.62

Table 16. Sample weights (in grams to 4 decimal places) and mineral content (expressed as percentage to 2 decimal places) of bony specimens taken from patients with a varus osteoarthritic wear pattern and with their corresponding age, sex and laterality matched controls. Pre and post EDTA weights are shown after the samples were freeze-dried.

The mean percentage mineral content within the osteoarthritic specimens with a varus wear pattern was 73.01% (Standard Deviation 3.36) and was found to be lower when compared to the mean from the matched controls (74.62%, standard deviation 1.88). However, this was not found to be a statistically significant ($p=0.29834$). No significant difference was observed in the proportion of mineral

between samples taken from the medial or lateral joint from patients with a varus osteoarthritis wear pattern (medial mean = 73.37%, lateral mean = 72.65%)

5.3.1.2 Balanced OA vs Matched controls

Sample	pre-EDTA weight (g)	post-EDTA weight (g)	mineral weight (g)	Percentage mineral of sample total
OA specimens				
4M	0.0363	0.0092	0.0271	74.66
4L	0.0423	0.0092	0.0331	78.25
12M	0.0425	0.0131	0.0294	69.18
12L	0.0524	0.0178	0.0346	66.00
13M	0.0450	0.0132	0.0318	70.69
13L	0.0340	0.0114	0.0226	66.46
14M	0.0363	0.0101	0.0262	72.18
14L	0.0537	0.0152	0.0385	71.69
15M	0.0208	0.0063	0.0145	69.65
15L	0.0408	0.0142	0.0266	65.22
18M	0.0403	0.0119	0.0284	70.49
18L	0.0575	0.0121	0.0454	78.96
21M	0.0330	0.0093	0.0237	71.82
21L	0.0295	0.0090	0.0205	69.49
23M	0.0525	0.0127	0.0398	75.82
23L	0.0505	0.0113	0.0392	77.60
Mean				71.76
Non-OA controls				
42-16 L medial	0.0536	0.0139	0.0397	74.07

42-16 L lateral	0.0601	0.0147	0.0454	75.54
48-16 L medial	0.0208	0.0060	0.0148	71.11
48-16 L lateral	0.0165	0.0041	0.0124	75.11
21-16 R medial	0.0420	0.0104	0.0316	75.21
21-16 R lateral	0.0677	0.0175	0.0502	74.14
53-16 R medial	0.0625	0.0182	0.0443	70.88
53-16 R lateral	0.0510	0.0138	0.0372	72.94
22-16 L medial	0.0234	0.0065	0.0169	72.27
22-16 L lateral	0.0337	0.0088	0.0249	73.92
64-16 R medial	0.0380	0.0084	0.0296	77.90
64-16 R lateral	0.0515	0.0107	0.0408	79.23
78-14 L medial	0.0636	0.0145	0.0491	77.19
78-14 L lateral	0.0710	0.0173	0.0537	75.63
51-16 L medial	0.0413	0.0106	0.0307	74.33
51-16 L lateral	0.0432	0.0117	0.0315	72.92
Mean				74.52

Table 17. Sample weights (in grams to 4 decimal places) and mineral content of bony specimens (expressed as % to 2 decimal places) taken from patients with a balanced osteoarthritic wear pattern and with their corresponding age, sex and laterality matched controls. Pre and post EDTA weights are shown after the samples were freeze-dried.

The mean percentage mineral content within the osteoarthritic specimens with a balanced wear pattern was 71.76% (Standard deviation 4.92) and was found to be lower when compared to the mean from the matched controls (74.52%, standard deviation: 2.30). This difference was found to be statistically significant ($p=0.03662$). No significant difference was observed in the proportion of mineral between samples taken from the medial or lateral joint from patients with a balanced osteoarthritis wear pattern (Medial mean = 71.81%, Lateral mean = 71.71%).

5.3.2 SDS-PAGE results

The molecular weight standard migration distance line is shown below in Figure 39.

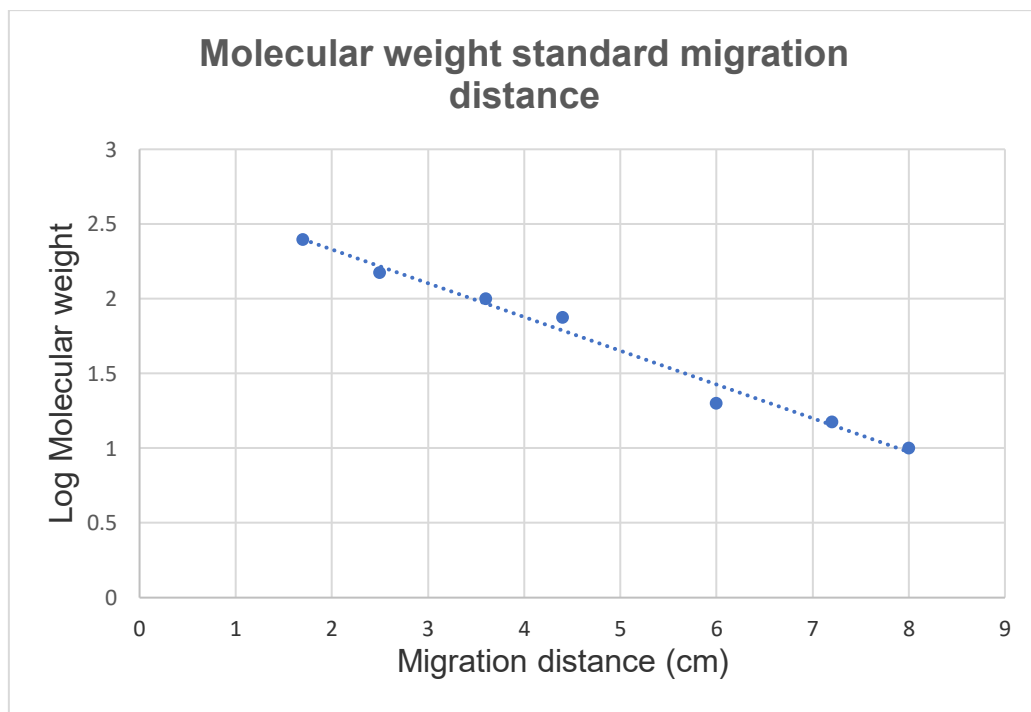


Figure 39. Migration distance (Rf) in cm of the molecular weight standard bands plotted against the Logarithm of their known molecular weights. The dashed line in blue represents the line of best fit.

The equation of the line of best fit was calculated to be where x is the migration distance in cm and y is the logarithm of the molecular weight:

$$y = -0.2258x + 2.7814$$

The equation was used to deduce the molecular weights of the α -1 and α -2 bands. This was calculated as 120Kda for the α -1 band and 109Kda for the α -2 band.

Almost all specimens obtained from patients with ankle osteoarthritis produced readable α -1 and α -2 bands on gels post SDS-PAGE. This contrasts to the non-osteoarthritis controls in which 13 (50%) produced α -1 and α -2 bands below the levels of detection (Table 18) under the conditions used. Given the slight difference in molecular weights between α -1 and α -2 bands, a correction factor of 1.1 was used in the quantification of the α -2 band.

Sample	α-1: α-2 ratio	Control sample	α-1: α-2 ratio
2M	1.64:1	10-16 L medial	Not detected
2L	2.25:1	10-16 L lateral	Not detected
4M	2.51:1	42-16 L medial	1.68:1
4L	2.59:1	42-16 L lateral	1.58:1
5M	Not detected	51-16 L medial	Not detected
5L	1.87:1	51-16 L lateral	Not detected
6M	2.70:1	53-16 R medial	Not detected
6L	1.86:1	53-16 R lateral	Not detected
10M	Not detected	78-14 L medial	1.12:1
10L	Not detected	78-14 L lateral	1.08:1
12M	1.90:1	64-16 R medial	1.83:1

12L	2.00:1	64-16 R lateral	1.34:1
13M	2.64:1	64-16 L medial	1.80:1
13L	2.54:1	64-16 L lateral	1.88:1
14M	2.08:1	21-16 R medial	Not detected
14L	2.05:1	21-16 R lateral	Not detected
15M	2.16:1	21-16 L medial	Not detected
15L	1.95:1	21-16 L lateral	Not detected
16M	2.52:1	22-16 L medial	1.39:1
16L	3.25:1	22-16 L lateral	1.43:1
17M	2.94:1	23-16 L medial	Not detected
17L	2.05:1	23-16 L lateral	Not detected
18M	1.86:1	48-16 R medial	1.75:1
18L	2.04:1	48-16 R lateral	Not detected
21M	Not detected	48-16 L medial	1.38:1
21L	2.64:1	48-16 L lateral	1.46:1
22M	2.12:1		
22L	1.92:1		
23M	1.93:1		
23L	1.96:1		
25M	2.32:1		
25L	2.21:1		
Mean ratios	2.23:1		1.52:1

Table 18. Table showing α -1 to α -2 band ratios quantified following SDS-PAGE from osteoarthritic patient samples and non-osteoarthritic control specimens. Ratios are shown to 2 decimal places.

Due to the lack of controls producing readable bands, osteoarthritic samples as a general group were compared to the control samples which produced readable bands i.e. Varus-wear OA and balanced-OA samples were grouped together for analysis.

Osteoarthritic specimens had a higher mean α -1: α -2 collagen ratio (mean: 2.23:1, standard deviation: 0.380) compared to non-osteoarthritic controls (mean: 1.52:1, standard deviation: 0.262). This difference was found to be statistically significant ($p < 0.0001$).

The α -1: α -2 collagen ratios from the medial joint were compared to results obtained from the lateral joint for samples obtained from patients with a varus and balanced osteoarthritic wear pattern. The results are shown below in tables 19 and 20.

Medial specimen	α -1: α -2 ratio	Lateral specimen	α -1: α -2 ratio
2	1.64:1	2	2.25:1
5	Not detected	5	1.87:1
6	2.70:1	6	1.86:1
10	Not detected	10	Not detected
16	2.52:1	16	3.25:1
17	2.94:1	17	2.05:1
22	2.12:1	22	1.92:1
25	2.32:1	25	2.21:1
Mean	2.37:1		2.20:1

Table 19. α -1: α -2 collagen ratios quantified from SDS-PAGE gels. Samples are from patients with a varus-OA wear pattern, taken from the medial and lateral sides of the joint. α -1: α -2 ratios have been rounded to 2 decimal places.

Medial specimen	α -1: α -2 ratio	Lateral specimen	α -1: α -2 ratio
4	2.51:1	4	2.59:1
12	1.90:1	12	2.00:1
13	2.64:1	13	2.54:1
14	2.07:1	14	2.42:1
15	2.16:1	15	1.94:1

18	1.86:1	18	2.03:1
21	Not detected	21	2.64:1
23	1.93:1	23	1.96:1
Mean	2.15:1		2.27:1

Table 20. α -1: α -2 collagen ratios quantified from SDS-PAGE gels. Samples are from patients with a balanced-OA wear pattern, taken from the medial and lateral sides of the joint. α -1: α -2 ratios have been rounded to 2 decimal places.

No differences were observed in the mean α -1: α -2 ratios taken from the medial and lateral joint for patients with both varus and balanced wear patterns, these were not found to be statistically significant.

5.4 Discussion

5.4.1 Levels of mineralisation

The results revealed that osteoarthritic specimens were found to have lower levels of mineralisation when compared to age (to within 8 years), sex and laterality matched controls. This was the case for both the varus and balanced wear groups with the later showing a statistically significant difference ($p= 0.035$) and was supportive of the hypothesis. Results were in keeping with significantly lower phosphate: amide I ratios deduced from Raman spectroscopy for osteoarthritic specimens which is also a marker of bone mineralisation.

The vast majority of literature has reported an association between hypomineralisation of subchondral bone with osteoarthritis. Grynpas et al., 1991 analysed subchondral hip bone from patients undergoing total hip arthroplasty using density fractionation and chemical analysis. They found that both weight-bearing and non-

weight-bearing surface subchondral bone became thickened but showed a lower degree of mineralization compared to non-OA controls. A study employing Raman spectroscopy to assess the compositional and structure of bone within the hip has also suggested that osteoarthritis is associated with hypomineralised subchondral bone (Buchwald 2012). Such changes are believed to be due to increased turnover and remodelling, a known finding during the progression of osteoarthritis (Li 2013) as well as the belief that increased levels of the α -1 homotrimer of type I collagen are not as readily mineralised as the normal type (Cucchiaroni 2016). As a consequence of hypomineralisation, osteoarthritic subchondral bone is believed to have a lower Young's modulus and has been shown using mechanical testing to be less stiff (Li 1997).

The results regarding levels of subchondral bone mineralisation contrasts with a single study utilising Raman spectroscopy to investigate the subchondral bone of osteoarthritic knees (Kearns 2014). In this study the authors observed increases in the phosphate: amide I ratios of osteoarthritic subchondral bone which is suggestive of bone hypermineralisation. Although this difference could be due to the different anatomical location of the joint being investigated, it could have also arisen due to a significant difference in the age of some of their controls. Half the control cohort within this study consisted of samples acquired from young patients undergoing lower leg amputation with bone mineralisation known to increase with age (Ager 2005).

No significant difference was observed in the levels of mineralisation from specimens taken from the medial or lateral joint for patient specimens with a varus or balanced wear pattern. In view of this finding in the relatively spared lateral joint surface from patients with a varus wear pattern, this would suggest that changes to the mineral content and/or cell metabolism/turnover within subchondral bone may occur before macroscopic evidence of the disease develops. This once again supports the notion that subchondral bone

changes develop in the whole joint irrespective of the degree of cartilage damage.

5.4.2 SDS-PAGE Results

The vast majority of osteoarthritic specimens produced stainable and readable α -1 and α -2 bands after SDS-PAGE was performed. This contrasts to 50% of the non-osteoarthritic controls producing interpretable bands. Interestingly, when subchondral knee specimens acquired from non-osteoarthritic controls i.e. both frozen cadaveric samples and fresh specimens obtained from patients undergoing above knee amputation (Gikas 2013) were processed and analysed using SDS-PAGE, the vast majority did not produce any readable bands following staining. This suggests that the difference in producing results may either be due to an inherent difficulty in isolating the collagen subunits from non-osteoarthritic specimens i.e. digestion of collagen using pepsin or inherent differences in the quantity or quality of collagen within osteoarthritic and non-osteoarthritic subchondral bone.

Indeed, increased turnover and remodelling are observed within osteoarthritic subchondral bone (Li 2013, Mansell 1998) including increased collagen synthesis (Bailey 2002, Cucchiari 2016) and this increased availability of collagen may explain why SDS-PAGE produced results more readily in the osteoarthritic specimens in this study as well as the aforementioned study analysing knee specimens (Gikas 2013).

After analysing the SDS-PAGE gels, the osteoarthritic specimens were found to have a higher α -1: α -2 ratio (mean of 2.23:1) when compared to the non-osteoarthritic controls (mean of 1.52:1) and was supportive of the hypothesis. However as only 50% of the control samples produced results, the controls were not necessarily age, sex and laterality matched. Despite this, the difference was found to be statistically significant. This increase in α -1: α -2 ratio suggests that the osteoarthritic specimens may have raised levels of α -1

collagen sub-units due to the presence of α -1 collagen homotrimers. Such results are consistent with increased α -1: α -2 ratios observed within bone from the osteoarthritic knee (Kearns 2014) and osteoarthritic hip (Bailey 2002) and suggest that alterations to the collagen structure are inherently associated with the osteoarthritic process irrespective of the joint affected. Furthermore, subchondral bone with this homotrimeric form of collagen type I is noted to have a reduced Young's modulus which may contribute to the progression of osteoarthritis (Li 2013).

The increased α -1: α -2 ratio was not as high as that reported in other studies. Kearns et al., 2014 who looked at osteoarthritic knee specimens had a ratio in the range of 1.58-9.09:1 whilst Bailey et al., 2002 who investigated the α -1: α -2 ratio in osteoarthritic hip bone was reported as a range of 4-17:1. Although such differences may be related to the fact that bone originated from different joints, the different methodologies may have had a greater impact. Bailey's study for example analysed cancellous bone rather than subchondral bone. Various differences in SDS-PAGE methodology may also have existed between the different studies.

No statistically significant difference was noted in the α -1: α -2 ratios between samples taken from the medial and lateral sides of the joint from osteoarthritic specimens. This included samples with a predominant varus wear pattern which have an asymmetrically affected joint surface i.e. osteoarthritis predominantly affects the medial compartment of the ankle. Our results therefore indicate that such subchondral bone changes associated with osteoarthritis are present even in areas of the joint with relatively well preserved macroscopic joint surfaces. This finding can be explained by the fact that subchondral bone changes develop in the whole joint irrespective of the degree of cartilage damage and support the possibility that subchondral bone changes precede macroscopic joint surface changes.

5.4.3 Summary of Biochemistry Results

Biochemical analysis of subchondral bone from osteoarthritic revealed that osteoarthritic specimens were hypomineralised compared to matched non-osteoarthritic controls. Further differences were elucidated from SDS-PAGE analysis revealing a significantly greater α -1: α -2 type I collagen ratio in osteoarthritic specimens. Furthermore, biochemical changes were also present in areas of the joint with relative cartilaginous sparing (i.e. lateral joint surface in patients with a varus wear pattern).

Biochemical results were supportive and complimentary of information inferred from Raman spectroscopy. The lower phosphate: amide I ratios calculated from spectra acquired from osteoarthritic specimens were suggestive of lower mineral content. This was validated by decalcification of specimens using EDTA revealing a lower mineral content in samples by weight. The higher α -1: α -2 ratios from SDS-PAGE analysis of OA samples were suggestive of altered collagen structure which was supported by lower amide I 1690:1660 ratios from Raman spectra sub-peak analysis which were indicative of disordered collagen structure/the presence of immature cross-links. Furthermore, both Biochemical analysis and Raman spectroscopy did not identify any differences in the subchondral bone from the medial or lateral sides of the joint.

CHAPTER 6-DISCUSSION & CONCLUSIONS

6.1 Study Discussion

The aims of this study were to investigate the chemical composition of subchondral bone in osteoarthritic ankle joints using Raman spectroscopy and biochemical analysis. Twenty-four patient osteoarthritic ankle specimens were analysed and compared to non-osteoarthritic controls. The data gained from these samples enabled the study objectives to be met i.e. to compare OA and non-OA samples in terms of Raman spectral signatures as well as to compare subchondral bone levels of mineralisation and alpha-1 to alpha-2 type I collagen ratios.

Analysis of Raman spectra from osteoarthritic specimens identified changes suggestive of subchondral bone hypomineralisation as well as increased levels of immature type I collagen crosslinks when compared to non-osteoarthritic controls. The results from biochemical analysis have supported and complemented results from Raman spectroscopy. The suggestion that a lower phosphate: amide I ratio (for osteoarthritic bone samples) detected from Raman spectra was indicative of hypomineralisation within osteoarthritic subchondral bone specimens was validated by a lower mineral content by weight following demineralisation of samples using EDTA. Likewise, the results acquired from deconvolution of the Amide I peak acquired from Raman spectroscopy was suggestive of disordered collagen structure which was supported by significantly different levels of α -1 to α -2 chains from biochemical analysis (a reflection of altered quaternary collagen structure).

Osteoarthritic subchondral bone hypomineralisation is believed to be a result of an overproduction of the homotrimeric (3 α -1 chains) as opposed to the standard (2 α -1 chains and 1 α -2 chain) form of collagen produced by osteoblasts with an altered phenotype (Mansell 1998, Bailey 2002, Couchourel 2009). A possible explanation is that

increased levels of the homotrimeric form of type I collagen are not as readily mineralised as the regular form of collagen (Cucchiari 2016).

Furthermore, both Raman spectroscopy and biochemical analysis did not identify differences in the subchondral bone taken from the medial or lateral aspects of the osteoarthritic joint. This was particularly interesting in the context of the samples with a predominantly varus wear pattern whereby Raman and biochemical changes were noted even in the relatively non-loaded lateral side of the joint. This was consistent with findings from the study of subchondral bone in varus osteoarthritic knees (Kearns 2014) which found that biochemical changes were also present in the macroscopically less worn lateral compartment. Such findings suggest that subchondral bone changes precede the onset of macroscopic damage to the articular surface and reconfirm the possibility of subchondral bone as a therapeutic target in the treatment of osteoarthritis (Castenada 2011).

Biochemical changes in the subchondral bone of ankle osteoarthritis as ascertained from the acquisition of Raman spectra and biochemical analysis has shown similarities to results from studies investigating the subchondral bone from hip and knee arthritis (Buchwald 2012, Kearns 2014, Kim 2015). These are primarily the indication of hypomineralised subchondral bone as well as increased levels of α -1 homotrimers within the type I collagen substructure. The fact that similar changes have been detected within subchondral bone from different joints suggests a common underlying disease pathoaetiology. However, ankle osteoarthritis is far less common than the disease affecting the hip and knee joints and is usually secondary to trauma in contrast to primary osteoarthritis of the hip or knee.

The nature of the ankle joint appears to be protective against primary osteoarthritis with only 7.7% of cases within a study cohort believed to be primary in origin (Valderrabano 2009). This is despite the ankle joint being exposed to similar forces to the hip and knee joints albeit with a smaller articular surface area (Michaels 2008). The congruence of the ankle joint is believed to provide resistance to

developing osteoarthritis (Wynarsky 1983, Barg 2013) with instability resulting from trauma (damage to supporting ligaments) causing a decrease in ankle joint congruence (McKinley 2008). Despite traumatic injuries to the ankle being extremely common (Doherty 2013), presentations of symptomatic ankle osteoarthritis remain relatively uncommon (Goldberg 2012).

A proposed theory for the development of Ankle osteoarthritis

In an attempt to explain why most cases of ankle arthritis are post-traumatic and yet everyone sustaining trauma does not get osteoarthritis, coupled with the findings of this thesis, a theory is proposed.

It is possible that those with a particular subchondral biochemical bone phenotype are more susceptible to developing osteoarthritic change and in the context of the ankle joint, a traumatic event or repeated trauma to the joint could trigger the development of the condition. The role of trauma and subchondral bone chemistry in the development of osteoarthritis of the ankle could be similar to the role of initiators and promoters in a two-stage model of cancer development whereby initiators predispose cells to develop mutations and promoters cause the proliferation of cancerous cells. Interestingly in this model of cancer development promoters themselves have no effect on cancer development without previous action from an initiator (Pitot 1981).

Adapting this model for the development of ankle osteoarthritis, the traumatic event or multiple traumatic events could act as an initiator for the condition whilst altered subchondral bone chemistry could act as a promoter. Although the mechanisms for how trauma in a joint/within close proximity to a joint increase the risk of developing osteoarthritis is unknown, it is believed that injury can lead to the direct rupture of collagen fibrils within the articular cartilage matrix and subsequently the loss of glycosaminoglycans (Punzi 2016). Both constituents are important contributors to the mechanical properties of

articular cartilage. In the context of individuals with particular forms of subchondral bone chemistry, such as altered levels of mineralisation and abnormal quantities of α -1: α -2 collagen ratios, the resultant mechanical properties caused by this change such as alterations in the stiffness of subchondral bone could lead to a loss of articular cartilage shock-absorbing ability and propagate the development of osteoarthritis (Li 2013).

Furthermore, inflammation has been linked with the development of post-traumatic osteoarthritis (Punzi 2016, Anderson 2011) with some individuals developing chronic inflammatory change due to injury (Liberthal 2015). The release of glycosaminoglycans and damage to articular cartilage are believed also to lead to the release of metalloproteinases and therefore the resultant degradation of proteins including type 2 collagen within the acute phase of trauma (Punzi 2016). Such damage in theory could be exacerbated by individuals with altered subchondral bone chemistry. For example, osteoarthritic subchondral bone with altered levels of α -1 homotrimers are known to have increased bone turnover which is associated with increased levels of collagen synthesis, increased immature crosslinking and collagen degradation by increased matrix metalloproteinase activity (Bailey 2002).

6.2 Study Conclusions

In summary, the results of this study support the following conclusions:

1. Subchondral bone chemistry is altered in ankle osteoarthritis with altered levels of mineralisation as well as altered collagen structure. Such differences re-affirm the role of subchondral bone in the disease process and may suggest that there is a population of individuals with subchondral bone chemistry which predisposes them to developing the condition.

2. Osteoarthritis of the ankle is a whole joint disease with associated subchondral bone changes present even in areas of relative macroscopic articular cartilage joint sparing.

6.3 Future work

The idea that there could be a population susceptible to developing ankle osteoarthritis in general due to their subchondral bone chemistry is an interesting notion. From our cohort of patients, only 3 were deemed to have a diagnosis of primary ankle osteoarthritis. Future work could involve comparing subchondral bone from a large number of patients with no history of trauma/primary ankle osteoarthritis with those with a clear traumatic aetiology. It would be important to see whether such patients have different subchondral bone chemistry.

Furthermore, it would be interesting to investigate whether patients who develop ankle osteoarthritis are prone to developing osteoarthritis in other major joints such as the hip or the knee. A starting point could be an epidemiological study investigating patients with ankle osteoarthritis whom have a concomitant diagnosis of primary hip or primary knee osteoarthritis. If the belief that certain populations are biochemically predisposed to developing osteoarthritis were to hold true, a significant proportion should indeed have ankle and hip/knee osteoarthritis. Raman spectroscopy and biochemical analysis could then be used to compare subchondral bone from the different major joints and if found to be biochemically similar would support the idea of a population of patients that are biochemically predisposed to developing osteoarthritis.

If such a cohort of individuals could be identified, it would be possible to investigate and isolate specific Raman spectroscopy “signatures” which identifies them as susceptible to developing ankle osteoarthritis. In order to confirm whether subchondral bone biochemical changes precede the onset of osteoarthritis and are

therefore intimately linked to the development of the condition rather than being an associated finding, it would be necessary to identify on a much larger scale people with this subchondral bone phenotype with no evidence of osteoarthritis of the ankle and to perform a prospective cohort study.

The results from this study have been based on the ex-vivo analysis of bone samples so in order to achieve this, the advancement of SORS is necessary in order to reliably acquire Raman spectra from patients non-invasively. At present this is possible but with practical limitations i.e. patients need to be “scanned” for relatively long periods of time e.g. 30 minutes whilst keeping still to gain meaningful spectra. Should SORS be optimised and a subchondral bone phenotype and/or phenotypes predisposing individuals to osteoarthritis of the ankle be identified and confirmed, it would then be possible to screen the population for “at-risk” patients and then to trial interventions in the hope of preventing the onset of the condition.

REFERENCES

- Abramson SB, Attur M. Developments in the scientific understanding of osteoarthritis. *Arthritis Res Ther.* 2009;11(3):227.
- Ager JW, Nalla RK, Breeden KL, Ritchie RO. Deep-ultraviolet Raman spectroscopy study of the effect of aging on human cortical bone. *J Biomed Opt.* 2005 May-Jun;10(3):034012.
- Akkus O, Adar F, Schaffler MB. Age-related changes in physicochemical properties of mineral crystals are related to impaired mechanical function of cortical bone. *Bone.* 2004 Mar;34(3):443-53.
- Ammann P, Rizzoli R. Bone strength and its determinants. *Osteoporos Int.* 2003;14 Suppl 3:S13-8.
- Andersen TL, Sondergaard TE, Skorzynska KE, Dagnaes-Hansen F, Plesner TL, Hauge EM, Plesner T, Delaisse JM. A physical mechanism for coupling bone resorption and formation in adult human bone. *Am J Pathol.* 2009 Jan;174(1):239-47.
- Anderson DD, Chubinskaya S, Guilak F et al. Post-traumatic osteoarthritis: improved understanding and opportunities for early intervention. *J Orthop Res* 2011;29:802–9
- Arias E. United States life tables, 2002. *Natl Vital Stat Rep.* 2004;53(6):1–38.
- Arthritis Research UK (2013). Osteoarthritis in General Practice. [online] Available at: <http://www.arthritisresearchuk.org/arthritis-information/data-and-statistics/~media/EFAEFCE432734F3AA5FB1C64329E02D1.ashx> [accessed 23. Feb 2018]
- Bailey AJ, Sims TJ, Knott L. Phenotypic expression of osteoblast collagen in osteoarthritic bone: production of type I homotrimer. *Int J Biochem Cell Biol.* 2002 Feb;34(2):176-82.

- Bakker AD, Soejima K, Klein-Nulend J, Burger EH. The production of nitric oxide and prostaglandin E(2) by primary bone cells is shear stress dependent. *J Biomech.* 2001 May;34(5):671-7.
- Bakker AD, Silva VC, Krishnan R, Bacabac RG, Blaauboer ME, Lin YC, Marcantonio RA, Cirelli JA, Klein-Nulend J. Tumor necrosis factor alpha and interleukin-1beta modulate calcium and nitric oxide signaling in mechanically stimulated osteocytes. *Arthritis Rheum.* 2009 Nov;60(11):3336-45.
- Barg A, Pagenstert GI, Leumann AG, Müller AM, Henninger HB, Valderrabano V. Treatment of the arthritic valgus ankle. *Foot Ankle Clin.* 2012 Dec;17(4):647-63.
- Barg A, Pagenstert GI, Hügler T, Gloyer M, Wiewiorski M, Henninger HB, Valderrabano V. Ankle osteoarthritis: etiology, diagnostics, and classification. *Foot Ankle Clin.* 2013 Sep;18(3):411-26.
- Bettica P, Cline G, Hart DJ, Meyer J, Spector TD. Evidence for increased bone resorption in patients with progressive knee osteoarthritis: longitudinal results from the Chingford study. *Arthritis Rheum.* 2002 Dec;46(12):3178-84.
- Bianco D, Todorov A, Čengić T, Pagenstert G, Schären S, Netzer C, Hügler T, Geurts J. Alterations of Subchondral Bone Progenitor Cells in Human Knee and Hip Osteoarthritis Lead to a Bone Sclerosis Phenotype. *Int J Mol Sci.* 2018 Feb 6;19(2). pii: E475.
- Borzi RM, Mazzetti I, Marcu KB, Facchini A. 2004. Chemokines in cartilage degradation. *Clin Orthop Relat Res.* 2004 Oct;(427 Suppl):S53-61.
- Boskey AL, Wright TM, Blank RD. Collagen and bone strength. *J Bone Miner Res.* 1999 Mar;14(3):330-5.
- Brockett CL, Chapman GJ. Biomechanics of the ankle. *Orthop Trauma.* 2016 Jun;30(3):232-238.

Buchwald T, Niciejewski K, Kozielski M, Szybowicz M, Siatkowski M, Krauss H. Identifying compositional and structural changes in spongy and subchondral bone from the hip joints of patients with osteoarthritis using Raman spectroscopy. *J Biomed Opt.* 2012 Jan;17(1):017007.

Buckley K et al. Raman spectroscopy reveals differences in collagen secondary structure which relate to the levels of mineralisation in bones that have evolved for different functions," *J. Raman Spectrosc.* 2012 43(9), 1237–1243.

Buettner O, Leumann A, Lehner R, Dell-Kuster S, Rosenthal R, Mueller-Gerbl M, Valderrabano V. Histomorphometric, CT arthrographic, and biomechanical mapping of the human ankle. *Foot Ankle Int.* 2013 Jul;34(7):1025-34.

Buckley K, Kerns JG, Birch HL, Gikas PD, Parker AW, Matousek P, Goodship AE. Functional adaptation of long bone extremities involves the localized "tuning" of the cortical bone composition; evidence from Raman spectroscopy. *J Biomed Opt.* 2014;19(11):111602.

Buckwalter JA, Glimcher MJ, Cooper RR, Recker R. Bone Biology. *J Bone Joint Surg Am.* 1995;77:1256-1275.

Burr DB, Radin EL. Microfractures and microcracks in subchondral bone: are they relevant to osteoarthrosis? *Rheum Dis Clin North Am.* 2003 Nov;29(4):675-85.

Calhoun JH, Li F, Ledbetter BR, Viegas SF. A comprehensive study of pressure distribution in the ankle joint with inversion and eversion. *Foot Ankle Int.* 1994 Mar;15(3):125-33.

Carden A, Rajachar RM, Morris MD, Kohn DH. Ultrastructural changes accompanying the mechanical deformation of bone tissue: A Raman imaging study. *Calcif Tissue Int.* 2003 Feb;72(2):166-75.

Castañeda S, Roman-Bias JA, Largo R, Herrero-Beaumont G. Subchondral bone as a key target for osteoarthritis treatment. *Biochem Pharmacol.* 2012 Feb 1;83(3):315-23.

Charles JF, Aliprantis AO. Osteoclasts: more than 'bone eaters'.
Trends Mol Med. 2014 Aug;20(8):449-59.

Civitelli R, Lecanda F, Jørgensen NR, Steinberg TH. Intercellular junctions and cell-cell communication in bone. Chapter 18 in Principles of Bone Biology, J. P. Bilezikian, L. Raisz, and G. A. Rodan, Eds., pp. 287–302, Academic Press, San Diego, Calif, USA, 2002.

Couchourel D, Aubry I, Delalandre A, Lavigne M, Martel-Pelletier J, Pelletier JP, Lajeunesse D. Altered mineralization of human osteoarthritic osteoblasts is attributable to abnormal type I collagen production. Arthritis Rheum. 2009 May;60(5):1438-50.

Crockett JC, Mellis DJ, Scott DI, Helfrich MH. New knowledge on critical osteoclast formation and activation pathways from study of rare genetic diseases of osteoclasts: focus on the RANK/RANKL axis. Osteoporos Int. 2011 Jan;22(1):1-20.

Cucchiaroni M, de Girolamo L, Filardo G, Oliveira JM, Orth P, Pape D, Reboul P. Basic science of osteoarthritis. J Exp Orthop. 2016 Dec;3(1):22.

Currey JD, Brear K, Zioupos P. The effects of ageing and changes in mineral content in degrading the toughness of human femora. J Biomech. 1996 Feb;29(2):257-60.

Currey JD, Foreman J, Laketic I, Mitchell J, Pegg DE, Reilly GC. Effects of ionizing radiation on the mechanical properties of human bone. J Orthop Res. J Orthop Res. 1997 Jan;15(1):111-7.

Currey JD. Role of collagen and other organics in the mechanical properties of bone. Osteoporos Int. 2003 Sep;14 Suppl 5:S29-36.

Currey JD. Bones: Structure and Mechanics. Princeton university press 2006.

Daniels T. Etiology and Biomechanics of Ankle Arthritis. Foot Ankle Clin. 2008 Sep;13(3):341-52.

Davies HE, Wathen CG, Gleeson FV. The risks of radiation exposure related to diagnostic imaging and how to minimise them. *BMJ*. 2011 Feb 25;342:d947.

Deland JT, Morris GD, Sung IH. Biomechanics of the ankle joint. A perspective on total ankle replacement. *Foot Ankle Clin*. 2000 Dec;5(4):747-59.

Dieppe P, Cushnaghan J, Young P, Kirwan J. Prediction of the progression of joint space narrowing in osteoarthritis of the knee by bone scintigraphy. *Ann Rheum Dis*. 1993 Aug;52(8):557-63.

Dumond H, Presle N, Terlain B, Mainard D, Loeuille D, Netter P, Pottie P: Evidence for a key role of leptin in osteoarthritis. *Arthritis Rheum* 2003, 48:3118-3129.

Egloff C, Hügle T, Valderrabano V. Biomechanics and pathomechanisms of osteoarthritis. *Swiss Med Wkly*. 2012 Jul 19;142:w13583.

Englund M, Lohmander LS. Risk factors for symptomatic knee osteoarthritis fifteen to twenty-two years after meniscectomy. *Arthritis Rheum*. 2004 Sep;50(9):2811-9.

Esmonde-White KA, Mandair GS, Raaii F, Jacobson JA, Miller BS, Urquhart AG, Roessler BJ, Morris MD. Raman spectroscopy of synovial fluid as a tool for diagnosing osteoarthritis. *J Biomed Opt*. 2009 May-Jun;14(3):034013.

Eyre DR. Collagens and cartilage matrix homeostasis. *Clin Orthop Relat Res*. 2004;(427 Suppl):S118–22.

Fermor B, Weinberg JB, Pisetsky DS, Misukonis MA, Banes AJ, Guilak F: The effects of static and intermittent compression on nitric oxide production in articular cartilage explants. *J Orthop Res* 2001, 19:729-737.

Ferraro, Nakamoto, Brown. (2003) Introductory Raman spectroscopy.

- Florencio-Silva R, Sasso GR, Sasso-Cerri E, Simões MJ, Cerri PS. Biology of Bone Tissue: Structure, Function, and Factors That Influence Bone Cells. *Biomed Res Int.* 2015;2015:421746.
- Gadjanski I, Spiller K, Vunjak-Novakovic G. Time-dependent processes in stem cell-based tissue engineering of articular cartilage. *Stem Cell Rev.* 2012 Sep;8(3):863-81
- Gardiner, D.J. (1989). *Practical Raman spectroscopy.* Springer-Verlag.
- Giannini S, Buda R, Faldini C, et al. The treatment of severe posttraumatic arthritis of the ankle joint. *J Bone Joint Surg Am* 2007;89(Suppl 3):15–28.
- Gikas P 2013. A study of the subchondral bone in human knee osteoarthritis using raman spectroscopy, MD (res) Thesis. University College London.
- Goldberg AJ, MacGregor A, Dawson J, Singh D, Cullen N, Sharp RJ, Cooke PH. The demand incidence of symptomatic ankle osteoarthritis presenting to foot & ankle surgeons in the United Kingdom. *Foot (Edinb).* 2012 Sep;22(3):163-6.
- Goldring MB, Goldring SR. Osteoarthritis. *J Cell Physiol.* 2007 Dec;213(3):626-34.
- Grynpas MD, Alpert B, Katz I, Lieberman I, Pritzker KP. Subchondral bone in osteoarthritis. *Calcif Tissue Int.* 1991 Jul;49(1):20-6.
- Guccione AA, Felson DT, Anderson JJ, Anthony JM, Zhang Y, Wilson PW, et al. The effects of specific medical conditions on the functional limitations of elders in the Framingham Study. *Am J Public Health.* 1994;84(3):351–8.
- Guilak F. Biomechanical factors in osteoarthritis. *Best Pract Res Clin Rheumatol.* 2011 December ; 25(6): 815–823.

Gupta S, Hawker GA, Laporte A, Croxford R, Coyte PC. The economic burden of disabling hip and knee osteoarthritis (OA) from the perspective of individuals living with this condition. *Rheumatology (Oxford)*. 2005;44(12):1531–7.

Hartley KG, Damon BM, Patterson GT, Long JH, Holt GE. MRI techniques: a review and update for the orthopaedic surgeon. *J Am Acad Orthop Surg*. 2012 Dec;20(12):775-87.

Hashimoto T, Inokuchi S. A kinematic study of ankle joint instability due to rupture of the lateral ligaments. *Foot Ankle Int*. 1997 Nov;18(11):729-34.

Helmark IC, Mikkelsen UR, Borglum J, Rothe A, Petersen MC, Andersen O, et al. Exercise increases interleukin-10 levels both intraarticularly and peri-synovially in patients with knee osteoarthritis: a randomized controlled trial. *Arthritis Res Ther*. 2010;12(4):R126.

Henrotin Y, Pesesse L, Sanchez C. Subchondral bone and osteoarthritis: biological and cellular aspects. *Osteoporos Int*. 2012 Dec;23 Suppl 8:S847-51.

Horisberger M, Valderrabano V, Hintermann B. Posttraumatic ankle osteoarthritis after ankle-related fractures. *J Orthop Trauma* 2009;23(1):60–7.

Huch K, Kuettner KE, Dieppe P. Osteoarthritis in ankle and knee joints. *Semin Arthritis Rheum*. 1997 Feb;26(4):667-74.

Imhof H, Sulzbacher I, Grampp S, Czerny C, Youssefzadeh S, Kainberger F. Subchondral bone and cartilage disease: a rediscovered functional unit. *Invest Radiol*. 2000 Oct;35(10):581-8.

Kadri A, Ea HK, Bazille C, Hannouche D, Liote´ F, Cohen-Solal ME. Osteoprotegerin inhibits cartilage degradation through an effect on trabecular bone in murine experimental osteoarthritis. *Arthritis Rheum*. 2008 Aug;58(8):2379-86.

Kawaguchi H: Endochondral ossification signals in cartilage degradation during osteoarthritis progression in experimental mouse models. *Mol Cells* 2008, 25:1-6.

Kawcak CE, McIlwraith CW, Norrdin RW, Park RD, James SP: The role of subchondral bone in joint disease: a review. *Equine Vet J.* 2001 Mar;33(2):120-6.

Kempson GE. Age-related changes in the tensile properties of human articular cartilage: a comparative study between the femoral head of the hip joint and the talus of the ankle joint. *Biochim Biophys Acta.* 1991 Oct 31;1075(3):223-30.

Kerns JG, Gikas PD, Buckley K, Shepperd A, Birch HL, McCarthy I, Miles J, Briggs TW, Keen R, Parker AW, Matousek P, Goodship AE. Evidence from Raman spectroscopy of a putative link between inherent bone matrix chemistry and degenerative joint disease. *Arthritis Rheumatol.* 2014 May;66(5):1237-46.

Kim KK, Won Y, Kim TG, Baek MH, Choi J. Comparison of the Chemical Composition of Subchondral Trabecular Bone of Medial Femoral Condyle between with Advanced Osteoarthritis and without Osteoarthritis. *J Bone Metab.* 2015 Aug;22(3):93-7.

Kouteva-Arguirova, S, Arguirov, T, Wolfframm, D.; Reif, J. Influence of local heating on micro-Raman spectroscopy of silicon. *J. Appl. Phys.* 2003, 94, 4946–4949.

Lajeunesse D, Reboul P. Subchondral bone in osteoarthritis: a biologic link with articular cartilage leading to abnormal remodeling. *Curr Opin Rheumatol.* 2003 Sep;15(5):628-33.

Leach RE, Baumgard S, Broom J: Obesity: its relationship to osteoarthritis of the knee. *Clin Orthop Relat Res* 1973, 93:271-273.

Lee MS, Trindade MC, Ikenoue T, Schurman DJ, Goodman SB, Smith RL. Intermittent hydrostatic pressure inhibits shear stress-induced

- nitric oxide release in human osteoarthritic chondrocytes in vitro. *J Rheumatol*. 2003 Feb;30(2):326-8.
- Legros R, Balmain N, Bonel G. Age-related changes in mineral of rat and bovine cortical bone. *Calcif Tissue Int*. 1987 Sep;41(3):137-44.
- Li B, Aspden RM. Composition and mechanical properties of cancellous bone from the femoral head of patients with osteoporosis or osteoarthritis. *J Bone Miner Res*. 1997 Apr;12(4):641-51.
- Li G, Yin J, Gao J, Cheng TS, Pavlos NJ, Zhang C, Zheng MH. Subchondral bone in osteoarthritis: insight into risk factors and microstructural changes. *Arthritis Res Ther*. 2013;15(6):223.
- Lieberthal J, Sambamurthy N, Scanzello CR. Inflammation in joint injury and post-traumatic osteoarthritis. *Osteoarthritis Cartilage* 2015;23:1825–34.
- Lindsjo U. Operative treatment of ankle fracture-dislocations. A follow-up study of 306/321 consecutive cases. *Clin Orthop Relat Res*. 1985 Oct;(199):28-38.
- Loeser RF. Molecular mechanisms of cartilage destruction: Mechanics, inflammatory mediators, and aging collide. *Arthritis Rheum*. 2006 May;54(5):1357-60.
- Loughlin J. Genome studies and linkage in primary osteoarthritis. *Rheum Dis Clin North Am*. 2002 Feb;28(1):95-109.
- Loughlin J. Polymorphism in signal transduction is a major route through which osteoarthritis susceptibility is acting. *Curr Opin Rheumatol*. 2005 Sep;17(5):629-33.
- Lu¨bbeke A, Salvo D, Stern R, et al. Risk factors for post-traumatic osteoarthritis of the ankle: an eighteen year follow-up study. *Int Orthop* 2012;36(7):1403–10.

- McCreadie BR, Goldstein SA. Biomechanics of fracture: is bone mineral density sufficient to assess risk? *J Bone Miner Res.* 2000 Dec;15(12):2305-8.
- McKinley TO, Tochigi Y, Rudert MJ, et al. The effect of incongruity and instability on contact stress directional gradients in human cadaveric ankles. *Osteoarthritis Cartilage* 2008;16(11):1363–9.
- Macko VW, Matthews LS, Zwirkoski P, Goldstein SA. The joint-contact area of the ankle. The contribution of the posterior malleolus. *J Bone Joint Surg Am.* 1991 Mar;73(3):347-51.
- Madry H, van Dijk CN, Mueller-Gerbl M. The basic science of the subchondral bone. *Knee Surg Sports Traumatol Arthrosc.* 2010 Apr;18(4):419-33 .
- Malinin T, Ouellette EA. Articular cartilage nutrition is mediated by subchondral bone: a long-term autograft study in baboons. *Osteoarthritis Cartilage.* 2000 Nov;8(6):483-91.
- Mandair GS, Morris MD. Contributions of Raman spectroscopy to the understanding of bone strength. *BoneKey Reports* 4. 2015. Article number: 620 (2015).
- Mann V, Huber C, Kogianni G, Jones D, Noble B. The influence of mechanical stimulation on osteocyte apoptosis and bone viability in human trabecular bone. *J Musculoskelet Neuronal Interact.* 2006 Oct-Dec;6(4):408-17.
- Mansell JP, Bailey AJ. Abnormal cancellous bone collagen metabolism in osteoarthritis. *J Clin Invest.* 1998 Apr 15;101(8):1596-603.
- Martin RB, Burr DB, Sharkey NA (1998) *Skeletal tissue mechanics.* Springer, Berlin Heidelberg New York.
- Martin JA, Buckwalter JA: Aging, articular cartilage chondrocyte senescence and osteoarthritis. *Biogerontology* 2002, 3:257-264

Matousek P, Clark IP, Draper ER, Morris MD, Goodship AE, Overall N, Towrie M, Finney WF, Parker AW. Subsurface probing in diffusely scattering media using spatially offset Raman spectroscopy. *Appl Spectrosc*. 2005 Apr;59(4):393-400.

Matousek P, Draper ER, Goodship AE, Clark IP, Ronayne KL, Parker AW. Noninvasive Raman spectroscopy of human tissue in vivo. *Appl Spectrosc*. 2006 Jul;60(7):758-63.

Michael JM, Golshani A, Gargac S, Goswami T. Biomechanics of the ankle joint and clinical outcomes of total ankle replacement. *J Mech Behav Biomed Mater*. 2008 Oct;1(4):276-94.

Millward-Sadler SJ, Salter DM. Integrin-dependent signal cascades in chondrocyte mechanotransduction. *Ann Biomed Eng*. 2004 Mar;32(3):435-46.

Morris MD, Mandair GS. Raman assessment of bone quality. *Clin Orthop Relat Res*. 2011 Aug;469(8):2160-9.

Mosley JR. Osteoporosis and bone functional adaptation: mechanobiological regulation of bone architecture in growing and adult bone, a review. *J Rehabil Res Dev*. 2000 Mar-Apr;37(2):189-99.

Muraoka T, Hagino H, Okano T, Enokida M, Teshima R. Role of subchondral bone in osteoarthritis development: a comparative study of two strains of guinea pigs with and without spontaneously occurring osteoarthritis. *Arthritis Rheum*. 2007 Oct;56(10):3366-74.

Nieves JW, Formica C, Ruffing J, Zion M, Garrett P, Lindsay R, Cosman F. Males have larger skeletal size and bone mass than females, despite comparable body size. *J Bone Miner Res*. 2005 Mar;20(3):529-35.

Oliveria SA, Felson DT, Cirillo PA, Reed JI, Walker AM. Body weight, body mass index, and incident symptomatic osteoarthritis of the hand, hip, and knee. *Epidemiology*. 1999 Mar;10(2):161-6.

Oliviero F, Ramonda R, Punzi L. New horizons in osteoarthritis. *Swiss Med Wkly*. 2010;140:w13098

Outerbridge RE. The etiology of chondromalacia patellae. *J Bone Joint Surg Br*. 1961 Nov;43-B:752-7.

Parker RD. Articular Cartilage and Meniscal Restoration. *Orthopedics*. 2005;28(9):980-982.

Paschalis EP, Tatakis DN, Robins S, Fratzi P, Manjubala I, Zoehrer R et al. Lathyrisms-induced alterations in collagen cross-links influence the mechanical properties of bone material without affecting the mineral. *Bone*. 2011 Dec;49(6):1232-41.

Pelton JT, McLean LR. Spectroscopic Methods for Analysis of Protein Secondary Structure. *Analytical Biochemistry* 2000;277:167–176.

Pezzotti G, Rondinella A, Marin E, Zhu W, Aldini NN, Ulian G, Valdrè G. Raman spectroscopic investigation on the molecular structure of apatite and collagen in osteoporotic cortical bone. *J Mech Behav Biomed Mater*. 2017 Jan;65:264-273.

Pitot, H.C., Goldsworthy, T., Moran, S. The natural history of carcinogenesis: Implications of experimental carcinogenesis in the genesis of human cancer. *J Supramol Struct Cell Biochem*. 1981;17(2):133-46.

Pope SJA, West YD. Use of the FT Raman spectrum of Na₂MoO₄ to study sample heating by the laser. *Spectrochim. Acta Part A*. 1995, 51, 2011-2017.

Punzi L, Galozzi P, Luisetto R, Favero M, Ramonda R, Oliviero F, Scanu A. Post-traumatic arthritis: overview on pathogenic mechanisms and role of inflammation. *RMD Open*. 2016; 2(2).

Ramachandran, M., 2017. *Basic Orthopaedic Sciences*. 3rd ed. United Kingdom: CRC Press.

Ramsey PL, Hamilton W. Changes in tibiotalar area of contact caused by lateral talar shift. *J Bone Joint Surg Am.* *J Bone Joint Surg Am.* 1976 Apr;58(3):356-7.

Robertson CM, Pennock AT, Harwood FL, Pomerleau AC, Allen RT, Amiel D: Characterization of pro-apoptotic and matrixdegradative gene expression following induction of osteoarthritis in mature and aged rabbits. *Osteoarthritis Cartilage* 2006, 14:471-476.

Robling AG, Castillo AB, Turner CH. Biomechanical and molecular regulation of bone remodeling. *Annu Rev Biomed Eng.* 2006;8:455-98.

Rocheftort GY, Pallu S, Benhamou CL. Osteocyte: the unrecognized side of bone tissue. *Osteoporos Int.* 2010 Sep;21(9):1457-69.

Sabokbar A, Crawford R, Murray DW, Athanasou NA: Macrophageosteoclast differentiation and bone resorption in osteoarthritic subchondral acetabular cysts. *Acta Orthop Scand.* 2000 Jun;71(3):255-61.

Saito M, Marumo K. Collagen cross-links as a determinant of bone quality: a possible explanation for bone fragility in aging, osteoporosis, and diabetes mellitus. *Osteoporos Int.* 2010 Feb;21(2):195-214.

Saltzman CL, Salamon ML, Blanchard GM, Huff T, Hayes A, Buckwalter JA, Amendola A. Epidemiology of ankle arthritis: report of a consecutive series of 639 patients from a tertiary orthopaedic center. *Iowa Orthop J.* 2005;25:44-6.

Saltzman CL, Zimmerman MB, O'Rourke M, Brown TD, Buckwalter JA, Johnston R. Impact of comorbidities on the measurement of health in patients with ankle osteoarthritis. *J Bone Joint Surg Am.* 2006;88(11):2366-72

Shepherd DE, Seedhom BB. Thickness of human articular cartilage in joints of the lower limb. *Ann Rheum Dis.* 1999 Jan;58(1):27-34.

- Sims NA, Gooi JH. Bone remodeling: Multiple cellular interactions required for coupling of bone formation and resorption. *Semin Cell Dev Biol.* 2008 Oct;19(5):444-51.
- Stufkens SA, Knupp M, Horisberger M, et al. Cartilage lesions and the development of osteoarthritis after internal fixation of ankle fractures: a prospective study. *J Bone Joint Surg Am* 2010;92(2):279–86.
- Takakura Y, Aoki T, Sugimoto K, et al. The treatment for osteoarthritis of the ankle joint. *Jpn J Joint Dis* 1986;5:347–52.
- Tanamas SK, Wluka AE, Pelletier JP, Martel-Pelletier J, Abram F, Wang Y, Cicuttini FM. The association between subchondral bone cysts and tibial cartilage volume and risk of joint replacement in people with knee osteoarthritis: a longitudinal study. *Arthritis Res Ther.* 2010;12(2):R58.
- Tetlow LC, Adlam DJ, Woolley DE: Matrix metalloproteinase and proinflammatory cytokine production by chondrocytes of human osteoarthritic cartilage: associations with degenerative changes. *Arthritis Rheum* 2001, 44:585-594.
- Tochigi Y, Rudert MJ, McKinley TO, et al. Correlation of dynamic cartilage contact stress aberrations with severity of instability in ankle incongruity. *J Orthop Res* 2008;26(9):1186–93.
- Tochigi Y, Buckwalter JA, Martin JA, et al. Distribution and progression of chondrocyte damage in a whole-organ model of human ankle intra-articular fracture. *J Bone Joint Surg Am* 2011;93(6):533–9.
- Todd Allen R, Robertson CM, Harwood FL, Sasho T, Williams SK, Pomerleau AC, Amiel D. Characterization of mature vs aged rabbit articular cartilage: analysis of cell density, apoptosis related gene expression and mechanisms controlling chondrocyte apoptosis. *Osteoarthritis Cartilage* 2004, 12:917-923.

- Valderrabano V, Horisberger M, Russell I, Dougall H, Hintermann B. Etiology of ankle osteoarthritis. *Clin Orthop Relat Res*. 2009 Jul;467(7):1800-6.
- Valdes AM, Loughlin J, Oene MV, Chapman K, Surdulescu GL, Doherty M, Spector TD. Sex and ethnic differences in the association of ASPN, CALM1, COL2A1, COMP, and FRZB with genetic susceptibility to osteoarthritis of the knee. *Arthritis Rheum*. 2007 Jan;56(1):137-46.
- Viguet-Carrin S, Garnero P, Delmas PD. The role of collagen in bone strength. *Osteoporos Int*. 2006;17(3):319-36.
- Wang X, Bank RA, TeKoppele JM, Agrawal CM (2001) The role of collagen in determining bone mechanical properties. *J Orthop Res* 19:1021–1026.
- Webster, S.S.J.(2001). *Integrated Bone Tissue Physiology*. Bone Mechanics Handbook 2nd edition. S.C.Cowin, CRC Press,USA.
- Weiner S. The Material Bone: Structure-Mechanical Function Relations. *Annual Review of Materials Science*. 1998 28(1):271-298.
- Westacott CI, Webb GR, Warnock MG, Sims JV, Elson CJ. Alteration of cartilage metabolism by cells from osteoarthritic bone. *Arthritis Rheum* 1997;40:1282–91.
- Wynarsky GT, Greenwald AS. Mathematical model of the human ankle joint. *J Biomech* 1983;16(4):241–51.
- Yerramshetty JS, Lind C, Akkus O. The compositional and physicochemical homogeneity of male femoral cortex increases after the sixth decade. *Bone*. 2006 Dec;39(6):1236-43.
- Zhai G, Hart DJ, Kato BS, MacGregor A, Spector TD. Genetic influence on the progression of radiographic knee osteoarthritis: a longitudinal twin study. *Osteoarthritis Cartilage* 2007, 15:222-225.

Zhao J, Lui H, McLean DI, Zeng H. Automated autofluorescence background subtraction algorithm for biomedical Raman spectroscopy. *Appl Spectrosc.* 2007 Nov;61(11):1225-32.

Zimmermann EA, Schaible E, Gludovatz B, Schmidt FN, Riedel C, Krause M, Vettorazzi E, Acevedo C, Hahn M, Püschel K, Tang S, Amling M, Ritchie RO Busse B. Intrinsic mechanical behavior of femoral cortical bone in young, osteoporotic and bisphosphonate-treated individuals in low- and high energy fracture conditions. *Sci Rep.* 2016 Feb 16;6:21072.

Zioupou P, Currey JD, Hamer AJ (1999) The role of collagen in the declining mechanical properties of aging human cortical bone. *J Biomed Mater Res.* 1999 May;45(2):108-16.

